

DEVELOPMENT OF A SURFACE ENHANCED RAMAN SPECTROSCOPY-BASED
ASSAY TO DETECT MALARIA BIOMARKERS IN BLOOD

by

Logan Hamm

A thesis submitted to the faculty of
The University of North Carolina at Charlotte
in partial fulfillment of the requirements
for the degree of Master of Science in
Chemistry

Charlotte

2020

Approved by:

Dr. Swarnapali De Silva Indrasekara

Dr. Joanna K. Krueger

Dr. Jordan C. Poler

Dr. Eugenia Lo

©2020
Logan Hamm
ALL RIGHTS RESERVED

ABSTRACT

LOGAN HAMM. Development of a Surface Enhanced Raman Spectroscopy-based Assay to Detect Malaria Biomarkers in Blood. (Under the direction of DR. SWARNAPALI DE SILVA INDRASEKARA)

Malaria is an infectious disease that affects many lives around the world and eradication efforts are focused on controlling the disease transmission; which requires early diagnosis of the infection before the onset of symptoms, i.e. at the asymptomatic stage. Blood smear microscopy is used for symptomatic malaria diagnosis, but it lacks the specificity and sensitivity required for asymptomatic diagnosis. Alternatively, polymerase chain reaction (PCR) can be used to detect the malaria (*plasmodium*) parasitic nucleic acids with high sensitivity and specificity, but the point-of-care (POC) implementation of PCR is not practical due to laborious procedures and expensive instrumentation. Recently, Surface Enhanced Raman Spectroscopy (SERS) has become a prominent analytical technique, because of its high molecular specificity and enhanced analytical sensitivity. The overall goal of this thesis is to develop a novel PCR amplification-free, SERS-based approach that can detect an asymptomatic malaria biomarker (Pfs25-mRNA) with sufficient sensitivity for POC applications. We developed a sandwich hybridization assay that captures Pfs25-mRNA target sequence using two partially complementary synthetic nucleic acid sequences attached to nanoparticles known as probes. One probe consists of a plasmonic core-shell nanoparticle with an embedded Raman tag to act as a SERS signal reporter. The other probe involves a magnetic bead allowing the separation of the captured Pfs25-mRNA from the blood matrix. Our work demonstrates the ability of the developed SERS hybridization assay to

specifically detect synthetic Pfs25-mRNA in buffer and spiked-in blood lysate without the need for amplification techniques. Along with development of the hybridization assay, a novel gold coated-silver nanostar substrate was developed for potential use in SERS-based applications.

ACKNOWLEDGEMENTS

I would like to first thank my thesis advisor Dr. Swarnapali De Silva Indrasekara here at the University of North Carolina at Charlotte. Dr. Indrasekara has always been willing to help guide me in the direction I needed to go while still making me learn important concepts and techniques. There were times I would allow the mishaps of research control my emotions but Dr. Indrasekara told me what I needed to hear to get back on track. I would also like to thank Dr. Eugenia Lo for her insight into the biology side of my research project, specifically topics on malaria that I did not understand. I would like to thank the rest of my thesis committee, Dr. Jordan Polar and Dr. Joanna Krueger, for being a part of my committee and giving insight on how to improve my thesis. Finally, a very special thanks to Dr. Thomas Walsh who graciously funded the second year of this program for me with his fellowship.

TABLE OF CONTENTS

LIST OF TABLES	viii
LIST OF FIGURES	ix
LIST OF ABBREVIATIONS	xi
CHAPTER 1: INTRODUCTION	1
1.1. Problem Statement – Unmet needs in Infectious Diseases Diagnostics	1
1.2. Background on Malaria and Malaria Diagnostics	1
1.3. Biosensor Development for Point-of-Care Diagnostics	3
1.4. Plasmonic Nanomaterials in Biosensing Applications	8
1.5. Plasmonic Nanoparticle- and SERS-based Optical Detection Method	11
1.6. Anisotropic Nanoparticle Characteristics and Synthesis	16
1.7. Nanoparticles Characterization using Dark-Field Scattering (DFS) Technique with Hyperspectral Imaging	19
1.8. Thesis Overview	21
CHAPTER 2: MATERIALS AND METHODS	23
2.1. Materials	23
2.2. Spherical Gold Nanoparticle Synthesis	24
2.3. Gold Nanostar Synthesis, Functionalization, and Coating with Silver	24
2.4. Silver Nanostar Synthesis, Functionalization, and Coating with Gold	26
2.5. Reporter and Capture Probe Functionalization	28
2.6. Pfs25-mRNA Sandwich Hybridization Event: Synthetic Target in Buffer	30
2.7. Lysis of Whole Blood and Hybridization Reactions in Blood	30
2.8. SERS measurements using Horiba XploRA ONE™ Raman microscope	31

2.9. DFS-Hyperspectral Imaging Acquisition using Cytoviva's Hyperspectral Microscope	32
2.10. Data and Statistical Analysis	32
CHAPTER 3: RESULTS AND DISSCUSION	34
*Section contains information included in a manuscript under submission process	
3.1. SERS Substrate Development: Silver Coated Gold Nanostars (Ag@AuNS)	34
3.2. Novel Substrate Development: Gold Coated Silver Nanostars (Ag@AuNS)	39
3.3. Fabrication and Optimization of Pfs25-mRNA and 18s-rRNA Probes in the Functional Interface	44
3.4. Comparison of Pfs25-mRNA & 18s-rRNA Hybridization Systems	48
3.5. Hybridization Reaction Results in Buffer	50
3.6. Sandwich Hybridization Reactions for Synthetic Biomarker Spiked-in Blood Lysate	51
CHAPTER 4: CONCLUSIONS AND FUTURE WORK	57
REFERENCES	61
APPENDIX A	74
APPENDIX B	102
APPENDIX C	107
APPENDIX D	111

LIST OF TABLES

TABLE 1: Synthetic sequence composition for two functional interface designs including melting temperature data	46
---	----

LIST OF FIGURES

FIGURE 1: World Health Organization malaria transmission map 2017	2
FIGURE 2: Schematic of sandwich hybridization assay and magnetic separation	7
FIGURE 3: Schematic of surface plasmon resonance application	9
FIGURE 4: Surface plasmon resonance versus localized surface plasmon resonance	11
FIGURE 5: Jablonski diagram of Raleigh versus Raman scattering	13
FIGURE 6: Dark field scattering with hyperspectral imaging diagram	21
FIGURE 7: Characterization of gold nanostars and silver coated gold nanostars	36
FIGURE 8: Dark field scattering-hyperspectral imaging results for silver coated gold nanostars	37
FIGURE 9: Surface enhanced Raman spectroscopy enhancement factor data	39
FIGURE 10: Characterization of three different silver nanostar synthesis methods	41
FIGURE 11: Coating method comparison of characterization for novel substrate	43
FIGURE 12: Scanning electron microscopy with elemental analysis of novel substrate	44
FIGURE 13: Schematic diagram of probe functionalization for hybridization reactions	46
FIGURE 14: Optimization of blank signal for hybridization reactions	48
FIGURE 15: Selectivity comparison of two functional interface systems for hybridization reactions in buffer	50
FIGURE 16: Calibration curve and surface enhanced Raman spectroscopy spectra from hybridization reactions in buffer for main target biomarker	51
FIGURE 17: Control measurements of whole blood and blood lysate	53
FIGURE 18: Time, purification and laser excitation study for reactions in blood	53
FIGURE 19: Comparison of three-hour blood lysate reaction measurements	54

FIGURE 20: Calibration curve and surface enhanced Raman spectroscopy spectra from hybridization reactions in blood lysate for main target biomarker	56
FIGURE B1: Spherical gold nanoparticle characterization	102
FIGURE B2: Characterization of silver nitrate coating trials onto gold nanostars	103
FIGURE B3: Comparison of blank spectra versus 200 nM reaction spectra	105
FIGURE B4: Raman tag selection spectra compared to blank measurement spectra	106
FIGURE C1: Ultraviolet-visible spectroscopy comparison for gold coating on silver nanostars trials with hexadecyltrimethylammonium bromide	108
FIGURE C2: Transmission electron microscopy images for gold coating trials with hexadecyltrimethylammonium bromide	109
FIGURE C3: Ultraviolet-visible spectroscopy and transmission electron microscopy comparison for gold coating trials of silver nanostars with chitosan	110
FIGURE D1: 785 nm laser excitation calibration curve and spectra in blood lysate reactions	112

LIST OF ABBREVIATIONS

RNA	ribonucleic acid
DNA	deoxyribonucleic acid
PCR	polymerase chain reaction
SERS	surface enhanced Raman spectroscopy
LSPR	localized surface plasmon resonance
EF	enhancement factor
AuNP	spherical gold nanoparticles
AuNS	gold nanostars
AgNS	silver nanostars
Ag@AuNS	silver coated gold nanostars
Au@AgNS	gold coated silver nanostars
DFS	dark-field scattering
UV-VIS	ultraviolet-visible spectroscopy
Pfs25-mRNA	<i>P. falciparum</i> microribonucleic acid biomarker
18s-rRNA	<i>P. falciparum</i> ribosomal ribonucleic acid biomarker
TEM	transmission electron microscopy
SEM	scanning electron microscopy
EDS	energy-dispersive x-ray spectroscopy
4-MBA	4-mercaptobenzoic acid
CVL	Crystal Violet Lactone
CTAB	hexadecyltrimethylammonium bromide

CHAPTER 1: INTRODUCTION

1.1. Problem Statement – Unmet needs in Infectious Diseases Diagnostics

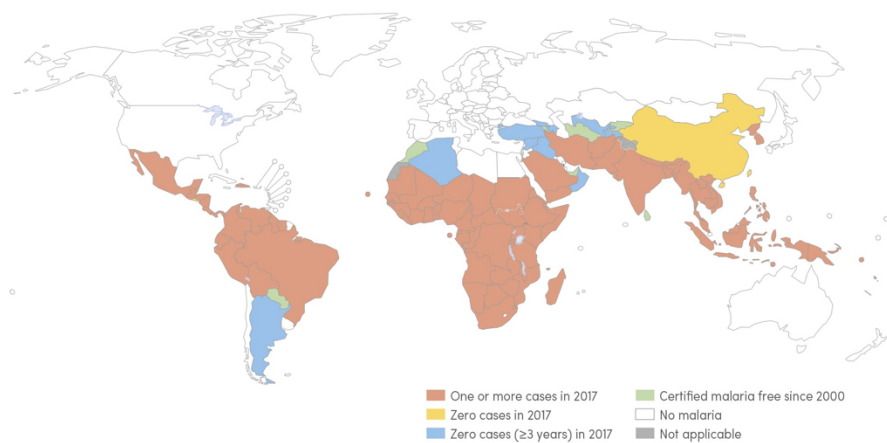
Infectious diseases are a global health issue requiring diagnostic detection methods to limit transmission or eradicate the disease. Current diagnostic testing is typically performed during the symptomatic stages of the disease. While some infectious diseases are treatable after diagnosis, the ability to limit transmission during the symptomatic stages is low. The main problem with current diagnostic methods is the shortcomings for asymptomatic detection. Which is why it's crucial to develop sensitive and selective diagnostic assays for asymptomatic detection of these diseases; especially for the detection of one of the most problematic infectious diseases, malaria.

1.2. Background on Malaria and Malaria Diagnostics

Many infectious diseases are the focus of diagnostic assay development; however, malaria is one of the highest life-threatening diseases with an estimated 228 million cases and 405,000 deaths worldwide in 2018 alone.² Malaria stems from *Plasmodium* parasites with transmission that occurs through female Anopheles mosquitos in tropical regions (Figure 1). While there are five total species of the *Plasmodium* parasite, two of these are the main causing agents of malaria; *P. falciparum* and *P. vivax* create a majority of the cases found worldwide. *P. falciparum* impacts these tropical areas with greater severity in comparison to *P. vivax* which is why it will be the focus of this work. Once the incubation period begins within the human host the disease can develop from uncomplicated malaria to complicated (severe) malaria. Uncomplicated malaria is present in the early symptomatic stage of the disease where symptoms such as fever, chills and body aches can occur.³ As the disease progresses it leads to complicated malaria which

can result in acute kidney injury, neurologic abnormalities and other severe conditions.³ Thus, showing the need for early detection of malaria to prevent these severe conditions from occurring.

Countries with indigenous cases in 2000 and their status by 2017 Countries with zero indigenous cases over at least the past 3 consecutive years are considered to be malaria free. All countries in the WHO European Region reported zero indigenous cases in 2016 and again in 2017. In 2017, both China and El Salvador reported zero indigenous cases. Source: WHO database.



WHO: World Health Organization.

Figure 1: World Health Organization malaria transmission map for 2017, reported in the world malaria report 2018¹.

For malaria detection researchers have developed clinical diagnostic methods using microscopic techniques for malaria detection.⁴⁻⁵ The most common clinical method used for the detection of malaria is the analysis of blood smears using microscopy.⁶⁻⁸ This method functions by taking a sample of blood that is obtained from an expected infected patient who shows many of the common symptoms of malaria. The blood sample is mixed with a dye, typically Giemsa, that binds to specific nucleic acid sequences of the parasites. This blood-dye mixture is then smeared onto a glass slide and observed using standard light microscopy or fluorescence microscopy. If the malaria parasite is present

in the blood, the dye will be displaying a distinct color difference between the red blood cells and the parasite when using light microscopy. In the case of fluorescence microscopy, the dye will produce a fluorescent response that can be observed. Yamamoto *et al.* developed a polycarbonate scan disc for fluorescence detection of *P. falciparum* infected red blood cells.⁸ By staining infected red blood cells with Hoechst 34580 fluorescent dye, they were able to detect a parasitemia range of 0.0001 – 1.0%. While the method of blood smear microscopy is useful for a confirmed diagnosis, it requires highly trained scientists to observe the parasites and lacks the sensitivity needed for early diagnosis. Rodulfo *et al.* compared microscopy to polymerase chain reaction and a rapid diagnostic test kit (OptiMAL) for malaria detection.⁹ Their results indicate as the parasitemia levels drop to 50 – 500 parasites/ μ L the ability of microscopy to correctly detect malaria drops to 42.9%. This demonstrates the issues with using microscopy for early diagnosis of malaria.

The biggest problem of the standard clinical methods is that malaria presents the onset of symptoms typically occurs 10 – 15 days after the infective bite from the *Anopheles* mosquito.² This is problematic because within that incubation period the parasite can develop into gametocytes where the uptake of the parasite can occur through a non-infected mosquito leading to further transmission of malaria.¹⁰⁻¹¹ While today's clinical methods of detection are helpful in determining the presence of malaria, it does not solve the problem of limiting the transmission or eradicating the disease. Which demonstrates the need for better diagnostic biosensors and testing methods that can be applied during the asymptomatic stages of malaria in a point-of-care setting.

1.3. Biosensor Development for Point-of-Care Diagnostics

The scientific community is continually working to develop these diagnostic biosensors for asymptomatic detection of infectious diseases like malaria. It is important for diagnostic biosensors to have rapid testing abilities, and offer sufficient analytical sensitivity and strong selectivity, to function at the point-of-care with limited resources.¹² A great benefit of biosensors is the fact they can be designed for detection of a single disease or can have multiplex capabilities¹³⁻¹⁵ to detect a catalogue of diseases, depending upon how they are developed.

The first step in biosensor development is determining the best biomarker from the disease of interest to target and determining a method to trap the biomarker for analysis. Biomarkers can range from nucleic acid sequences¹⁶⁻²² to specific proteins²³⁻²⁹ to macromolecules such as lipids and carbohydrates.³⁰⁻³² Detecting the biomarker in a complex matrix such as blood or urine, requires specific molecular recognition moieties and a signal transduction element in order to trap the target and produce a signal response, respectively. Proteins and nucleic acids are the most commonly used biomarkers due to the increased number of recognition elements present for biomarker capture compared to other target types.³³⁻³⁶

Nucleic acid biomarker detection usually involves nucleic acid hybridization. For instance, in 2014, Wang *et al.* used a single complementary nucleic acid sequence, bound to a dye molecule, to hybridize with RSAD2 RNA biomarker for the detection of respiratory infections.³⁷ Using a surface enhanced Raman spectroscopy detection method, the dye molecule provided the signal output for the hybridization assay where they were able to achieve a detection limit of 1 nM for the RSAD2 RNA biomarker. Protein biomarkers where antigens are the established target, antibodies can be used as the

molecular recognition moieties or vice versa for detection of a disease.²⁵⁻²⁶ Recently an immunosensor was designed to detect a Zika specific envelope antibody through a gold array micro-electrode with a detection limit of 10 pM.³⁸ While proteins are common targets and useful for diagnostic assays; they are not ideal for asymptomatic stage detection due to the concentration of antibodies being low from the lack of RNA translation into amino acid sequences. Nucleic acid sequences are of very high priority in comparison to proteins as biomarkers due to a higher presence of nucleic acids in the early stages of diseases and an increased specificity of the sequences for a singular disease. For example, Chang *et al.* compared the protein makeup of Zika to other arthropod-borne viruses like dengue and determined that Zika shares 55.6% amino acid sequence identity with dengue.³⁹ However, determining the method of isolation for nucleic acid biomarkers for specific and sensitive detection is a challenging task.

There is a significant focus on the isolation followed by detection methods in regard to the nucleic acid hybridization -based diagnostic assays. The most common approach is the sandwich hybridization-based assays.⁴⁰⁻⁴⁵ Designing two partially, complementary nucleic acid sequences to hybridize directly to the target sequence is highly efficient. Once the biomarker is trapped in the sandwich assay (Figure 2), it has to be isolated from any other biological material that could interfere in signal production. There are a variety of ways the assay can be developed for biomarker isolation and separation. It is common that one of the molecular recognition elements is bound to a substrate that can easily be removed from a matrix or a method in which the matrix can be removed without removal of the target-receptor system. Substrate types could include glass slides, magnetic beads, or a paper-based substrate. A good example of an in-solution separation technique is the

application of magnetic nanoparticles as one of the molecular recognition elements functionalized with one of the complementary sequences to the biomarker; most often referred to as a capture probe.^{20, 46} Zhang *et al.* utilized a sandwich hybridization assay with magnetic separation for the detection of a DNA biomarker of West Nile virus⁴⁶, which allowed to enrich the hybridized complexes into one location for surface enhanced Raman spectroscopy-based detection of the target. Magnetic separation (Figure 2) is a widely used choice for isolation of the biomarker because of the simplicity it adds to the procedure in comparison to other vigorous and time-consuming methods. Along with isolation of the nucleic acid biomarker, a signal response must be detected to clearly demonstrate the isolation of the biomarker of interest occurred. Determining how to detect the isolated biomarker sequence is another important step in biosensor development.

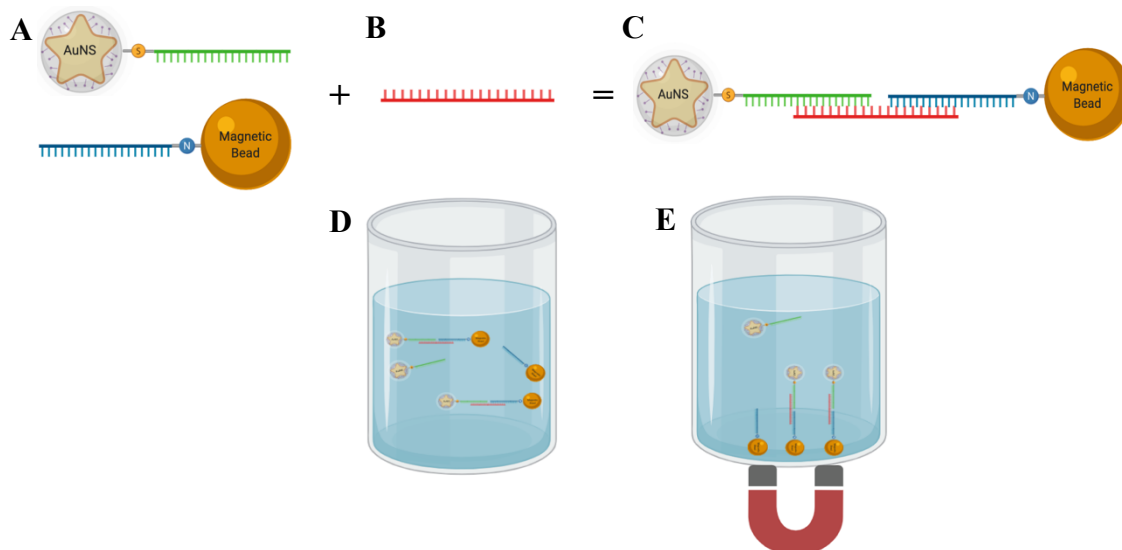


Figure 2. Representative schematic diagram of a sandwich hybridization reaction and the magnetic separation of the complexes in solution. A) Two probes used for isolation of the target nucleic acid biomarker containing partially complementary sequences to the biomarker. One typically acts as the reporter probe (top) to relay a signal response while the other is the capture probe for target separation (bottom). B) Desired target sequence for isolation and detection. C) Sandwich hybridization complex after incubation of the two probes with the target biomarker. D) The reaction in solution with the hybridized complexes. E) Magnetic separation of the complexes and residual capture probes when magnet placed in close proximity to reaction vessel.

The next step in developing a capable diagnostic biosensor for nucleic acid biomarkers is determining the detection method. Common methods of nucleic acid detection are PCR and fluorescence. For research purposes, PCR has been the predominate detection method of nucleic acid biomarkers for biosensing applications.⁴⁷⁻⁵⁴ PCR is an amplification technique that takes small concentrations of a target sequence and can create millions of copies of the target. This is a huge advantage of using PCR for detecting small quantities of the target in early stages of disease progression. However, there is a downside to the use of PCR as a Rapid Diagnostic Test (RDT) or an POC diagnostic assay. PCR is very expensive and many areas of the highest infection rate

from malaria do not have access to PCR instrumentation in a point-of-care setting. PCR is also laborious and required specialized personnel to perform the assay. Diagnostic assays need rapid, simplified procedural detection methods that can report results in a timely manner. A method that can meet a majority of these criteria is the use of fluorescence-based techniques.⁵⁵⁻⁵⁸ Fluorescent tags can be incorporated to a nucleic acid sequence that can interact with the target sequence and create a fluorescent signal. Liu *et al.* published a good example for fluorescent detection of DNA in a sandwich hybridization based lateral flow assay.⁵⁶ This group utilized fluorescent carbon nanoparticles as a tag for a nucleic acid sequence complementary to the DNA target. As a proof-of-concept assay, they demonstrated the ability to detect a 21mer sequence down to femtomolar concentrations. Researchers have been able to develop biosensors using fluorescence that can report results anywhere from minutes to a few hours.^{57, 59} Fluorescence does present some issues like photobleaching and short lifetimes of the fluorescent dyes. One field of detection systems that has been making a strong impact on biosensor development is optical diagnostics based on plasmonic nanoparticles.

1.4. Plasmonic Nanomaterials in Biosensing Applications

In general, the field of plasmonics relates to the study of light interacting with free conduction band electrons of certain metals.⁶⁰ When this occurs, the light causes these electrons to have a resonant oscillation around the metal. This produces an intense electromagnetic field that can scatter the light with the same or different energy than the energy of the incidental light source creating surface plasmon resonance (Figure 3).⁶¹ Plasmonic materials can consist of metals like silver and gold, metal oxides or semiconducting materials.⁶² When surface plasmons form they can propagate like waves

across the plasmonic material being used. The highest intensity of this electromagnetic field is at the point of interaction between the light and the metal-dielectric interface.⁶³ As the wave propagates away from the point of interaction, the electromagnetic field weakens.

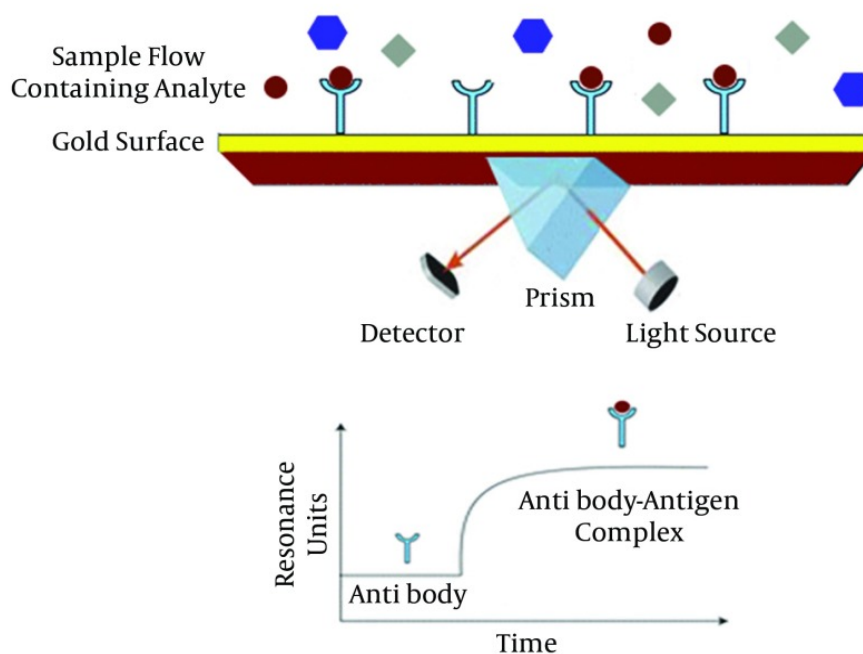


Figure 3. Schematic diagram displaying the use of surface plasmon resonance for protein detection with a gold film substrate.⁶⁴

An important feature of surface plasmon resonance is its sensitivity to changes in the environment of the plasmonic metals.⁶⁵ Due to having a high sensitivity, it is necessary to consider how different changes to this environment could impact how the surface plasmon resonance will act. For instance, Omar *et al.* used surface plasmon resonance to detect the binding of a dengue antigen to an antibody immobilized on a sensor-gold layered film.⁶⁶ When the antigen would bind and change the local environment near the

plasmonic metal, they were able to detect a change in the surface plasmon resonance angle producing a limit of detection of 0.08 pM within 8 minutes. Surface plasmon resonance can be paired with certain detection systems like PCR or fluorescence to provide added signal based on the environmental changes in the system; like the added presence of a specific biomarker for detection. This broad applicability of plasmonics makes it a suitable candidate for biosensors.^{63, 67-69} For instance, surface plasmon resonance has been used to detect PCR-amplified *E. coli* biomarkers in stool samples.⁷⁰ They were able to compare the total resonance units of control spiked samples (251.1 resonance units) to infected samples (220.2 resonance units) and determine the developed assay was successful in discriminating *E. coli* infected samples from non-infected samples (128.5 resonance units). While there are many benefits of surface plasmon resonance, some issues can arise that could negatively impact the developed biosensor. The biggest issue of surface plasmon resonance is the bulk effect. When using surface plasmon resonance as the main detection method on a substrate such as a plasmonic film, the area of sensing can range up to hundreds of nanometers into the present matrix. This means that even if you have the desired biomarkers present at the plasmonic surface, other biomolecules may be detected that aren't wanted in the assay. The size of the plasmonic material has significant influence on this bulk effect behavior of the plasmon resonance. When light interacts with a plasmonic material that is larger than the incoming frequency the surface plasmon resonance propagates across the surface and the dielectric medium. Issues like bulk effect when using surface plasmon resonance can create analytical detection problems. However, when the size of the plasmonic particles is smaller than the wavelength of incidental light it creates what is called localized surface

plasmon resonance (LSPR).⁷¹ One of the main differences between surface plasmon resonance and LSPR is the size of the produced plasmonic field. As stated by the name, LSPR is a localized plasmonic field at the point of interaction between the incidental laser source and the nanoparticle interface; whereas surface plasmon resonance produces a much larger plasmonic field (Figure 4). Which is why over the last 20 years one of the most widely used diagnostic detection methods that can eliminate this bulk effect with the use of LSPR in biosensors is SERS.

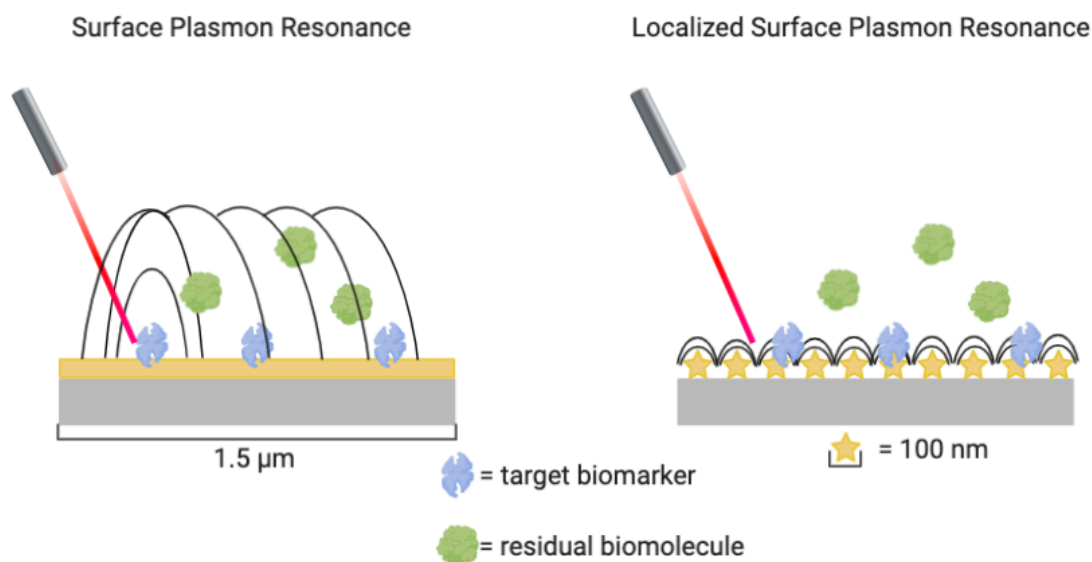


Figure 4: Surface plasmon resonance bulk effect versus localized surface plasmon resonance fields.

1.5. Plasmonic Nanoparticle- and SERS-based Optical Detection Method

SERS has grown to become one of the most widely used detection methods for biosensors.^{15, 19, 30, 46, 72-79} SERS functions by utilizing the phenomena of Raman scattering as the basis of the detection method. When light, from a laser source, interacts with an analyte there are two types of scattering that occur: Rayleigh scattering and

Raman scattering. The difference between these two are the energy exchange from the point of the incidental light interacting with the analyte and the energy of the light scattered. Rayleigh scattering is a display of inelastic scattering where there is no energy difference between the incidental light and the scattered light; this scattering type composes almost all of the reflected light. Raman scattering is elastic scattering where the energy of the scattered light can be greater or smaller than the incidental light's energy; this is also known as anti-stokes and stokes scattering, respectively (Figure 5). Only a small fraction of scattered light demonstrates this Raman scattering effect. Employing Raman scattering can be useful for a diagnostic biosensor due to the produced signal being a spectral fingerprint of the sample being analyzed. This is beneficial for discriminating between two diseases that could be similar in genetic makeup or for standard multiplexing applications.^{15, 44, 74} However, Raman spectroscopy is not very sensitive since only a small portion of all scattered light (0.000001%)⁸⁰ is Raman and it has limitations in its ability as a detection method for disease diagnostics. SERS has the ability to eliminate many of the limitations Raman spectroscopy demonstrates through Raman signal enhancement.

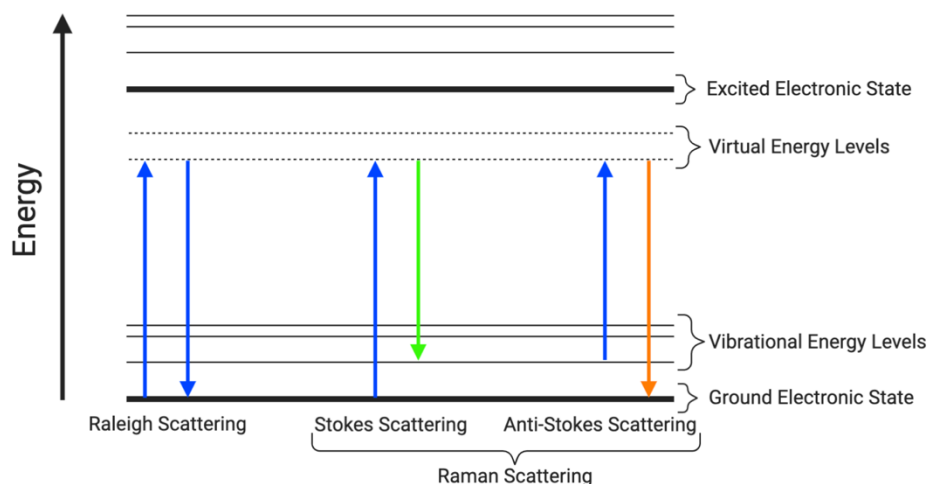


Figure 5: Jablonski diagram depicting Raleigh versus Raman scattering; including the two types of Raman scattering: Stokes and Anti-Stokes scattering.

SERS signal enhancement of Raman scattering stems from two main types of enhancement: electromagnetic and chemical.⁷² Electromagnetic enhancement originates from the localization of light on the SERS substrate surface.⁸¹ This localization of the light induces the surface plasmon resonance with an amplified intensity due to the interaction of the plasmonic metal's electrons with the light source. The electromagnetic enhancement mechanism solely focuses on the magnitude of enhancement produced from the SERS substrate. However, when a biomarker or general molecule reside in close proximity to the SERS substrate surface, there is also a chemical enhancement mechanism that changes how the electromagnetic enhancement occurs.⁸² While the electromagnetic mechanism remains independent of the molecule near the substrate surface, the electromagnetic mechanism properties applies to the intrinsic properties of the molecule.⁸² The chemical enhancement mechanism is important for understanding the spectral fingerprint produced by an adsorbate on the SERS substrate. Contributions of the chemical enhancement come from a temporary charge transfer between the adsorbate and

the metal or strictly from the polarization of the adsorbate from the light source.⁸¹ The produced Raman bands in the spectral profile from the chemical enhancement depends upon the factors like: the orientation of the adsorbate on the substrate, the structure of the adsorbate, and excitation wavelength of the adsorbate.⁸³⁻⁸⁵ Both of these enhancement mechanisms are important for SERS enhancement of the Raman scattering effect. The most common way to show how well a SERS substrate enhances a signal is by calculating the SERS enhancement factor (EF). There are many ways to calculate the SERS EF depending upon the manner in which the SERS substrate is being used.⁸⁶ Generally, the SERS EF calculation takes the Raman signal intensity of an analyte at one Raman band and compares it to the SERS signal intensity when the analyte is near the SERS substrate. Taking these two intensities and factoring in the number of analytes present in each measurement can give an analytical enhancement factor.⁸⁶ The analyte being used for these measurements is determined by the designed system the SERS substrate will in. This requires a conceptual understanding of direct versus indirect SERS-based detection.

When performing SERS-based detection there are two main methods of acquiring a spectral signature from an analyte: direct and indirect detection. Direct detection indicates that the analyte or biomarker of interest is in close proximity to the SERS substrate and produces the fingerprint spectra; enabling direct quantification of the biomarker.^{79, 87-89} Xu *et al.* used iodine-modified silver nanoparticles for direct SERS detection of DNA sequences with varying composition down to 3.5 μM .⁹⁰ The other method, indirect detection, functions through the use of a molecular moiety acting as a Raman tag to produce the fingerprint profile rather than the biomarker.⁹¹⁻⁹⁴ This method requires

adsorption, binding or embedding of the Raman tag onto the SERS substrate surface to relay the signal output. Gracie *et al.* used Raman tags bound to nucleic acid sequences for the multiplexed detection of three bacterial meningitis pathogens (down to picomolar region) using SERS.⁴⁵ Indirect detection is useful for developing SERS substrates with the ability to bind to the biomarker for quantification. Since the electromagnetic mechanism drives a majority of the SERS enhancement of the biomarker or Raman tag, it is important to study the design of SERS substrates used in a biosensing system.

The SERS performance is mainly determined by the plasmonic metal substrate, which is commonly referred to as the SERS substrate. The composition, size and shape all play a role in how the surface plasmons will act; thus, also impacting how intense the provided signal amplification is from SERS. The composition of the plasmonic metal plays an important role in how the laser light will interact with the sample. The best choices for plasmonic metals are ones that display a low damping rate and a high frequency of onset for interband transitions.⁹⁵ Silver displays one of the highest interband transition frequency out of plasmonic metals like gold, copper and aluminum; which allows it to function in a SERS system across the visible and near-infrared regions. However, silver can easily be oxidized which can change the optical properties of the system if the substrate is not properly designed. Gold is a beneficial choice for biosensing applications due to the biocompatibility and lack of oxidation in comparison to silver.⁹⁶⁻⁹⁷ Gold does have a higher damping rate than silver which can cause a lower Raman scattering intensity.⁹⁵ Both of these plasmonic metals are great choices for SERS detection in the visible or near-infrared regions.⁹⁸

The size of the SERS substrate is also important to the functionality of it in a system. As previously mentioned, size can change the plasmon resonance effect and how a substrate will function in a biosensing system. Surface plasmon resonance can negatively impact an assay due to the bulk effect compared to LSPR which can overcome this issue. This difference is in large part why the focus of SERS and biosensing applications relies on LSPR. When biomarkers are being targeted in a complex matrix as previously discussed, the plasmonic field produces the Raman scattering effect through an energy change. A larger plasmonic field employed by a system creates a bulk effect which can lead to quantitative and qualitative issues such as poor limits of detection, poor spectral resolution, and extra peak signals that do not represent the biomarker. Which is why it is important to use nanoparticles to provide the LSPR in biosensing systems for disease detection. Not only can the size of the plasmonic metals impact the LSPR, but the shape can as well.

Spherical nanoparticles are useful in biosensor development and can induce a LSPR. However, the magnitude of the LSPR for spherical nanoparticles in comparison to anisotropic shapes can be minute. Common nanoparticles used in biosensing with complex features includes nanorods and nanostars. These shapes can produce more areas on the nanoparticles with an amplified LSPR; these areas are called SERS hotspots. Hotspots contain a higher density of conduction band electrons from the nanoparticle which helps when the light-plasmonic metal interaction occurs. Choosing which anisotropic nanoparticle to use in a SERS-biosensor is based on the synthesis methods, functional use, and SERS signal enhancement.

1.6. Anisotropic Nanoparticle Characteristics and Synthesis

Obtaining hotspots for SERS is important in biosensing applications. Generating plasmonic hotspots allows for the ability to concentrate the electromagnetic field to a confined area around the surface of the plasmonic substrate.⁹⁹ Doing this increases the Raman scattering effect which can increase the sensitivity and produce lower limits of detection for biosensors. So it is necessary to synthesize anisotropic nanoparticle shapes when developing a biosensor to create more hotspots. With the work of many researchers, synthesizing complex shapes like nanostars, nanorods, and other anisotropic particles has been simplified from previously challenging methods and used for biosensing applications.^{27, 76, 100-107} Anisotropic nanoparticles are capable of creating multiple hotspots because of the sharp facets formed like edges and branches. The added benefit of anisotropic nanoparticles is the ability to tailor the LSPR through synthesis changes so the hotspots created are optimized for the biosensor.¹⁰⁸ Of these commonly used shapes and many others that have been designed, nanostars tend to obtain the highest SERS EF or show the best analytical sensitivity.^{75, 78, 103, 109} The SERS EF looks at how well the nanoparticles can amplify the signal intensity of the biomarker or tag being used to produce the signal. Nanostars tend to produce the highest signal depending upon branch density, tip length and tip width.¹⁰⁸ These three characteristics of nanostars are very sensitive to the reaction conditions used during the synthesis.¹¹⁰ This sensitivity is beneficial for researchers as it allows for tuning of the nanostars; which is another reason they are being used more frequently in SERS-based detection. Tip length and width are the two most important characteristics to consider when producing nanostars.¹¹⁰ The sharper the produced branches, the higher intensity of the LSPR from those

hotspots.¹¹¹ In order to synthesize nanostars that optimize the designed biosensor, the different synthetic approaches are necessary to consider.

For nanostar synthesis there are two main methods: seed mediated growth^{106, 110, 112} and one-step procedures.^{105, 113-114} Seed mediated growth methods requires the synthesis of spherical nanoparticles¹¹⁵⁻¹¹⁶ to act as the core for the nanostar. Then the production of branches through the addition of the plasmonic metal of interest and reducing agents to the already synthesized core. One-pot method is the complete formation of the nanostars all in one reaction. Both methods can be useful in producing nanostars with optical properties that can match the needs of the system being developed. No matter which method is preferred, it is important to develop methods that remove the need for surfactants. The use of a surfactant can cause complications depending upon how the nanostars applied in the biosensor. In some cases, nanostars have been used in-vivo where having a surfactant toxic to living organism and interfere with the biosensor. Another downfall for using surfactants in synthesis is the growing demand to create green synthesis methods to help with the environment. There are very good methods published by researchers that show a high tunability of the nanostar morphology and are surfactant free. Employing surfactant-free, seed mediated growth nanostars is the method used throughout this thesis project.

Another well-developed nanoparticle design in biosensors is the use of core-shell and bimetallic nanoparticles.¹¹⁷⁻¹²² Synthesizing core-shell particles can lead to vast capabilities of how the nanoparticles can be used. They can be designed to ensure the entrapment of the biomarker or a Raman tag. Some core-shell nanoparticles are designed to be plasmonic and magnetic to remove procedural steps and simplify the assay¹²³. By

applying a gold coating to magnetic nanoparticles, researchers can use these without the worry of toxicity to cells because of the high biocompatibility of gold within the body. Core-shell nanoparticles are predominantly being used in diagnostic assays like the ones used in this thesis. Not only can a core-shell nanoparticle be synthesized containing one plasmonic metal, i.e. gold shell around gold nanostars, but two metals can be used to create a bimetallic nanoparticle substrate. The use of bimetallic substrates in SERS-based detection can lead to higher signal amplification and the use of the LSPR from both of the metals used.¹¹⁸⁻¹¹⁹ In the case of a gold core with a silver shell, the LSPR of the overall particle will shift from the original gold core LSPR. This can also be tuned by whether or not the entire core is coated and the thickness of the coating. However, with advantages there are always some disadvantages which could cause issues with the detection method. An outer coating of silver is more susceptible to oxidation which can ultimately lead to the degradation of the coating or the entire nanoparticles, creating a shorter shelf life than a gold coating layer. Another issue for some developed assays would be the toxicity of silver on biological materials in comparison to gold which is highly biocompatible. An important part of synthesizing any SERS substrate for biosensing applications is understanding the optical properties through characterization. One characterization method which is beneficial for finding out the optical properties is dark-field scattering (DFS) microscopy technique paired with hyperspectral imaging capabilities.

1.7. Nanoparticles Characterization using Dark-Field Scattering (DFS) Technique with Hyperspectral Imaging

DFS microscopy and spectroscopy can be used to characterize optical properties of nanomaterials in optical biosensor development.¹²⁴⁻¹²⁸ DFS works by adjusting the

distance of the condenser in a microscope so that the light source passes directly through the sample itself and not the entire background. This produces the dark field image so all light being received by the detector comes from the scattering of the nanoparticles or in some cases the biomarker being targeted. The hyperspectral imaging system produces a three-dimensional data cube that contains spectral information for each pixel of the dark-field image (Figure 6). The benefit of a DFS technique with the added hyperspectral imaging system is the determination of the max wavelength of scattering for the nanoparticles; thus, also providing the wavelength at which the LSPR will have the greatest magnitude. Knowing this information is critical for optimizing any diagnostic biosensor. By understanding the LSPR wavelength, other parameters for the assay can be manipulated like laser excitation choice or nanoparticle synthesis until a desired LSPR wavelength is achieved. DFS-hyperspectral imaging not only has the capabilities to detect the LSPR of the particles as a whole but can provide single particle measurements; which can provide better quantitative specificity on how the entire sample population of the nanoparticles are behaving in comparison to a technique like ultraviolet-visible spectroscopy.

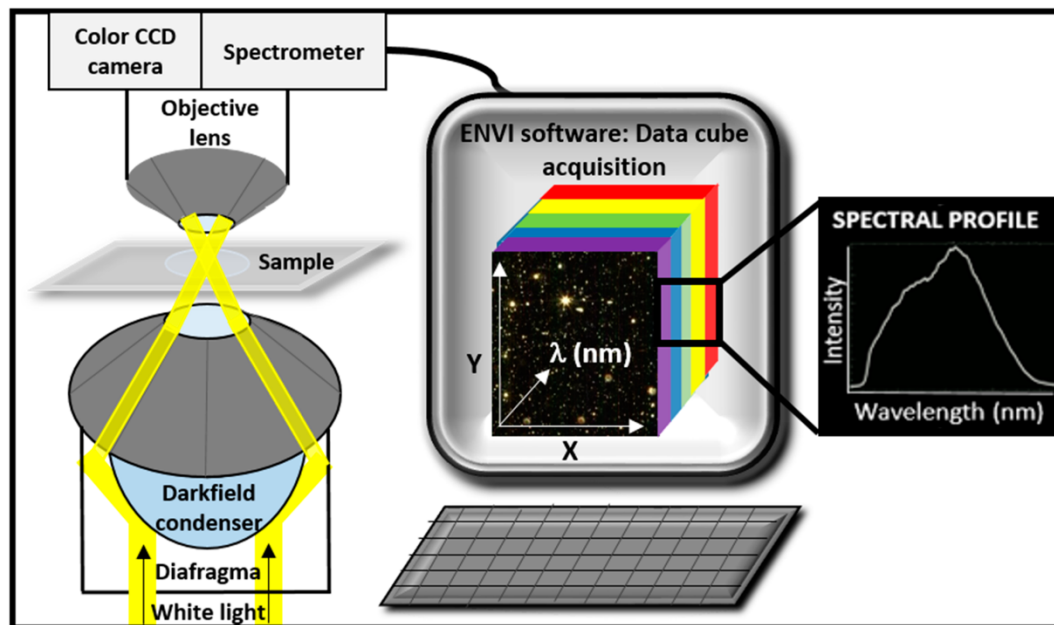


Figure 6: Schematic diagram for a DFS-hyperspectral imaging acquisition set up. Figure obtained from Zamora-Perez *et al.*¹²⁶

1.8. Thesis Overview

In this thesis we investigated the development of a SERS-based biosensor for asymptomatic detection of a malaria nucleic acid biomarker (Pfs25-mRNA). We focused on two specific aims for the assay development: (i) SERS substrate development and (ii) functional interface development. For the purpose of this thesis, the focus was on synthesizing and using silver-coated gold nanostars (Ag@AuNS). The advantages of using Ag@AuNS is the higher enhancement due to the bimetallic nature, the properties of a nanostar core in comparison to a spherical core, and the capabilities of trapping a Raman tag (Rose Bengal dye) for indirect SERS detection. Knowing that silver can oxidize over time, gold-coated silver nanostars (Au@AgNS) were synthesized to combat this issue while maintaining the bimetallic nature. At the point of this thesis, there have been no reports of an Au@AgNS substrate being developed or used in a biosensing assay.

The functional interface development focused on utilizing a sandwich hybridization event to trap the synthetic nucleic acid biomarker and produce an indirect signal response with the Raman tag embedded in the bimetallic substrate (reporter probe). Simple separation of the target from the buffer matrix in the initial development phases was completed using a magnetic bead (capture probe) that binds to the Pfs25-mRNA biomarker. To ensure the designed system probes would work specifically for Pfs25-mRNA biomarker and could work for other systems, a 18s-rRNA system was designed and used for comparison. After the development and optimization of the Pfs25-mRNA system in buffer, the synthetic target was used to spike blood lysate for determining the feasibility of the assay in blood. Experimental details are provided along with the results of the experiments and a discussion as to how this assay functions for the possibility of use at the point-of-care. Along with the work completed for the SERS-based assay development, this thesis includes a review paper published (Appendix A) on the topic of SERS detection of infectious diseases after completing an intensive literature survey for this thesis project⁷⁹.

CHAPTER 2: MATERIALS AND METHODS

2.1. Materials

Outlined here are all the materials and reagents used throughout this thesis work. Similar reagents were used in the SERS substrate synthesis of AuNP, AuNS, and AgNS. SERS substrate synthesis reagents gold (III) chloride trihydrate, gold (III) chloride solution, hydrochloric acid, sodium hydroxide, hydroxylamine, ammonium hydroxide, L-ascorbic acid, silver nitrate, trisodium citrate dihydrate, Rose Bengal Dye (95%), 4-mercaptobenzoic acid (4-MBA), Crystal Violet Lactone (CVL), chitosan (medium MW), hexadecyltrimethylammonium bromide (CTAB), and O-2-(3-Mercaptopropionylamino)ethyl-O'-methylpolyethylene glycol (PEG, MW: 5000) were purchased and obtained from Sigma-Aldrich. A VWR spin bar and hot/stir plate were used during the syntheses; reaction containers included Erlenmeyer flasks and scintillation vials.

Some of the reagents from the SERS substrate syntheses are used for the reporter and capture probes in the functional interface. Other reagents not yet mentioned for the probes include tris(2-carboxyethyl)phosphine hydrochloride (Thermo Fisher Scientific), tris(hydroxymethyl)aminomethane-diaminoethanetetraacetic acid (TE, Sigma Aldrich), synthetic capture/reporter sequences (Integrated DNA Technologies), phosphate buffered saline (PBS, Thermo Fisher Scientific), tween20 (TW20, Thermo Fisher Scientific), Dynabeads M-270 (magnetic beads, Thermo Fisher Scientific), dimethyl sulfoxide (DMSO, Sigma Aldrich), Dibenzocyclooctyne-N-hydroxysuccinimidyl ester (DBCO-NHS, Santa Cruz Biotechnology), and Ultrapure DNase/RNase free water (Thermo Fisher Scientific). For the hybridization reactions saline-sodium citrate (SSC, Promega),

sodium dodecyl sulfate (SDS, Sigma Aldrich), and bovine serum albumin (BSA, Sigma Aldrich) were purchased. DynaMag™-2 Magnet (Thermo Fisher Scientific) was purchased for magnetic separation of the hybridization complexes. Materials include 2-mL microcentrifuge tubes and VWR pipettes. General instruments used for these procedures include a Horiba XploRA ONE™ Raman microscope, Cytoviva® Hyperspectral Imaging system, Thermo Scientific™ Sorvall™ Legend™ X1 centrifuge and micro 21R microcentrifuge, Thermo Scientific™ thermal mixer, Branson 2800 ultrasonic cleaner, vortex-genie 2 from Scientific Industries, and a VWR-164AC balance.

2.2. Spherical Gold Nanoparticle Synthesis

AuNP seeds of 12 nm in diameter were synthesized following the Turkevich method¹¹⁶ with some modifications. 1 mL of a 10 mg/mL solution of HAuCl₄ was diluted in 194 mL of MilliQ water. The reaction solution was heated to a boil (150 °C, VWR plate setting) in an Erlenmeyer flask containing a stir bar and placed under stirring conditions. Stirring conditions varied depending upon formation of a vortex so that it did not make contact with stir bar. After five minutes, 5.0 mL of 1% citric acid trisodium salt was added and the flask was covered with foil under the same conditions. After 30 minutes of boiling, a color change of the solution to red occurred indicating the formation of AuNP; the heating of the solution was carried out for another 30 minutes. The solution was cooled to room temperature under the same stirring speed. The resultant colloidal solution was then purified by centrifugation at 10,000 g for 60 minutes. The resultant pellet was resuspended in 20 mL of MilliQ water and kept in the refrigerator for long-term use.

2.3. Gold Nanostar Synthesis, Functionalization, and Coating with Silver

Synthesis of AuNS was performed using Indrasekara *et al.* procedure with some modifications.¹²⁹ To start the synthesis, 492 μL of 5.08 mM HAuCl_4 solution was added to 10 mL of MilliQ water in a plastic scintillation vial with a stir bar and placed under stirring conditions at room temperature for 10 seconds. Then 20 μL of 1N HCl was added and allowed to mix for 10 seconds. 900 μL of 12 nm AuNP seeds ($A_{519} = 0.449$ from Nanodrop) was added then added to the reaction mixture and allowed to mix for another 10 seconds. Volume of the seeds were adjusted according to absorbance of the seeds to ensure the same number of spherical nanoparticles were added during each batch synthesis. 34 μL of 3 mM silver nitrate was added to the resultant solution as a shaping agent for branch formation and allowed to mix for 5 seconds followed by the addition of 100 μL of 100 mM L-ascorbic acid. The time between steps is crucial for batch-to-batch consistency when synthesizing AuNS and was determined in literature.¹²⁹ Within seconds of the L-ascorbic acid addition, the solution turned bluish green and was kept under stirring conditions for another minute. For long term stability, the resultant gold nanostars were functionalized with PEG. The nanostars were incubated with 40 μL of 1 mg/mL PEG for 10 minutes after the synthesis. If AuNS were immediately used, no PEG addition was necessary. After the synthesis of the nanostars, purification was performed by centrifuging the AuNS at 3,000 g for 10 minutes. The resultant pellet was then resuspended in 1.5 mL of MilliQ water and stored in the refrigerator.

The surface functionalization of these AuNS with a Raman tag, Rose Bengal dye, was performed. The functionalization was designed for 60% surface saturation of the tag on the surface of the nanostars. Surface area of nanostars was calculated by using tip-to-tip diameter and assuming the AuNS were spherical shape since no nanostar surface area

equation is currently available. The Raman tag was added to 1 mL of AuNS and mixed for 3 hours at 350 rpm on the thermal shaker with foil covering the sample. To this 1 mL sample of Raman tagged AuNS, the silver coating procedure was implemented. The silver coating method for the AuNS samples with the Rose Bengal Raman tag used 4 μL of 0.05 M silver nitrate and 4 μL of 0.1 M ascorbic acid added to the 1 mL Raman tagged AuNS sample. Immediately following that, 2 μL of 28.5% ammonium hydroxide solution was added to the microcentrifuge tube. The sample was promptly placed in the thermal shaker and mixed for 5 minutes at 1000 rpm. Centrifugation at 2,000 g for 10 minutes was next, followed by the supernatant being removed and pellet resuspended in 1 mL of MilliQ water; producing a stock solution of Ag@AuNS.

2.4. Silver Nanostar Synthesis, Functionalization, and Coating with Gold

A two-step reduction method, obtained from Garcia-Leis *et al.*⁷⁶, was used for the synthesis of AgNS. In order to optimize synthesis conditions, varying concentrations of certain reagents were originally used in the following protocol however the described protocol below was determined as the best synthesis method for AgNS formation. A plastic scintillation vial was rinsed with hot MilliQ water prior to the synthesis. To the scintillation vial, 500 μL of 0.13 M hydroxylamine and 500 μL of 0.05 M sodium hydroxide were added along with a stir bar. The VWR stir plate was set to just above 600 rpm for stirring conditions. While mixing, 9 mL of 1.1×10^{-4} M silver nitrate was added dropwise at a rate of 50 $\mu\text{L}/\text{sec}$. Five minutes after all of the silver nitrate was added, 100 μL of 0.03 M trisodium citrate was added to the solution. Synthesis was left to mix for 48 hours at room temperature with a lid covering the vial. Due to the formation of a solid precipitate, the sample was sonicated for 2 minutes and then transferred to

microcentrifuge tubes for centrifugation at 3,500 g for 10 minutes. The resulting pellet was resuspended in 1 mL of MilliQ water then PEG-functionalized by adding 40 μ L of 1 mg/mL of PEG for 10 minutes under shaking conditions. These PEG-coated AgNS are centrifuged for a second time using the same conditions. The final pellet was resuspended in 1 mL of MilliQ water and placed in the refrigerator.

Surface functionalization of the AgNS with Rose Bengal dye followed the same procedure as the AuNS functionalization found in the previous section. Multiple gold coating attempts (CTAB and chitosan) were performed to synthesize Au@AgNS substrates and are described below.

For CTAB coating method, 8 mL of 50 mM CTAB was added to a 20 mL scintillation vial with a small stir bar. 200 μ L of Rose Bengal adsorbed AgNS solution were added to the vial; sample mixed at a rate of 400 rpm on stir plate. After turning stir plate on, 400 μ L of 0.1 M ascorbic acid was added to solution; sample mixed for 20-30 seconds. Following ascorbic acid addition, different volumes of 0.1 M gold (III) chloride solution were added for different trials. Sample mixed for 5 minutes and then centrifuged at 3,000 g for 10 minutes. The resulting substrate pellet was kept and resuspended in 1 mL of MilliQ water.

For the chitosan method, chitosan stock solution prepped by creating a 1 mg/mL solution in 4% (v/v) 1 N hydrochloric acid at 40°C. Stir bar added to chitosan solution and mixed at 200 rpm (40°C) until ready to use. The Rose Bengal adsorbed AgNS solution was placed in a 20 mL scintillation vial with a small stir bar. 3 mL of MilliQ water were added then 1 mL of the 1 mg/mL chitosan solution. Sample mixed for 5 minutes at 375 rpm (40°C). While mixing, various amounts of 0.1 M gold solution were

added for different trials. After 10 seconds 400 μL of 0.1 M ascorbic acid was added to vial and allowed to stir for 18 hours at 375 rpm (40°C). Following the 18-hour incubation, the sample was sonicated for two minutes and then centrifuged at 3000 g for 10 minutes. Substrate pellet was kept and resuspended in 1 mL of MilliQ water.

2.5. Reporter and Capture Probe Functionalization

The method used for the functionalization of the reporter probes was first performed by Vo-Dinh *et al*⁷⁷. The procedure required 5 μL of 100 mM TCEP in TE 1X which was added to 50 μL of 100 μM thiolated synthetic mRNA reporter probes. The volume of synthetic mRNA sequences used was varied between reporter probe stock solutions based upon the concentration of substrates being functionalized (60% surface saturation). The mixture was incubated for 1 hour at room temperature and 700 rpm on the thermal shaker before being added to 1 mL of Raman tagged SERS substrate. After the adding the sequences to the SERS substrate was incubated for 1 hour at 700 rpm in the thermal shaker. Then 10 μL of citrate-HCl buffer (300 mM trisodium citrate, pH adjusted to 3.1 using 1 M HCl) was added to promote loading of synthetic mRNA onto the SERS substrate. One hour later the mixture was centrifuged at 6,500 rpm for 10 minutes. Fifty microliters of 1 mM PEG were added to the pellet followed by addition of 1 mL PBS 1X with 0.01% TW20 and sonication until mixed (2 minutes). The solution was centrifuged at 6,500 rpm for 5 minutes. The pellet was washed once with TE 1X followed by centrifuging at 6,500 rpm for 5 minutes. Pellet resuspended in TE 1X and stored in refrigerator prior to use.

The capture probe method is also originally from Vo-Dinh *et al.*⁷⁷, which involves magnetic beads being removed from refrigerator approximately 15 minutes before use.

Twenty-two μL of stock Dynabeads M-270 were washed three times with 1.5 mL DMSO. Then 1.5 milligrams of a linker molecule, DBCO-NHS, was dissolved in 10 mL of 3.73×10^{-4} M DMSO. 13.4 μL of DBCO-NHS solution was mixed with the magnetic beads in 500 μL of Ultrapure (DNAse and RNAse free) water. The mixture was wrapped with aluminum foil and placed on shaker for 1 hour. After 1 hour, the magnetic bead-linker complexes were washed three times with 1.5 mL Ultrapure water using magnetic separation. The pellet was resuspended in 500 μL of Ultrapure water. 75 μL of the 100 μM synthetic capture probe sequence was placed in 500 μL of coupling buffer (PBS pH=7.4, 1X, Gibco). The magnetic bead-linker complexes were mixed with the azide-containing sequences, wrapped in foil, and placed on the thermal mixer for 1 hour at room temperature. Capture probe solution was placed in the refrigerator for 18 hours. The supernatant was removed, and the pellet was resuspended in 1 mL of coupling buffer. Capture probes transferred to a new 1.5 mL microcentrifuge tube and washed three times with 1 mL increments of coupling buffer. Final capture probe pellet resuspended in 1 mL of coupling buffer to create capture probe stock solution.

For surface passivation of free amine groups for the capture probe, supernatant from the stock solution removed and washed twice with 1 mL of passivation buffer (150 mM PBS with 150 mM sodium chloride, pH = 7.4). Supernatant removed after last washing step. To the pellet, 1 mL of 22 mM of sulfo-NHS-acetate (in passivation buffer) was added. Solution mixed for one hour at 700 rpm with foil covering the solution. Supernatant removed and capture probes washed three times with 1.5 mL of passivation buffer. Microcentrifuge tube switched between the second and third washing step. After the final passivation buffer washing step, with supernatant removed, pellet resuspended

in 1 mL of TE (1X) buffer. Supernatant removed for final time and pellet resuspended in 1 mL TE (1X) to create passivated capture probe stock solution.

2.6. Pfs25-mRNA Sandwich Hybridization Event: Synthetic Target in Buffer

Following the Vo-Dinh *et al.* article⁷⁷ with some modifications, the hybridization reaction involving a synthetic target sequence was completed. Varying volumes of the 100 μ M synthetic target mRNA was added to a hybridization buffer (SSC 5X, BSA 1%, and SDS 0.02%) in a microcentrifuge tube. A probe molar ratio of 784765 reporter probes/capture probe were added to the target sequence in buffer; total volume of hybridization reactions was kept consistent at 20 μ L. Hybridization samples were incubated for 3 hours at 40°C and 550 rpm on a thermal mixer with foil covering reactions. The hybridization complexes were washed three times with hybridization buffer, once with Ultrapure DNase/RNase free water and concentrated using magnetic separation. Once final supernatant was removed, 1 μ L of the Ultrapure water was added to complexes and solution was removed from microcentrifuge tube via pipetting. The complexes were drop casted onto a clean silicon wafer resting on the magnet. Complexes were pipetted up and down to concentrate them into one uniform pellet. Samples were then ready to be analyzed using Raman microscope.

2.7. Lysis of Whole Blood and Hybridization Reactions in Blood

Whole blood samples (anticoagulant heparin sodium) were obtained from Dr. Kausik Chakrabarti's lab in the Biology Department at UNC Charlotte and Zen-Bio, Inc located at Research Triangle Park in Raleigh, North Carolina. A QuantiGene® sample processing kit was obtained from Thermo Fisher Scientific for lysing whole blood samples. For lysing the whole blood, the QuantiGene® procedure was followed with some variations;

32 μL of Lysis Mixture solution pre-warmed at 40 °C for 30 minutes while shaking at 550 rpm on the Thermo Scientific™ thermal mixer. After 30 minutes of warming 50 μL of ultrapure RNase free water, 2 μL of proteinase K, and 12 μL of whole blood were added to the warmed Lysis Mixture. Immediately following, the new working solution was vortexed for 30 – 60 seconds and then incubated at 60 °C for one hour at a shaking rate of 550 rpm. Lysed blood allowed to cool for 10 minutes and then was ready to use for hybridization reactions. Volumes for lysis procedure were scaled up based on volume of lysate needed for hybridization reactions.

Hybridization reactions in blood lysate followed the same procedure as in buffer but with the use of the blood lysate as a replacement for the hybridization buffer. Varying volumes of the 100 μM synthetic target mRNA was added to fresh blood lysate in a microcentrifuge tube. A probe molar ratio of 784765 reporter probes/capture probe were added to the target sequence in buffer. Hybridization samples were incubated for 3 hours at 40°C and 550 rpm on a thermal mixer with foil covering reactions. The hybridization complexes were washed three times with hybridization buffer, once with Ultrapure DNase/RNase free water and concentrated using magnetic separation. Once final supernatant was removed, 1 μL of the Ultrapure water was added to complexes and solution was removed from microcentrifuge tube via pipetting. The complexes were drop casted onto a clean silicon wafer resting on the magnet. Complexes were pipetted up and down to concentrate them into one uniform pellet. Samples were then ready to be analyzed using Raman microscope.

2.8. SERS measurements using Horiba XploRA ONE™ Raman microscope

A clean silicon wafer holding the hybridized complexes was placed on a glass microscope slide which was added to the microscope stage for analysis. List of parameters for sandwich hybridization measurements includes: 10x objective lens, 638 nm laser operating on 25% power (~7 mW), grating 1200 (750 nm), hole: 500 μm , slit: 200 μm , 1 second acquisition time, 10 accumulations, and spectral range 700 – 2400 cm^{-1} . For hybridized complexes, five measurements were taken per replicate and ten measurements were taken for one sample of synthesized SERS substrate to determine the SERS EF. Any measurements taken with the 785 nm laser were also performed at 25% operating power (~11.7 mW) and other parameters remained the same.

2.9. DFS-Hyperspectral Imaging Acquisition using CytoViva® Hyperspectral Microscope

The white light source given by CytoViva® was always set to deliver 100% of the light to the sample. Oil immersion technique was used, for acquiring every image with spectral information, with the 60x oil immersion objective from Olympus. Conditions such as exposure time, size of scan, and size of the iris opening for the objective were optimized based on providing particles that produced between 1,000 – 16,200 counts while observing the live feed of the detector. When completing scans for a comparison between different samples, all of the relevant parameters were kept constant.

2.10. Data and Statistical Analysis

Multiple programs were used to analyze the data acquired in this thesis for the SERS substrate characterization and hybridization reactions. For substrate characterization, ultraviolet-visible spectroscopy (UV-VIS) figures and data were processed in Igor Pro 8 software. Transmission electron microscopy (TEM) images were analyzed with ImageJ

in order to determine average size of nanoparticles for each synthesis step. For DFS-hyperspectral imaging, the initial analysis of the images was conducted in ENVI software provided by CytoViva®. The processed data cubes for the substrates were sent through a MATLAB® code in order to retrieve the sample population's spectral information. Histograms were made using this code for information such as maximum wavelength of scattering, maximum intensity of scattering at each wavelength and the full width at half maximum. A separate MATLAB® code was used to plot the scattering versus wavelength spectrum of a singular particle. SERS spectra were averaged, baseline subtracted and initially analyzed for peak intensities in LabSpec6 software provided by HORIBA. All SERS spectra and calibration curves obtained for SERS measurements were processed in Igor Pro 8.

CHAPTER 3: RESULTS AND DISCUSSION

3.1. SERS Substrate Development: Silver-Coated Gold Nanostars (Ag@AuNS)

Optical and chemical properties of the nanoparticles are critical to achieve required SERS sensitivity in our assay. Here in, we synthesized and characterized Silver-Coated Gold Nanostars (Ag@AuNS) as the SERS substrate. By adding a silver coating to the gold nanostar core, the Raman tag is embedded between the substrate layers and the bimetallic nature can serve to further enhance the produced SERS signal.¹¹⁸⁻¹¹⁹ Fan *et al.* demonstrated the ability of bimetallic substrates to achieve the highest SERS signal enhancement by comparing gold-silver metal alloys of varying composition with four different Raman tags.¹¹⁸ The gold nanostar (AuNS) core of the Ag@AuNS was synthesized using a seed mediated approach with two steps; first for the formation of 12 nm spherical gold nanoparticles (Appendix B) and the second step of reducing gold onto the spherical core to create branch formation on the surface. Following the AuNS synthesis, was adsorbing the Raman tag molecules, Rose Bengal dye, to the AuNS surface and the addition of a silver coating to embed the Raman tag in the SERS substrate. Applying the silver coating was performed using a gradient of silver nitrate concentrations (50 mM, 25 mM and 10 mM) to understand how the coating can impact the optical properties of the substrate. Three different coatings were applied to the Raman tag adsorbed AuNS; characterization of the substrates was performed using UV-VIS and TEM (Appendix B). The UV-VIS results displayed the 50 mM silver nitrate addition having a spectral profile with a strong peak and improved batch homogeneity of the formed particles in comparison to the other silver nitrate additions; which is demonstrated by the peak width compared to the other samples. The TEM image for sample 50 mM

indicates that the silver was deposited on the AuNS because of the change in morphology and the dark coloration at the core of the observed particles. While all of the samples indicated some formation of the desired substrates, the 50 mM silver nitrate coating method for SERS substrate synthesis was employed for all future work.

TEM and UV-VIS characterization data for AuNS with the Ag@AuNS can be found below in Figure 7. The sizes of the particles were calculated using ImageJ: AuNS was $64.1 \text{ nm} \pm 9.6 \text{ nm}$ tip-to-tip diameter and the Ag@AuNS SERS substrate was $74 \text{ nm} \pm 8 \text{ nm}$. Although the TEM image displays AuNS branches that are partially coated, the increase in size between the AuNS and the substrate indicated the successful deposition of Ag on AuNS. The blue-shift from 671.5 nm to 546 nm displayed in the UV-VIS spectra from the coating of the AuNS also indicated that silver is present on the surface of the AuNS; as silver nanoparticles characteristically display an absorbance peak in the 400 – 600 nm portion of the visible region. In an article published by Vo-Dinh's group, they analyzed different silver coatings of gold nanostars and determined that substrates with the highest SERS enhancement stemmed from particles with a partial coating and exposed branch tips.¹³⁰ Ag@AuNS were also further characterized by dark-field scattering microscopy coupled with a hyperspectral imaging technique, to provide an in-depth analysis of the Ag@AuNS substrate scattering properties with single particle measurements for a larger sample population.

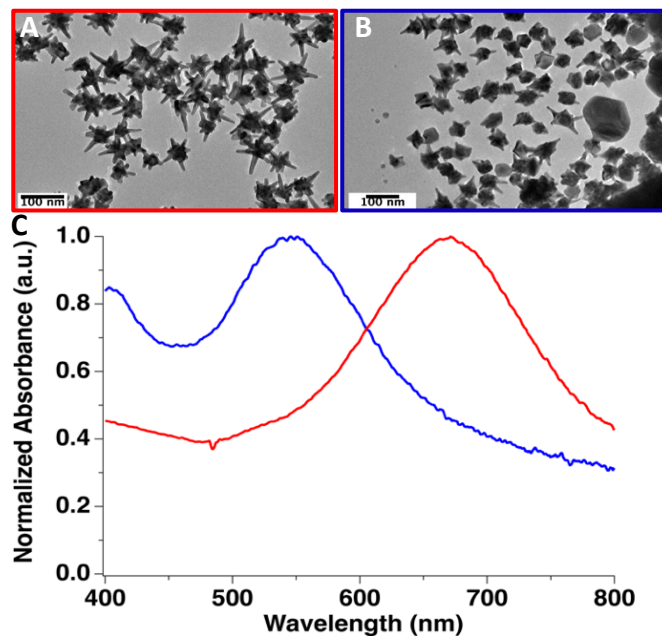


Figure 7. TEM images for AuNS (A) and the Ag@AuNS SERS Substrate (B). C) UV-VIS spectra with normalized absorbance for those nanoparticles as displayed by corresponding spectral color. Spectral shift in wavelength observed from AuNS max at 671.5 nm to Ag@AuNS max at 546 nm.

Dark-field scattering microscopy coupled with hyperspectral imaging was added for an improved characterization of the SERS substrate light scattering properties. Knowing this detail of how individual particles will scatter light is important for the substrate's functional ability in a scattering based detection system like SERS. Figure 8 displays a dark-field scattering image of a SERS substrate stock solution along with a representative individual particle scattering profile obtained from the hyperspectral imaging capabilities. These images with the hyperspectral information were processed through a MATLAB code to determine optical characteristics such as scattering wavelength, intensity of scattering, and the Full Width Half Max (FWHM) of each particle spectral profile. The most important characteristic to acknowledge is the maximum wavelength of scattering.

This information can be displayed as a histogram (Figure 8) to show how these particles can be implemented in a SERS system. With a λ -max in the region of 525 – 575 nm, this information can help determine parameters such as laser wavelength to use or what Raman reporter molecule could work best with the system moving forward.

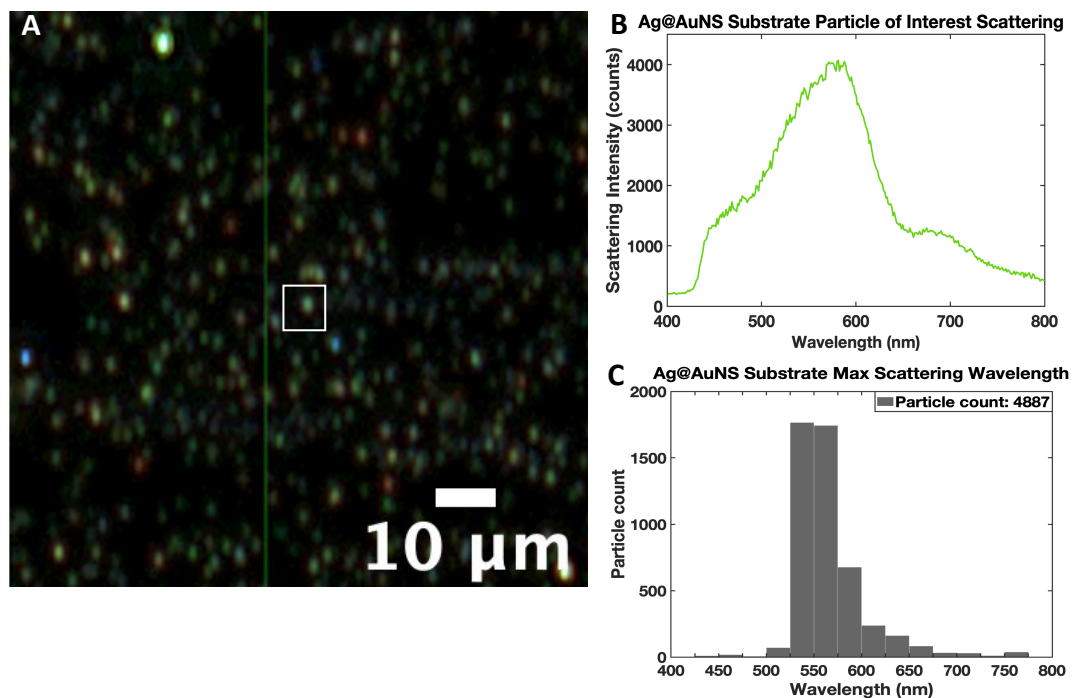


Figure 8. DFS image (A) of SERS substrates with a single particle max scattering spectrum (B) of the particle located in the white box and a cumulative histogram (C) of the whole sample's max wavelength of scattering, at 545 nm, with a total particle count of 4887. Image acquired using a 60x oil immersion objective with a full scan setting (696 x 696 pixels) and 500 millisecond exposure time.

In order to use this SERS substrate with SERS detection, Raman measurements of the Rose Bengal dye and SERS measurements of the substrate were required to observe the level of signal enhancement the substrate provides using this spectroscopic method. More information on the decision to incorporate Rose Bengal dye as the Raman tag can be found in Appendix B. Ten measurements were acquired for both a dried Rose Bengal

solution drop, and a dried SERS substrate drop using 638 nm laser excitation with a one second acquisition time and a 10x objective lens. More information on Raman tag selection of Rose Bengal can be found in the supporting information. The spectra were averaged, and baseline subtracted to remove background noise (Figure 9). A known formula for SERS analytical enhancement factor calculations⁸⁶ was used for processing the order of magnitude increase in the SERS signal compared to the Rose Bengal dye signal and can be seen in Figure 9. In this equation the variables " $I_{\text{SERS}}/I_{\text{Raman}}$ " are the intensity of the SERS signal at a single Raman shift value. Rose Bengal dye displays multiple strong Raman peaks that could be used for SERS analysis; however, only one peak was used for determining the presence of Rose Bengal. In this thesis the strong SERS peak at 1489.11 cm^{-1} , corresponding to asymmetric C=C ring stretching¹⁰⁰, was used and the intensity of the Raman signal at this peak for the enhancement factor calculation. The variable " $N_{\text{SERS}}/N_{\text{Raman}}$ " is the number of tag molecules present in the measurements for both the SERS substrate and Rose Bengal dye, respectively. This N-value for the SERS measurements was estimated through calculating the concentration of substrates present in the stock solution with Beer's Law and knowing the number of tag molecules that should be present per SERS substrate, based a 60% surface saturation calculation. This calculation does imply some assumptions, for instance all of the Rose Bengal molecules that were added during the synthesis were all adsorbed to the AuNS and not lost during washing steps. Another critical assumption is an equal dispersion of the substrates during the drying of the droplet, which can impact the overall signal intensity for the SERS measurements. The laser area does not completely cover the area of the dried drops and can result in varying intensities depending upon the location of the

measurements within the dried sample area. These assumptions indicate not all of the Raman tags are being measured which can impact the calculated enhancement factor value by lowering the overall magnitude enhancement when the calculation is performed assuming all tags are measured. However, the enhancement can still be observed through obtaining the Raman and SERS spectra. The SERS substrate has a calculated two order of magnitude enhancement when compared to Raman measurements for Rose Bengal. With the SERS substrate characterized and established as functional for the system, the functional interface could be developed for this SERS-based assay.

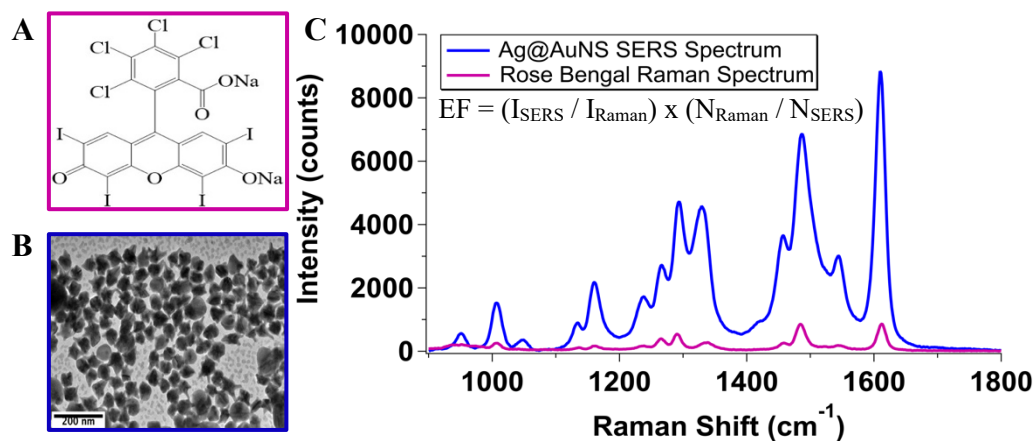


Figure 9. Comparison of Rose Bengal dye (A) versus SERS substrate (B) for determining the SERS enhancement factor. C) Spectral profiles for Raman and SERS measurements using 638 nm laser excitation with a 10x objective and one second acquisition time. The main peak used for calculations with the enhancement factor equation (inset) resides at 1489.11 cm⁻¹ and the overall signal enhancement was calculated to be a two order of magnitude increase.

3.2. Novel Substrate Development – Gold Coated Silver Nanostars (Au@AgNS)

Developing SERS substrates for potential biosensing applications requires careful consideration of composition, size and shape. While this thesis focuses on the use of an Ag@AuNS SERS substrate for assay development, we worked on developing a novel

Au@AgNS substrate. The purpose of switching the composition of the substrate is for concealing silver with gold to prevent oxidation of the outer surface; which could degrade the SERS substrate. Another improvement of developing the novel Au@AgNS substrate was that the bulk of the core-shell nanoparticle would be of silver composition to potentially increase the SERS enhancement factor in comparison to the Ag@AuNS.

Three different silver nanostars (AgNS) were synthesized in order to compare the LSPR and morphology. These trials differed by using various concentrations of silver nitrate and reducing agents; based on work performed by Garcia-Leis *et al.*⁷⁶ This two-step reduction method utilizes hydroxylamine for formation of the silver core while the trisodium citrate used in the reduction is for branch formation. All three of these methods obtained from Garcia-Leis *et al.*⁷⁶ used the same concentration of trisodium citrate (297 μM). Two methods (AgNS-31 and AgNS-71) required 2.98 mM of hydroxylamine while the third method (AgNS-51) required 6.44 mM hydroxylamine. For the concentration of silver nitrate, AgNS-31 and AgNS-51 methods called for 989 μM ; AgNS-71 only required 98 μM of silver nitrate. The UV-VIS and TEM of the AgNS trials can be seen below in Figure 10. The results of UV-VIS indicate only AgNS-31 and AgNS-51 formed a homogenous batch of nanoparticles based on the narrow absorbance peak. AgNS-31 had a max wavelength at 389.5 nm while AgNS-51 had a max wavelength of absorbance at 384.5 nm. TEM images were used to determine which AgNS synthesis was ideal for SERS substrate development based on nanostar morphology. AgNS-51 was chosen for the Au@AgNS substrate development out of the three synthesized samples due to the longer branch formation and homogenous morphology.

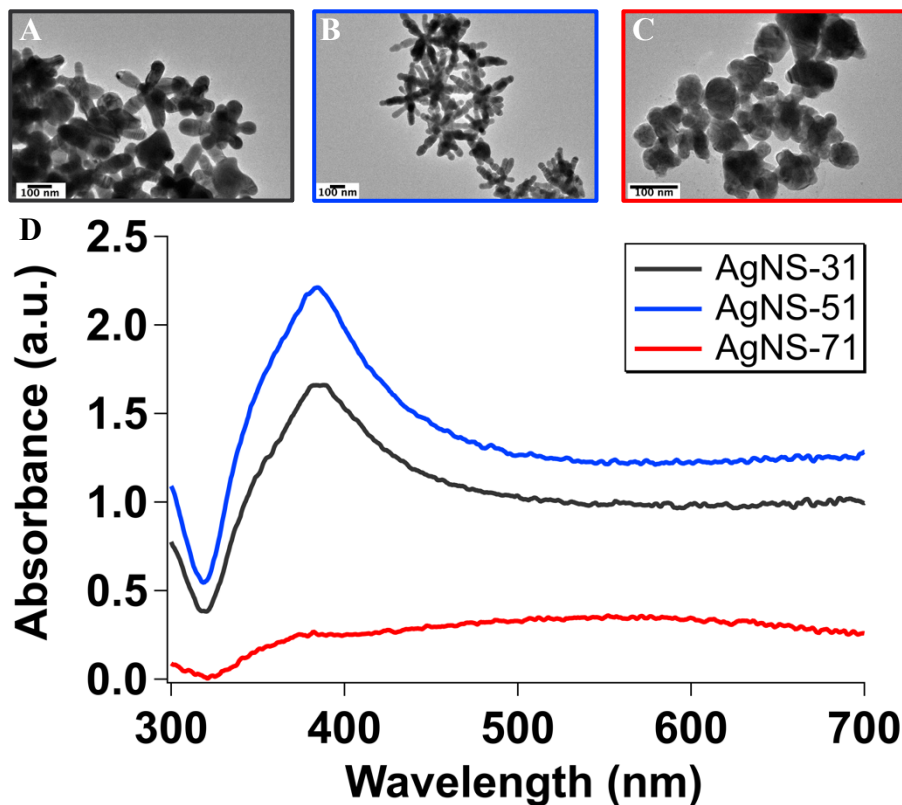


Figure 10. UV-VIS and TEM results for AgNS synthesis of three samples using various reagent additions. TEM images represent sample AgNS-31 (A), AgNS-51 (B) and AgNS-71 (C). D) UV-VIS of the synthesized AgNS.

After discovering the best AgNS synthesis parameters out of the three samples, next was the functionalization with the Rose Bengal Raman tag and gold coating. The adsorption of the Raman tag was performed in the same manner as the Ag@AuNS SERS substrate by saturating 60% of the nanostar surface. The challenge of developing this substrate became prominent in the gold coating. Following a similar reduction method as Ag@AuNS for the outer layer addition to the nanostar core, the gold did not deposit on the surface. In order to increase the chances of the gold to deposit onto the surface of the AgNS, two different approaches were considered: surfactant stabilization (CTAB) and employing a biopolymer (chitosan) for stabilization. Comparatively, using chitosan is

more advantageous due to its biocompatibility and environmentally friendly nature. Various trials were performed individually for both CTAB and chitosan in order to add a gold coating (Appendix C). Once the best methods for both coating types were determined, the two results were compared using UV-VIS and TEM (Figure 11). Both UV-VIS spectra display broad peaks over a large range of wavelengths (500 -850 nm). When examining the TEM images of the two samples, the chitosan method coating produced the best substrates based on the AgNS morphology remaining present. The CTAB method for coating reduces the branches from the AgNS down to a more spherical or popcorn-like morphology. Keeping the branch formation is important for inducing the localized hot spots as discussed earlier in this thesis. Since the UV-VIS spectrum for the chitosan sample is broad it is hard to tell how well gold is distributed across the nanostars. However, the shift in this broad peak from the AgNS max wavelength of 384.5 nm to this range of wavelengths (500 – 850 nm) is a good indicator that some gold is present.

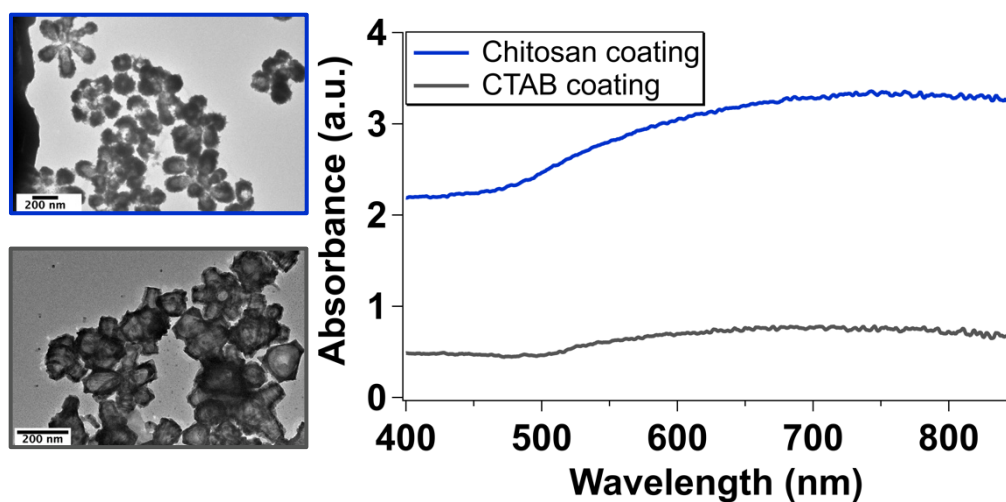


Figure 11. TEM and UV-VIS results for chitosan and CTAB coating methods for the addition of gold onto AgNS. TEM image border color correspond to the colors found in the UV-VIS. Scale bars for TEM images set to 500 nm.

In order to confirm the presence of gold on the surface of the chitosan coated Au@AgNS substrates, scanning electron microscopy (SEM) with energy-dispersive x-ray spectroscopy (EDS). Applying SEM-EDS can confirm gold was successfully deposited on the surface of the AgNS due to EDS acting as an elemental analysis technique. Results for the chitosan Au@AgNS substrate SEM-EDS analysis can be found below in Figure 12. EDS confirms the presence of gold (18.2%) on the AgNS (11.5%) with a 1.58 gold per silver ratio. Silicon makes up a majority of the elemental analysis (56.1%) due to the Au@AgNS sample residing on a silicon wafer. The high percent of carbon present (11.7%) is most likely from the chitosan addition to the coating method. This confirms the development of a novel plasmonic Au@AgNS substrate for potential use in SERS-based applications.

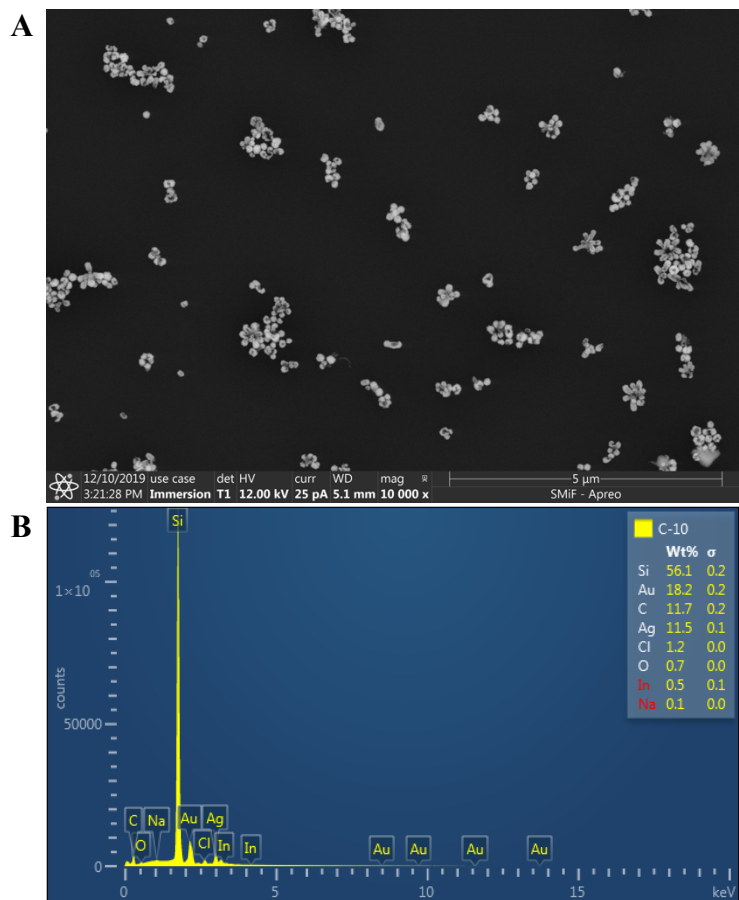


Figure 12. SEM-EDS analysis of Au@AgNS substrates using chitosan for stabilization of the gold coating. A) SEM image of the chitosan substrates on a silicon wafer. B) EDS analysis of the chitosan substrates displaying the presence of gold and silver.

3.3. Fabrication and Optimization of Pfs25-mRNA and 18s-rRNA Probes in the Functional Interface

Once the SERS substrate was synthesized and characterized, the reporter and capture probe functionalization reactions were the next step in designing the biosensor. The reporter probe and capture probe sequences used in the functionalization were designed to be partially complementary to the two individual systems target biomarkers, Pfs25-

mRNA and 18s-rRNA. This allows for both probes to bind to the biomarker of interest on opposite ends and form the desired hybridized complexes in the presence of the specific biomarker. The capture probe synthesis (Figure 13) was functionalized by conjugating amine terminated magnetic beads with azide- terminated synthetic nucleic acid sequence, using Cu-free click chemistry, with the aid of DBCO-NHS ester linker molecule. Click chemistry was chosen for conjugating the capture probe sequence to the magnetic bead over other conjugation methods because the reactions are spontaneous and proceed at room temperature. Thus, increasing the simplicity of the functional interface design for possible POC use. Developing the capture probe to include magnetic beads was also an important step in devising a protocol with simplified techniques. Using the magnetic beads allows for simple magnetic separation of the hybridized complexes without the need for extensive separation methods²⁰.

For the reporter probe, the synthetic nucleic acid sequence was designed with a thiol group present because of the known binding affinity of thiol groups towards metals such as gold (Figure 13). The loading of the reporter probe sequences onto the SERS substrate was promoted with the use of a citrate-HCl buffer (pH = 3.1). Once the loading step was completed, PEG-SH (MW: 5000) was used to provide an added stability for the reporter probe stock solution. Surface saturation of the synthetic sequences on the surface of the SERS substrates and magnetic beads was performed to achieve 60% saturation. The designs for the sequences used can be found in Table 1 below along with the melting temperature of the sequences.

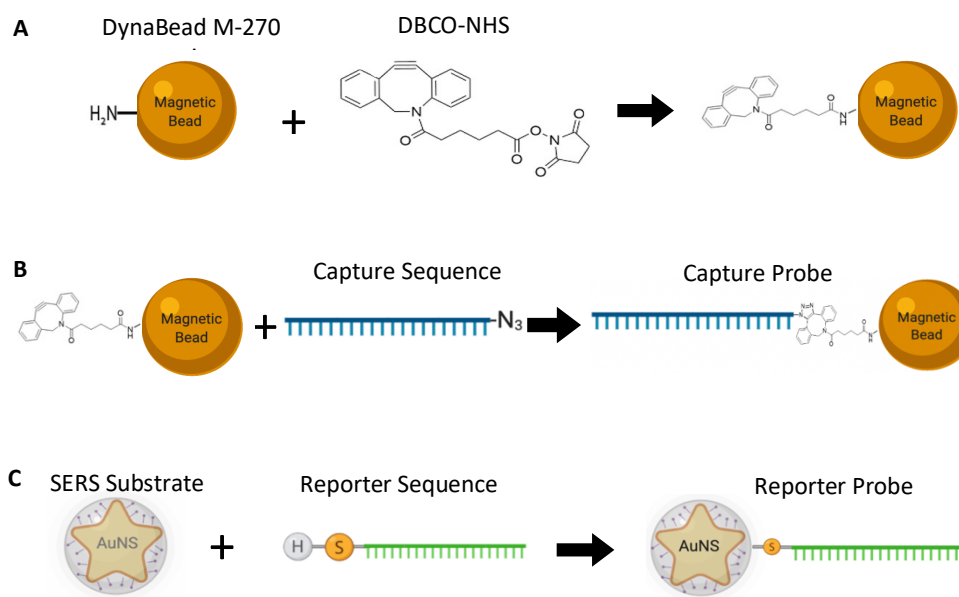


Figure 13. Schematic diagram of click chemistry reaction for capture probe functionalization: (A) represents the binding of the DBCO-NHS ester linker to the amine functionalized surface of the magnetic beads through a substitution reaction (B) displays the binding of the capture probe sequence azide functional group to the cyclooctyne triple bond present in the linker molecule. C) Reporter probe functionalization using a thiolated reporter sequence to bind to the SERS substrate surface.

Table 1. sequences for the Pfs25-mRNA and 18s-rRNA systems including the capture, reporter, and target probes. The reporter and capture probe for the Pfs25-mRNA system were designed to have a polyA chain on the same end as the desired functional groups to increase the melting temperatures above the hybridization reaction temperature (40°C).

System	Sequence	Length	Melting Temperature (ΔT_m)
Pfs25	RP: 5'-/ThioMC6-D//iSp18//iSp18//iSp18/AAA AAA AAA AAT GAA TAA ATT TTA-3'	24mer	42.9°C
	CP: 5'-GTT TGT TTC TTT TCC AAA AAA AAA AAA AAA/iSp18//iSp18//iSp18//3AzideN/-3'	30mer	51.5°C
	TP: 5'-GGA AAA GAA ACA AAC TGT. AAA GTT TAT TCA T-3'	31mer	53.7°C
18s	RP: 5'-CAA TTT CAA ATA AGA ATA TAG TGT ACT CGC CGC/iSp18//iSp18//iSp18//3ThioMC3-D/-3'	33mer	52.8°C
	CP: 5'-/5AzideN//iSp18//iSp18//iSp18/CCT AAT TTG ATT ACT GAA TAA ATG TAT AGT TAC CTA TG-3'	38mer	54.7°C
	TP: 5'-GCG GCG AGT ACA CTA TAT TCT TAT TTG AAA TTG AAC ATA GGT AAC TAT ACA TTT ATT CAG TAA TCA AAT TAG G-3'	73mer	64.6°C

An issue that became prevalent with the developed interface in buffer after the sequence functionalization was completed, was a high blank signal for the Pfs25-mRNA system. Blank reactions for this research was running the hybridization reactions in the

absence of the target biomarker. Having a high average blank signal for a system limits the functional interface's ability to get a low limit of detection. Originally the approach for changing this high blank signal was to reduce the number of capture probes used in the reactions to change the molar ratio from 155153 reporter probes/capture probe to 174395 reporter probes/capture probe. However, this approach still displayed a large blank signal for the Pfs25-mRNA system with an intensity at 1489.11 cm^{-1} of 3274 ± 1828 counts. This indicated the possible presence of unbound reporter probe in the pellet following the washing steps since the high intensity spectral profile was still identical to the Ag@AuNS substrate measurements when Rose Bengal is present. The next attempt to lower the blank signal was manipulating the washing steps by involving different washing platforms (microcentrifuge or capillary tube), increasing the number of washing steps from two to three, and changing washing solutions from buffer to Ultrapure (DNase and RNase free) water. The lowest possible blank signal of 1108 ± 1036 counts (Figure 14) was obtained from optimizing the number of washing steps to three, continuing to use buffer for washing steps and the microcentrifuge platform; the blank signal improved by three orders of magnitude but still showed the Rose Bengal in the spectra.

In order to minimize any nonspecific binding that may be occurring, the surface of the magnetic beads was passivated with sulfo-NHS acetate. The free amine groups on the surface of the magnetic beads could be a possible source for the nonspecific binding between the probes that produced the high blank signal of the Rose Bengal Raman tag. After passivating the capture probes ($3.61 \times 10^{-16} \text{ M}$) with 1 mL of 11.2 mM sulfo-NHS acetate, the lowest blank signal without eliminating the ability of the capture probe to

bind to the target was achieved (Figure 14). With the Rose Bengal profile reduced from the blank signal due to passivation, the molar ratio of the reporter to capture probes was optimized again to further improve a lower background signal; less magnetic beads were used to increase the molar ratio from 174395 reporter probes/capture probe to 784765 reporter probes/capture probe. After doing so, the blanks provided low-signal spectra with an intensity at 1489.11 cm^{-1} of 125 ± 65 counts and no Rose Bengal profile being evident in the spectra. Future use of these systems in hybridization reactions followed the same optimized washing procedure as previously stated along with passivation of the capture probes.

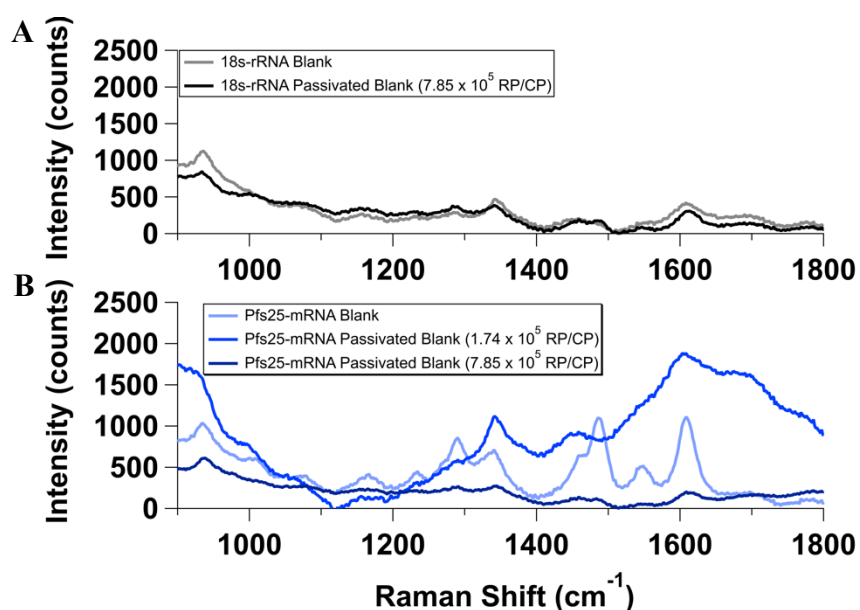


Figure 14. SERS spectra of blank signal optimization for both 18s-rRNA (A) and Pfs25-mRNA (B) systems. Each sample was performed with five replicates using 638 nm laser excitation at ~ 7 mW power with one second acquisition.

3.4. Comparison of Pfs25-mRNA & 18s-rRNA Hybridization Systems

After functionalization and optimization of the probes for blank measurements were performed, the functional interface designs for the Pfs25-mRNA and 18s-rRNA

systems were tested using sandwich hybridization reactions in buffer. Other hybridization conditions were necessary to consider for the reactions when detecting the synthetic targets. The washing steps found in the previous section were used along with setting the mixing rate to 550 rpm and dropcasting the hybridized complexes onto a silicon wafer placed on a magnet. The SERS measurements taken following the reactions were with 638 nm excitation, one second acquisition time, 10x objective and with ten accumulations per measurement. The first reaction attempts SERS spectra using 10 μM of target biomarker for the Pfs25-mRNA and 18s-rRNA systems in buffer can be found in Figure 15. The successful detection of the target was proven by the Rose Bengal profile being present in the SERS spectra. In order to display the specificity of the designed probes for the different systems, selectivity experiments were performed using 10 μM hybridization reactions in buffer (Figure 15). Pfs25-mRNA probes with the Pfs25-mRNA biomarker forms the hybridized complexes thus displaying a strong Rose Bengal signal at 1489.11 cm^{-1} with an intensity of 6806 counts. When performing the Pfs25-mRNA probe selectivity with 18s-rRNA target in place of the correct Pfs25-mRNA target, the intensity at 1489.11 cm^{-1} was 19 counts.

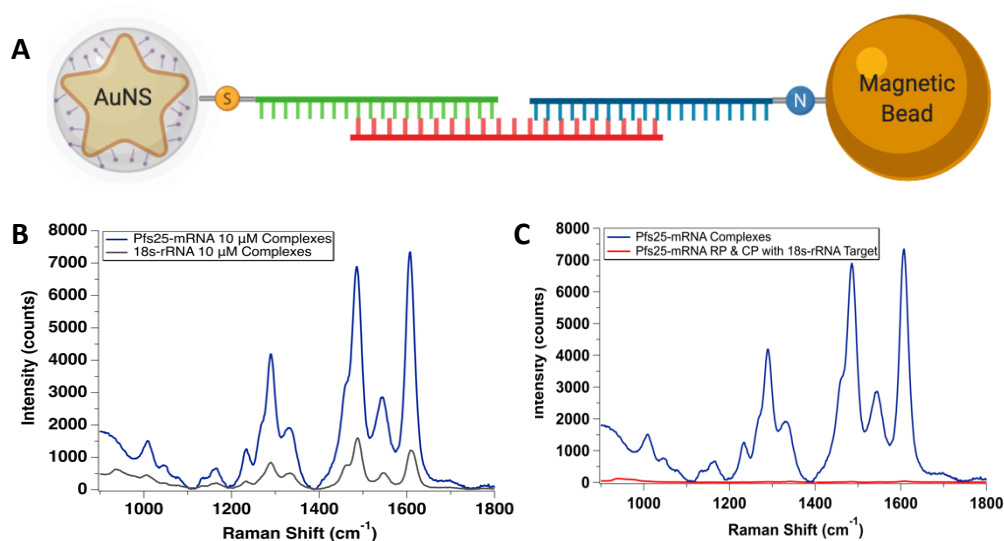


Figure 15. A) Schematic representation of the hybridized complexes when performing sandwich hybridization reactions with the synthetic target biomarker present. B) SERS spectra of 10 μM hybridized complexes for Pfs25-mRNA and 18s-rRNA systems. C) System probe selectivity for 10 μM with Pfs25-mRNA hybridized complexes and Pfs25-mRNA probe selectivity using the 18s-rRNA target.

3.5. Hybridization Reaction Results in Buffer

Using the optimized capture probes and reporter probes, a calibration curve was obtained to perform quantitative analysis for the biosensor in buffer. Concentrations used for the calibration curve ranged from 250 nM to 10 μM (Figure 16) along with blank measurements; five replicate reactions for each sample were performed. Ten measurements per replicate were obtained for each sample concentration. These measurements were acquired using the 638 nm laser excitation with an operating power of ~ 7 mW, a 10x objective and ten accumulations per sample measurement. The standard deviation from each sample can possibly be attributed to factors such as pellet formation of the hybridized complexes when concentrating them with a magnet onto the silicon wafer and how the complexes are distributed across the hybridized complex pellet. As a

result, some of the higher concentrations present in the calibration curve display large variations in signal intensity between the replicates. The limit of detection was calculated using the standard equation $LOD = (3 * Std Dev_{intercept})/slope$, from a linear model obtained from the calibration curve. The linear model was derived from the plotting the averaged blank measurements and the approximate linear range (250 nM to 1 μ M). The calculated limit of detection was determined to be 280 nM or 3.4×10^{12} RNA copies based on the hybridization reaction volumes of 20 μ L. These results indicated that the system can function in buffer down to nanomolar concentrations. With the successful detection of the Pfs25-mRNA biomarker in buffer hybridization reactions, the next step was to determine the functional ability of the assay using a synthetic target spiked-in blood lysate.

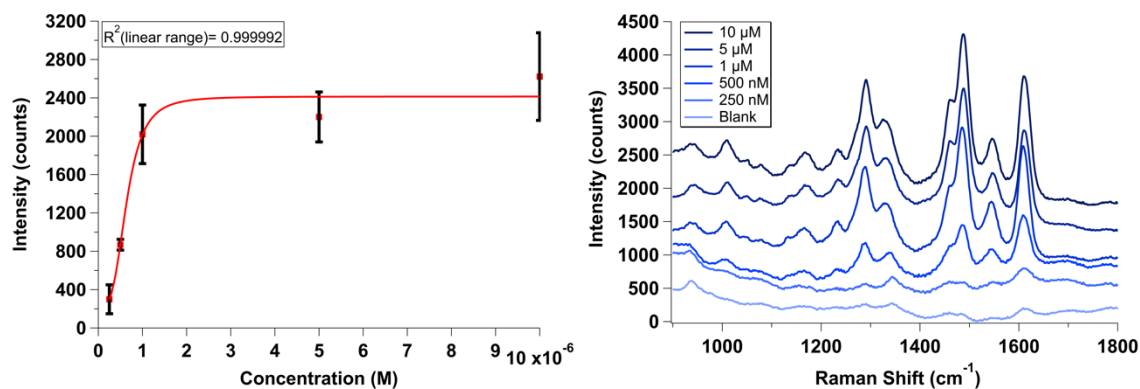


Figure 16. Left) Pfs25-mRNA system in buffer calibration curve with best fit and coefficient of determination for the linear range. Right) Average, stacked SERS spectra at each concentration of the calibration curve, including the averaged blank signal.

3.6. Sandwich Hybridization Reactions for Synthetic Biomarker Spiked-in Blood Lysate

For testing the application of this assay in blood, it was necessary to use a protocol for lysing the whole blood since the genetic material and the biomarker of interest would reside within the infected red blood cells. Prior to analyzing the ability of the assay to

detect the synthetic biomarker spiked-in blood lysate, control measurements were required to understand what signal convolution could occur due to the blood matrix. Whole blood and blood lysate control measurements were performed using the same operating parameters for the Raman microscope as the hybridization reactions in buffer. Additional control measurements were obtained by mixing the reporter probe with blood lysate to observe the SERS substrate signal in this matrix without running hybridization reactions. These three controls were tested using the 638 nm laser excitation but also with the 785 nm laser to see how changing the laser excitation for measurements in blood could impact the spectral profile of the Rose Bengal tag. The control measurements for the whole blood and blood lysate showed little to no signal at the Raman shift region of interest ($1480 - 1490 \text{ cm}^{-1}$) which indicated no signal interference should occur due to the blood matrix (Figure 17). The reporter probe in blood lysate produced the SERS signal to demonstrating the ability of the 1489.11 cm^{-1} peak to be observed in this matrix (Figure 17). These controls were performed with no washing steps or purification steps. With the washing steps in the hybridization reactions the high baseline signal observed across the large range of Raman shift values for blood lysate will be reduced. Following these control experiments, incubation time dependence studies were performed to optimize the hybridization efficiency in blood. Along with understanding the effects of time on the reactions another variable, purification after blood lysis procedure, was adjusted during these time trials to try and improve overall signal. Triplicates were completed for each time interval (three hours, four hours, & five hours) and for the blood lysate with and without purification (Figure 18) at a concentration of $10 \mu\text{M}$. Based on the signal

intensity of the different time intervals, three hour incubation was determined to produce the highest overall signal.

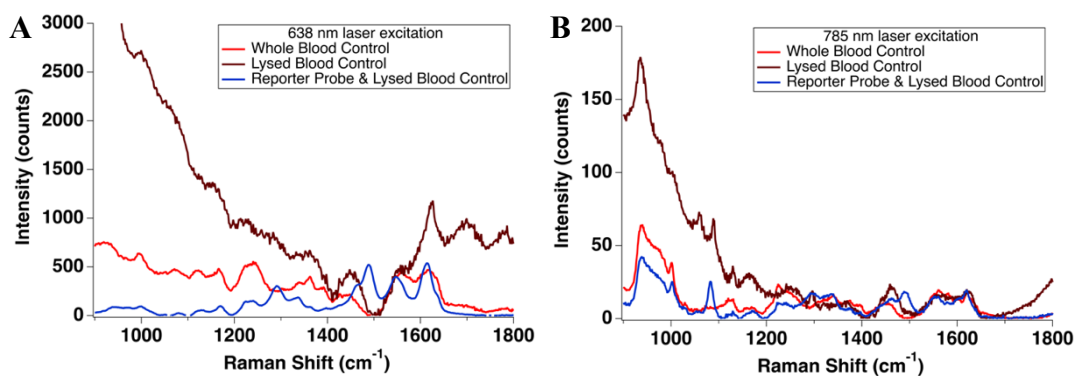


Figure 17. Blood control measurements using whole blood, lysed blood and reporter probe with lysed blood mixture. A) Represents the measurements taken with the 638 nm excitation at ~ 7 mW power, one second acquisition time, 10x objective and performed in triplicate. B) Represents 785 nm measurements taken using the same parameters as 638 nm with the exception of laser power (~ 12 mW).

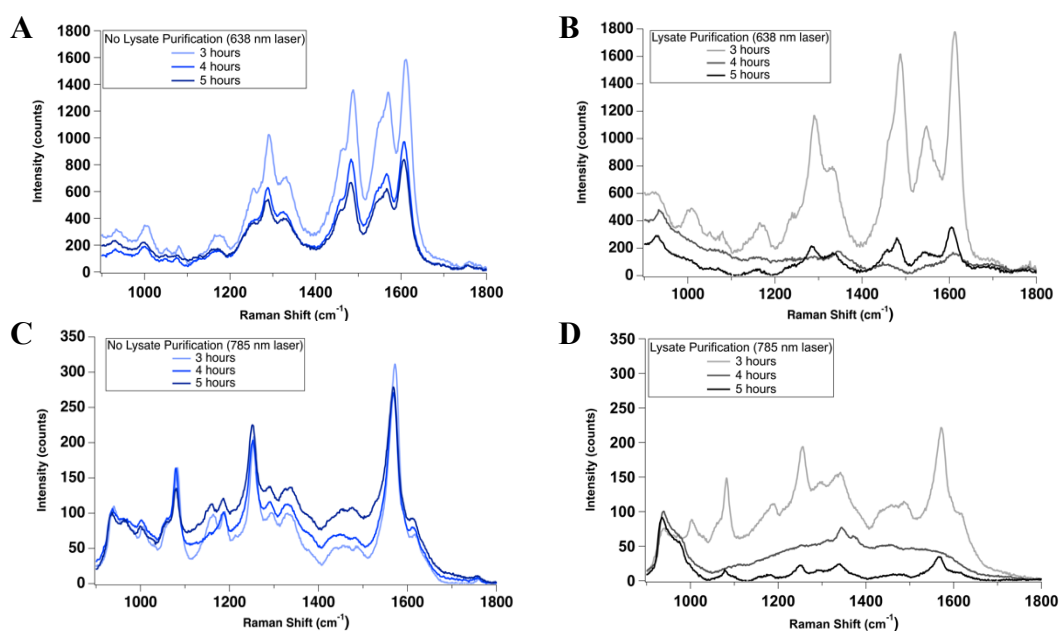


Figure 18. 10 μ M Pfs25-mRNA system measurements for blood lysate trials with manipulating time of incubation, lysate purification protocol, and laser excitation. A & B) Compares the results for the 638 nm laser excitation without lysate purification and reactions with lysate purification, respectively. C & D) Comparison of 785 nm excitation results without lysate purification and with lysate purification, respectively.

After baseline subtraction of the averaged profiles for each variable, the signal intensity was compared for the peak residing around 1489.11 cm^{-1} . The 638 nm laser excitation results were the main focus due to much higher signal intensity for every reaction with changing the variables in comparison to 785 nm laser excitation. The hybridization results indicated that the three-hour incubation period produced the best signal intensity for both methods of lysing the blood with and without purification. The increase in time does not increase the signal, possibly due to settling of the capture probes causing less interactions between the capture probes and the target/reporter probes. After determining the optimal time of the hybridization reactions in blood lysate, next the intensity of the three-hour incubation between the two types of lysate methods were compared (Figure 19).

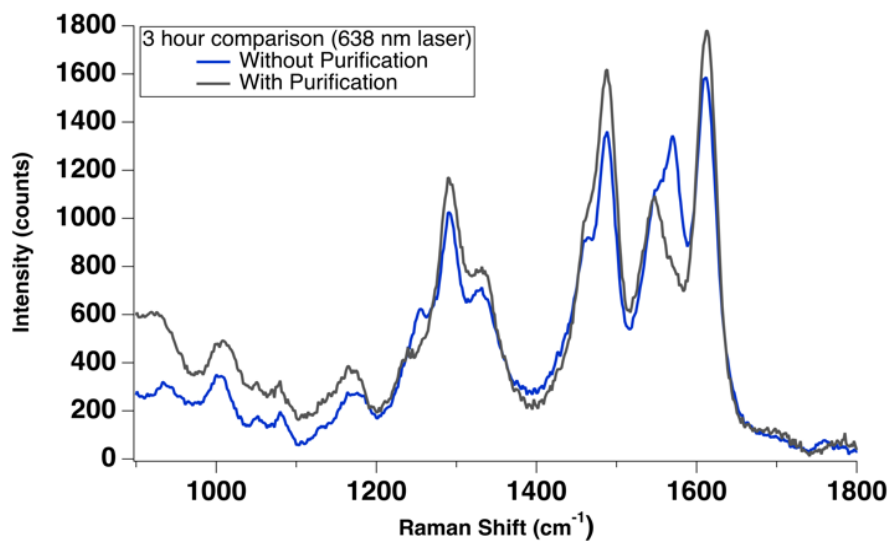


Figure 19. Comparison of purification methods, for the three-hour incubation with 638 nm excitation, on SERS signal output.

Further comparing the intensity at the 1489.11 cm^{-1} peak for the two lysing purification methods with the 638 nm excitation; the results show the purified lysate sample having an average intensity of 1571 ± 771 counts and the method without lysate purification producing an average signal of 1331 ± 120 counts. These results indicated the method using the three-hour incubation without purification of the lysate was the best moving forward. While the signal intensity from the purified lysate displayed a 240 average count higher intensity than the non-purified lysate, the standard deviation between replicates for the purified lysate samples was seven-times higher than that of the method without lysate purification. Having a protocol that limits the variability of the results and can function with removing purification steps simplifies the protocol and improves the possibility of the assay to function in a POC setting. Which is why the three-hour incubation with no blood lysate purification protocol was used to quantify a limit of detection for the Pfs25-mRNA system with target spiked-in blood lysate.

Once the optimized parameters for lysing the whole blood and the hybridization reactions were determined, a calibration curve was obtained for Pfs25-mRNA reactions in the blood lysate matrix from $10\text{ }\mu\text{M}$ to 125 nM (Figure 20) using the 638 nm excitation. 785 nm excitation calibration curve with averaged spectra can be found in Appendix D. Similar to the buffer reactions, five replicates were performed at each sample concentration, including blank reactions. For these measurements the 638 nm laser excitation was used with the 10x objective, one second acquisition and 10 accumulations. As expected from the control measurements, the blood lysate matrix after washing steps in the hybridization reactions showed little interference. This allowed for 125 nM to be tested which was an improvement in comparison to the lowest concentration when using

the buffer matrix (250 nM). The averaged spectra for each concentration and blank measurements can be found in Figure 20 as well. The approximate linear range was determined to be 125 nM to 1 μ M. The limit of detection calculation was performed using the same equation as the buffer. However, the standard deviation value used for blood came from the replicates of the lowest standard used in the calibration curve, 125 nM. The calculated limit of detection for target spiked-in blood lysate was 99 nM or 1.2×10^{12} RNA copies based on 20 μ L reaction volume.

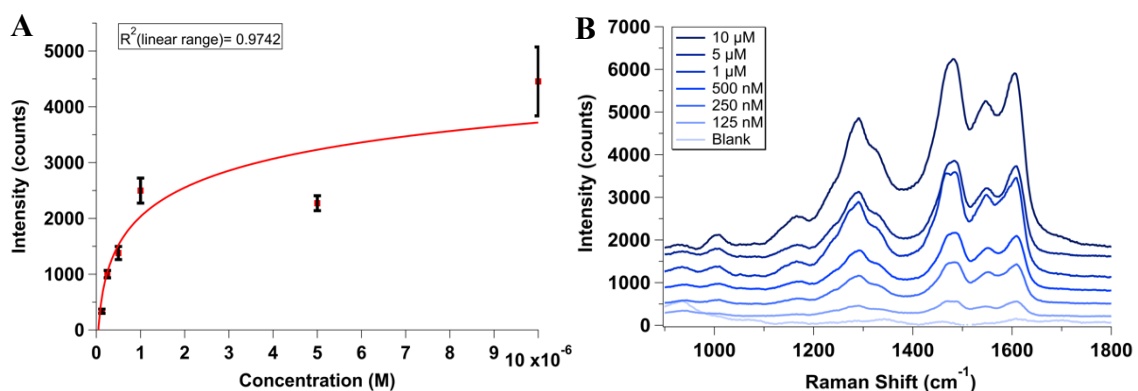


Figure 20. Calibration data for spiked-in synthetic Pfs25-mRNA reactions in blood lysate. A) Calibration curve from 125 nM up to 10 μ M with error bars. B) Averaged, stacked SERS spectra for each calibration curve concentration plus the averaged blank reaction spectrum. Five replicate reactions performed for each concentration and measured using 638 nm laser with 10x objective and one second acquisition time.

CHAPTER 4: CONCLUSIONS AND FUTURE WORK

The successful development of a SERS-based assay for detection of malaria nucleic acid biomarker, Pfs25-mRNA, was demonstrated in this thesis. A SERS substrate, Ag@AuNS, was synthesized with a two order of magnitude SERS EF for use in the functional interface as an optical transducer for indirect detection. A new, novel SERS substrate, Au@AgNS was developed for future potential use in a SERS-based assay for biosensors. Synthetic Pfs25-mRNA sequences were successfully detected in buffer down to the nanomolar region after careful optimization of the sandwich hybridization reaction parameters. Pfs25-mRNA probes were able to differentiate between a Pfs25-mRNA target and a 18s-rRNA biomarker, thus displaying the selectivity of the probe design. Blood lysate showed little interference in the Raman tag signal based on control measurements of just blood and blood with the reporter probe. Reaction optimization in blood lysate for time, laser type and purification steps were performed to achieve the highest possible signal in blood lysate.

The results of this thesis indicate the possible use of this SERS assay in a POC setting. However, the use for asymptomatic detection may be limited due to the detection limit of the system. This work benefits the biosensor community for malaria detection due to the novel SERS substrate that was developed, and the simplified procedural steps needed to develop the assay. Having reagents that can be made within 24 hours and then run reactions with detection after only 4 – 5 hours is valuable for POC diagnostics. While this thesis covered a large basis for asymptomatic malaria detection, there is plenty of future work that can be done.

The next step for the developed biosensor would be to test clinical blood samples for patients who have tested malaria positive. Reactions and detection would be conducted using the same parameters as the spiked-in blood lysate work. Issues may arise during the lysing process when compared to spiked-in synthetic sequences. Control measurements of lysed infected blood would be necessary to see how the parasites might impact the background spectral profile when using SERS. A calibration curve would be made using similar concentrations as the buffer and spiked-in blood lysate samples to determine the limit of detection. The hope would be that as seen with comparing the buffer to blood lysate matrix in this work, clinical infected samples would be able to be detected at even lower concentrations. This would further indicate the possible use of this developed assay for not only a POC setting but for asymptomatic detection as well. Beyond the use of this system for infected clinical blood samples, challenging this system to be used in a field transferable POC setting would be necessary as well.

The current system was performed in a laboratory using a large, non-portable Raman microscope. There are some issues with this for POC diagnosis, but the most problematic issue is that most countries with high malaria cases and transmission do not have the resources necessary to use this system in the same conditions. A portable, handheld Raman system would be used to make the field transferable applications more likely to work for this assay. With using a new detection system many controls and optimization steps will have to be performed to ensure the same detection abilities are possible with the handheld Raman. Synthetic target in buffer, spiked-in blood lysate and infected clinical sample reactions would all have to be repeated to obtain the figures of merit. Not

only would the experiments need to be repeated using the handheld Raman system, but also in conditions similar to the tropical countries where malaria is a serious problem.

Since there are many countries where malaria can be a serious concern, finding conditions to use like temperature and humidity could prove difficult to determine. Since *P. falciparum* makes up a larger portion of the cases in Africa, the average climate taken from the most infected countries in Africa could be used as set parameters to mimic for future work. Attempting to run reactions in similar conditions to Africa and outside of a lab setting could be useful to understanding the assay's capacity to function in a field transferable POC setting. Ideally, all that would be needed in those countries are the minimum equipment to store the reagents, run the reactions and collect the data. Outside of those factors the high temperatures of that region could prove to disrupt the ability of the assay to function because of the melting temperature of the probe sequences. Running hybridization reactions as the temperature of the climate in the African countries would provide meaningful information. Not only would the reaction conditions possibly be impacted by the tropical climate, but the stability of the reporter and capture probes would need to be considered.

Stability time studies would be performed to determine how long one stock solution of each probe could be used for in both a laboratory and field transferable setting. Stock solutions in the laboratory setting would be refrigerated as they were throughout this thesis to function as control samples. Field transferable setting stock solutions would be left out under two conditions: room temperature and under the temperature conditions similar to the climate in the tropical countries. On a weekly basis, the reporter probe stock solution would be tested using UV-VIS and DFS-hyperspectral imaging to check

for the LSPR. SERS measurements would also be acquired to test the stability of the Raman tag profile and SERS EF over time. The capture probe would also be checked using UV-VIS, along with checking the magnetic abilities of the capture probe by placing the solution near the magnet used during hybridization reactions. It would be beneficial to not only check the stability of these probes in the matrices mentioned in the experimental section but to also consult literature on other possible matrices that could be used to store these solutions for longer periods of time. If a reputable matrix can be found in literature for these types of probes, they would be tested the same way as the above-mentioned samples for a stability time study. Beyond further developing the present system, the novel substrate (Au@AgNS) should be tested in hybridization reactions.

This Au@AgNS substrate was designed for future use in SERS-based assays but should be tested in buffer before consideration in blood lysate. Similar to the SERS substrate used for the hybridization reactions in this thesis, Au@AgNS would be tested using higher concentrations of the synthetic Pfs25-mRNA in buffer before creating a calibration curve. Further optimization of washing steps, probe molar ratio and other parameters would probably be necessary in order to collect analytical figures of merit. All of these experiments listed for future work would be a great foundation for truly understanding the potential for this SERS assay to be used in a POC setting.

REFERENCES

1. Organization, W. H., *World Malaria Report 2018*. World Health Organization, 2019: 2019; p 204.
2. Organization, W. H. Malaria. <https://www.who.int/news-room/fact-sheets/detail/malaria>.
3. Prevention, C. f. D. C. a. Malaria Disease. <https://www.cdc.gov/malaria/about/disease.html>.
4. Prevention, C. f. D. C. a. Malaria Diagnosis (U.S.). https://www.cdc.gov/malaria/diagnosis_treatment/diagnosis.html.
5. Poostchi, M.; Ersoy, I.; McMenamin, K.; Gordon, E.; Palaniappan, N.; Pierce, S.; Maude, R. J.; Bansal, A.; Srinivasan, P.; Miller, L.; Palaniappan, K.; Thoma, G.; Jaeger, S., Malaria parasite detection and cell counting for human and mouse using thin blood smear microscopy. *Journal of Medical Imaging* **2018**, 5 (4).
6. Guy, R.; Liu, P.; Pennefather, P.; Crandall, I., The use of fluorescence enhancement to improve the microscopic diagnosis of falciparum malaria. *Malaria Journal* **2007**, 6.
7. Murphy, S. C.; Shott, J. P.; Parikh, S.; Etter, P.; Prescott, W. R.; Stewart, V. A., Review Article: Malaria Diagnostics in Clinical Trials. *American Journal of Tropical Medicine and Hygiene* **2013**, 89 (5), 824-839.
8. Yamamoto, T.; Yatsushiro, S.; Hashimoto, M.; Kajimoto, K.; Ido, Y.; Abe, K.; Sofue, Y.; Nogami, T.; Hayashi, T.; Nagatomi, K.; Minakawa, N.; Oka, H.; Mita, T.; Kataoka, M., Development of a highly sensitive, quantitative, and rapid detection system for Plasmodium falciparum-infected red blood cells using a fluorescent blue-ray optical system. *Biosensors & Bioelectronics* **2019**, 132, 375-381.
9. Rodulfo, H.; De Donato, M.; Mora, R.; Gonzalez, L.; Contreras, C. E., Comparison of the diagnosis of malaria by microscopy, immunochromatography and PCR in endemic areas of Venezuela. *Brazilian Journal of Medical and Biological Research* **2007**, 40 (4), 535-543.
10. Siciliano, G.; Alano, P., Enlightening the malaria parasite life cycle: bioluminescent Plasmodium in fundamental and applied research. *Front. Microbiol.* **2015**, 6, 8.
11. Ngwa, C. J.; Rosa, T. F. D.; Pradel, G., *The Biology of Malaria Gametocytes*. 2016; p 117-144.

12. Metkar, S. K.; Girigoswami, K., Diagnostic biosensors in medicine - A review. *Biocatal. Agric. Biotechnol.* **2019**, *17*, 271-283.
13. Maiti, K. K.; Dinish, U. S.; Samanta, A.; Vendrell, M.; Soh, K.-S.; Park, S.-J.; Olivo, M.; Chang, Y.-T., Multiplex targeted in vivo cancer detection using sensitive near-infrared SERS nanotags. *Nano Today* **2012**, *7* (2), 85-93.
14. Wang, Y.; Tang, L.-J.; Jiang, J.-H., Surface-Enhanced Raman Spectroscopy-Based, Homogeneous, Multiplexed Immunoassay with Antibody-Fragments-Decorated Gold Nanoparticles. *Analytical Chemistry* **2013**, *85* (19), 9213-9220.
15. Sanchez-Purra, M.; Carre-Camps, M.; de Puig, H.; Bosch, I.; Gehrke, L.; Hamad-Schifferli, K., Surface-Enhanced Raman Spectroscopy-Based Sandwich Immunoassays for Multiplexed Detection of Zika and Dengue Viral Biomarkers. *Acs Infectious Diseases* **2017**, *3* (10), 767-776.
16. Xu, W.; Jin, T.; Dai, Y. F.; Liu, C. C., Surpassing the detection limit and accuracy of the electrochemical DNA sensor through the application of CRISPR Cas systems. *Biosensors & Bioelectronics* **2020**, *155*.
17. Huertas, C. S.; Bonnal, S.; Soler, M.; Escuela, A. M.; Valcarcel, J.; Lechuga, L. M., Site-Specific mRNA Cleavage for Selective and Quantitative Profiling of Alternative Splicing with Label-Free Optical Biosensors. *Analytical Chemistry* **2019**, *91* (23), 15138-15146.
18. Caneira, C. R. F.; Soares, R. R. G.; Pinto, I. F.; Mueller-Landau, H. S.; Azevedo, A. M.; Chu, V.; Conde, J. P., Development of a rapid bead-based microfluidic platform for DNA hybridization using single- and multi-mode interactions for probe immobilization. *Sensors and Actuators B-Chemical* **2019**, *286*, 328-336.
19. Ngo, H. T.; Wang, H.-N.; Fales, A. M.; Nicholson, B. P.; Woods, C. W.; Vo-Dinh, T., DNA bioassay-on-chip using SERS detection for dengue diagnosis. *Analyst* **2014**, *139* (22), 5655-5659.
20. Strelau, K. K.; Brinker, A.; Schnee, C.; Weber, K.; Moeller, R.; Popp, J., Detection of PCR products amplified from DNA of epizootic pathogens using magnetic nanoparticles and SERS. *Journal of Raman Spectroscopy* **2011**, *42* (3), 243-250.
21. Negri, P.; Dluhy, R. A., Detection of genetic markers related to high pathogenicity in influenza by SERS. *Analyst* **2013**, *138* (17), 4877-4884.
22. Indrasekara, A. S. D.; Fabris, L., SERS-based approaches toward genetic profiling. *Bioanalysis* **2015**, *7* (2), 263-278.

23. Ozgur, E.; Uyanik, H. U.; Senel, S.; Uzun, L., Immunoaffinity biosensor for neurofilament light chain detection and its use in Parkinson's diagnosis. *Materials Science and Engineering B-Advanced Functional Solid-State Materials* **2020**, 256.
24. Fang, C.; Wang, Z. R.; Dai, Y. Y.; Chang, W. J.; Sun, L. N.; Ma, X. L., Serum human neutrophil lipocalin: An effective biomarker for diagnosing bacterial infections. *Clinical Biochemistry* **2020**, 75, 23-29.
25. Amor-Gutierrez, O.; Costa-Rama, E.; Arce-Varas, N.; Martinez-Rodriguez, C.; Novelli, A.; Fernandez-Sanchez, M. T.; Costa-Garcia, A., Competitive electrochemical immunosensor for the detection of unfolded p53 protein in blood as biomarker for Alzheimer's disease. *Analytica Chimica Acta* **2020**, 1093, 28-34.
26. George, A.; Amrutha, M. S.; Srivastava, P.; Sai, V. V. R.; Sunil, S.; Srinivasan, R., Label-Free Detection of Chikungunya Non-Structural Protein 3 Using Electrochemical Impedance Spectroscopy. *Journal of the Electrochemical Society* **2019**, 166 (14), B1356-B1363.
27. Hennigan, S. L.; Driskell, J. D.; Ferguson-Noel, N.; Dluhy, R. A.; Zhao, Y.; Tripp, R. A.; Krause, D. C., Detection and Differentiation of Avian Mycoplasmas by Surface-Enhanced Raman Spectroscopy Based on a Silver Nanorod Array. *Applied and Environmental Microbiology* **2012**, 78 (6), 1930-1935.
28. Fan, Z.; Senapati, D.; Khan, S. A.; Singh, A. K.; Hamme, A.; Yust, B.; Sardar, D.; Ray, P. C., Popcorn-Shaped Magnetic CorePlasmonic Shell Multifunctional Nanoparticles for the Targeted Magnetic Separation and Enrichment, Label-Free SERS Imaging, and Photothermal Destruction of Multidrug-Resistant Bacteria. *Chemistry-a European Journal* **2013**, 19 (8), 2839-2847.
29. Wang, Y.; Rauf, S.; Grewal, Y. S.; Spadafora, L. J.; Shiddiky, M. J. A.; Cangelosi, G. A.; Schluecker, S.; Trau, M., Duplex Microfluidic SERS Detection of Pathogen Antigens with Nanoyeast Single-Chain Variable Fragments. *Analytical Chemistry* **2014**, 86 (19), 9930-9938.
30. Mircescu, N. E.; Zhou, H. B.; Leopold, N.; Chis, V.; Ivleva, N. P.; Niessner, R.; Wieser, A.; Haisch, C., Towards a receptor-free immobilization and SERS detection of urinary tract infections causative pathogens. *Analytical and Bioanalytical Chemistry* **2014**, 406 (13), 3051-3058.
31. Fan, Z.; Kanchanapally, R.; Ray, P. C., Hybrid Graphene Oxide Based Ultrasensitive SERS Probe for Label-Free Biosensing. *Journal of Physical Chemistry Letters* **2013**, 4 (21), 3813-3818.
32. Lu, X.; Samuelson, D. R.; Xu, Y.; Zhang, H.; Wang, S.; Rasco, B. A.; Xu, J.; Konkel, M. E., Detecting and Tracking Nosocomial Methicillin-Resistant Staphylococcus

- aureus Using a Microfluidic SERS Biosensor. *Analytical Chemistry* **2013**, *85* (4), 2320-2327.
33. Hermann, T.; Patel, D. J., Biochemistry - Adaptive recognition by nucleic acid aptamers. *Science* **2000**, *287* (5454), 820-825.
34. Kent, A. D.; Spiropulos, N. G.; Heemstra, J. M., General Approach for Engineering Small-Molecule-Binding DNA Split Aptamers. *Analytical Chemistry* **2013**, *85* (20), 9916-9923.
35. Sela-Culang, I.; Kunik, V.; Ofran, Y., The structural basis of antibody-antigen recognition. *Frontiers in Immunology* **2013**, *4*.
36. Santosh, B.; Yadava, P. K., Nucleic Acid Aptamers: Research Tools in Disease Diagnostics and Therapeutics. *Biomed Research International* **2014**.
37. Wang, H.-N.; Fales, A. M.; Zaas, A. K.; Woods, C. W.; Burke, T.; Ginsburg, G. S.; Vo-Dinh, T., Surface-enhanced Raman scattering molecular sentinel nanoprobe for viral infection diagnostics. *Analytica Chimica Acta* **2013**, *786*, 153-158.
38. Kaushik, A.; Yndart, A.; Kumar, S.; Jayant, R. D.; Vashist, A.; Brown, A. N.; Li, C. Z.; Nair, M., A sensitive electrochemical immunosensor for label-free detection of Zika-virus protein. *Scientific Reports* **2018**, *8*.
39. Chang, H. H.; Huber, R. G.; Bond, P. J.; Grad, Y. H.; Camerini, D.; Maurer-Stroh, S.; Lipsitch, M., Systematic analysis of protein identity between Zika virus and other arthropod-borne viruses. *Bulletin of the World Health Organization* **2017**, *95* (7), 517-525.
40. Yrad, F. M.; Castanares, J. M.; Alocilja, E. C., Visual Detection of Dengue-1 RNA Using Gold Nanoparticle-Based Lateral Flow Biosensor. *Diagnostics* **2019**, *9* (3).
41. Xu, X. M.; Chen, J. Y.; Li, B. R.; Tang, L. J.; Jiang, J. H., Single particle ICP-MS-based absolute and relative quantification of E-coli O157 16S rRNA using sandwich hybridization capture. *Analyst* **2019**, *144* (5), 1725-1730.
42. Miyagawa, A.; Harada, M.; Okada, T., Multiple MicroRNA Quantification Based on Acoustic Levitation of Single Microspheres after One-Pot Sandwich Interparticle Hybridizations. *Analytical Chemistry* **2018**, *90* (22), 13729-13735.
43. Cai, J.; Ding, L. Y.; Gong, P. F.; Huang, J., A colorimetric detection of microRNA-148a in gastric cancer by gold nanoparticle-RNA conjugates. *Nanotechnology* **2020**, *31* (9).
44. Kang, T.; Yoo, S. M.; Yoon, I.; Lee, S. Y.; Kim, B., Patterned Multiplex Pathogen DNA Detection by Au Particle-on-Wire SERS Sensor. *Nano Letters* **2010**, *10* (4), 1189-1193.

45. Gracie, K.; Correa, E.; Mabbott, S.; Dougan, J. A.; Graham, D.; Goodacre, R.; Faulds, K., Simultaneous detection and quantification of three bacterial meningitis pathogens by SERS. *Chemical Science* **2014**, *5* (3), 1030-1040.
46. Zhang, H.; Harpster, M. H.; Park, H. J.; Johnson, P. A., Surface-Enhanced Raman Scattering Detection of DNA Derived from the West Nile Virus Genome Using Magnetic Capture of Raman-Active Gold Nanoparticles. *Analytical Chemistry* **2011**, *83* (1), 254-260.
47. Sea-liang, N.; Sereemasapun, A.; Patarakul, K.; Gaywee, J.; Rodkvamtook, W.; Srisawat, N.; Wacharaplusadee, S.; Hemachudha, T., Development of multiplex PCR for neglected infectious diseases. *Plos Neglected Tropical Diseases* **2019**, *13* (7), 12.
48. Viedma, M. D. M.; Puri, V.; Oldfield, L. M.; Shabman, R. S.; Tan, G. S.; Pickett, B. E., Optimization of qRT-PCR assay for zika virus detection in human serum and urine. *Virus Research* **2019**, *263*, 173-178.
49. Udoh, B. E.; Iwalokun, B. A.; Etukumana, E.; Amoo, J., Asymptomatic falciparum Malaria and its Effects on Type 2 Diabetes Mellitus Patients in Lagos, Nigeria. *Saudi Journal of Medicine & Medical Sciences* **2020**, *8* (1), 32-40.
50. Taghdiri, A.; Almani, P. G. N.; Sharifi, I.; Mohammadi, M. A.; Salari, S., Detection of malaria with light microscopy and Nested polymerase chain reaction (Nested PCR) methods in peripheral blood expansions and investigation of the genetic diversity of Plasmodium species by 18S rRNA gene in Southeast of Iran. *Microbial Pathogenesis* **2019**, *137*.
51. Mehta, N.; Perrais, B.; Martin, K.; Kumar, A.; Hobman, T. C.; Cabalfin-Chua, M. N.; Donald, M. E.; Painaga, M. S. S.; Gaite, J. Y.; Tran, V.; Kain, K. C.; Hawkes, M. T.; Yanow, S. K., A Direct from Blood/Plasma Reverse Transcription-Polymerase Chain Reaction for Dengue Virus Detection in Point-of-Care Settings. *American Journal of Tropical Medicine and Hygiene* **2019**, *100* (6), 1534-1540.
52. Leski, T. A.; Taitt, C. R.; Swaray, A. G.; Bangura, U.; Reynolds, N. D.; Holtz, A.; Yasuda, C.; Lahai, J.; Lamin, J. M.; Baio, V.; Jacobsen, K. H.; Ansumana, R.; Stenger, D. A., Use of real-time multiplex PCR, malaria rapid diagnostic test and microscopy to investigate the prevalence of Plasmodium species among febrile hospital patients in Sierra Leone. *Malaria Journal* **2020**, *19* (1).
53. Araujo, R. V.; Feitosa-Suntheimer, F.; Gold, A. S.; Londono-Renteria, B.; Colpitts, T. M., One-step RT-qPCR assay for ZIKV RNA detection in Aedes aegypti samples: a protocol to study infection and gene expression during ZIKV infection. *Parasites & Vectors* **2020**, *13* (1).

54. Amaral, L. C.; Robortella, D. R.; Guimaraes, L. F. F.; Limongi, J. E.; Fontes, C. J. F.; Pereira, D. B.; de Brito, C. F. A.; Kano, F. S.; de Sousa, T. N.; Carvalho, L. H., Ribosomal and non-ribosomal PCR targets for the detection of low-density and mixed malaria infections. *Malaria Journal* **2019**, *18*.
55. Zheng, J.; Li, N. X.; Li, C. R.; Wang, X. X.; Liu, Y. C.; Mao, G. B.; Ji, X. H.; He, Z. K., A nonenzymatic DNA nanomachine for biomolecular detection by target recycling of hairpin DNA cascade amplification. *Biosensors & Bioelectronics* **2018**, *107*, 40-46.
56. Takalkar, S.; Baryeh, K.; Liu, G. D., Fluorescent carbon nanoparticle-based lateral flow biosensor for ultrasensitive detection of DNA. *Biosensors & Bioelectronics* **2017**, *98*, 147-154.
57. Park, K. S.; Charles, R. C.; Ryan, E. T.; Weissleder, R.; Lee, H., Fluorescence Polarization Based Nucleic Acid Testing for Rapid and Cost-Effective Diagnosis of Infectious Disease. *Chemistry-a European Journal* **2015**, *21* (46), 16359-16363.
58. Adegoke, O.; Morita, M.; Kato, T.; Ito, M.; Suzuki, T.; Park, E. Y., Localized surface plasmon resonance-mediated fluorescence signals in plasmonic nanoparticle-quantum dot hybrids for ultrasensitive Zika virus RNA detection via hairpin hybridization assays. *Biosensors & Bioelectronics* **2017**, *94*, 513-522.
59. Hassan, S. E. H.; Haggaz, A. E. D.; Mohammed-Elhassan, E. B.; Malik, E. M.; Adam, I., Fluorescence microscope (Cyscope (R)) for malaria diagnosis in pregnant women in Medani Hospital, Sudan. *Diagnostic Pathology* **2011**, *6*.
60. Stockman, M. I.; Kneipp, K.; Bozhevolnyi, S. I.; Saha, S.; Dutta, A.; Ndukaife, J.; Kinsey, N.; Reddy, H.; Guler, U.; Shalaev, V. M.; Boltasseva, A.; Gholipour, B.; Krishnamoorthy, H. N. S.; MacDonald, K. F.; Soci, C.; Zheludev, N. I.; Savinov, V.; Singh, R.; Gross, P.; Lienau, C.; Vadai, M.; Solomon, M. L.; Barton, D. R.; Lawrence, M.; Dionne, J. A.; Boriskina, S. V.; Esteban, R.; Aizpurua, J.; Zhang, X.; Yang, S.; Wang, D. Q.; Wang, W. J.; Odom, T. W.; Accanto, N.; de Roque, P. M.; Hancu, I. M.; Piatkowski, L.; van Hulst, N. F.; Kling, M. F., Roadmap on plasmonics. *Journal of Optics* **2018**, *20* (4).
61. Yu, H. K.; Peng, Y. S.; Yang, Y.; Li, Z. Y., Plasmon-enhanced light-matter interactions and applications. *Npj Computational Materials* **2019**, *5*.
62. Boriskina, S. V.; Ghasemi, H.; Chen, G., Plasmonic materials for energy: From physics to applications. *Materials Today* **2013**, *16* (10), 375-386.
63. Sipova, H.; Homola, J., Surface plasmon resonance sensing of nucleic acids: A review. *Analytica Chimica Acta* **2013**, *773*, 9-23.
64. Heiat, M.; Ranjbar, R.; Alavian, S. M., Classical and Modern Approaches Used for Viral Hepatitis Diagnosis. *Hepatitis Monthly* **2014**, *14* (4).

65. Miller, M. M.; Lazarides, A. A., Sensitivity of metal nanoparticle surface plasmon resonance to the dielectric environment. *Journal of Physical Chemistry B* **2005**, *109* (46), 21556-21565.
66. Omar, N. A. S.; Fen, Y. W.; Abdullah, J.; Sadrolhosseini, A. R.; Kamil, Y. M.; Fauzi, N. I. M.; Hashim, H. S.; Mahdi, M. A., Quantitative and Selective Surface Plasmon Resonance Response Based on a Reduced Graphene Oxide-Polyamidoamine Nanocomposite for Detection of Dengue Virus E-Proteins. *Nanomaterials* **2020**, *10* (3).
67. Masson, J. F., Surface Plasmon Resonance Clinical Biosensors for Medical Diagnostics. *Acs Sensors* **2017**, *2* (1), 16-30.
68. Liu, J. J.; Jalali, M.; Mahshid, S.; Wachsmann-Hogiu, S., Are plasmonic optical biosensors ready for use in point-of-need applications? *Analyst* **2020**, *145* (2), 364-384.
69. Fathi, F.; Rashidi, M. R.; Omid, Y., Ultra-sensitive detection by metal nanoparticles-mediated enhanced SPR biosensors. *Talanta* **2019**, *192*, 118-127.
70. Kai, E.; Ikebukuro, K.; Hoshina, S.; Watanabe, H.; Karube, I., Detection of PCR products of Escherichia coli O157 : H7 in human stool samples using surface plasmon resonance (SPR). *Fems Immunology and Medical Microbiology* **2000**, *29* (4), 283-288.
71. Unser, S.; Bruzas, I.; He, J.; Sagle, L., Localized Surface Plasmon Resonance Biosensing: Current Challenges and Approaches. *Sensors* **2015**, *15* (7), 15684-15716.
72. Langer, J.; de Aberasturi, D. J.; Aizpurua, J.; Alvarez-Puebla, R. A.; Auguie, B.; Baumberg, J. J.; Bazan, G. C.; Bell, S. E. J.; Boisen, A.; Brolo, A. G.; Choo, J.; Ciialla-May, D.; Deckert, V.; Fabris, L.; Faulds, K.; de Abajo, F. J. G.; Goodacre, R.; Graham, D.; Haes, A. J.; Haynes, C. L.; Huck, C.; Itoh, T.; Ka, M.; Kneipp, J.; Kotov, N. A.; Kuang, H.; Le Ru, E. C.; Lee, H. K.; Li, J. F.; Ling, X. Y.; Maier, S. A.; Mayerhofer, T.; Moskovits, M.; Murakoshi, K.; Nam, J. M.; Nie, S.; Ozaki, Y.; Pastoriza-Santos, I.; Perez-Juste, J.; Popp, J.; Pucci, A.; Reich, S.; Ren, B.; Schatz, G. C.; Shegai, T.; Schlucker, S.; Tay, L. L.; Thomas, K. G.; Tian, Z. Q.; Van Duyne, R. P.; Vo-Dinh, T.; Wang, Y.; Willets, K. A.; Xu, C.; Xu, H.; Xu, Y.; Yamamoto, Y. S.; Zhao, B.; Liz-Marzan, L. M., Present and Future of Surface-Enhanced Raman Scattering. *Acs Nano* **2020**, *14* (1), 28-117.
73. Chon, H.; Lim, C.; Ha, S. M.; Ahn, Y.; Lee, E. K.; Chang, S. I.; Seong, G. H.; Choo, J., On-Chip Immunoassay Using Surface-Enhanced Raman Scattering of Hollow Gold Nanospheres. *Analytical Chemistry* **2010**, *82* (12), 5290-5295.
74. Paul, A. M.; Fan, Z.; Sinha, S. S.; Shi, Y. L.; Le, L. D.; Bai, F. W.; Ray, P. C., Bioconjugated Gold Nanoparticle Based SERS Probe for Ultrasensitive Identification of Mosquito-Borne Viruses Using Raman Fingerprinting. *Journal of Physical Chemistry C* **2015**, *119* (41), 23669-23675.

75. Oliveira, M. J.; Quaresma, P.; de Almeida, M. P.; Araujo, A.; Pereira, E.; Fortunato, E.; Martins, R.; Franco, R.; Aguas, H., Office paper decorated with silver nanostars - an alternative cost effective platform for trace analyte detection by SERS. *Scientific Reports* **2017**, *7*.
76. Garcia-Leis, A.; Rivera-Arreba, I.; Sanchez-Cortes, S., Morphological tuning of plasmonic silver nanostars by controlling the nanoparticle growth mechanism: Application in the SERS detection of the amyloid marker Congo Red. *Colloids and Surfaces a-Physicochemical and Engineering Aspects* **2017**, *535*, 49-60.
77. Ngo, H. T.; Freedman, E.; Odion, R. A.; Strobbia, P.; Indrasekara, A. S. D.; Vohra, P.; Taylor, S. M.; Tuan, V. D., Direct Detection of Unamplified Pathogen RNA in Blood Lysate using an Integrated Lab-in-a-Stick Device and Ultrabright SERS Nanorattles. *Scientific Reports* **2018**, *8*.
78. Li, M.; Cushing, S. K.; Zhang, J. M.; Lankford, J.; Aguilar, Z. P.; Ma, D. L.; Wu, N. Q., Shape-dependent surface-enhanced Raman scattering in gold-Ramanprobe-silica sandwiched nanoparticles for biocompatible applications. *Nanotechnology* **2012**, *23* (11).
79. Hamm, L.; Gee, A.; Indrasekara, A. S. D., Recent Advancement in the Surface-Enhanced Raman Spectroscopy-Based Biosensors for Infectious Disease Diagnosis. *Applied Sciences-Basel* **2019**, *9* (7).
80. Integrated Optics, U. Raman Spectroscopy. <https://integratedoptics.com/Raman-Spectroscopy>.
81. Pilot, R.; Signorini, R.; Durante, C.; Orian, L.; Bhamidipati, M.; Fabris, L., A Review on Surface-Enhanced Raman Scattering. *Biosensors-Basel* **2019**, *9* (2).
82. LeRu, E. C.; Etchegoin, P. G., *Principles of Surface-Enhanced Raman Spectroscopy: And Related Plasmonic Effects*. 2009; p 1-663.
83. Otto, A., SURFACE-ENHANCED RAMAN-SCATTERING - CLASSICAL AND CHEMICAL ORIGINS. *Topics in Applied Physics* **1984**, *54*, 289-418.
84. Morton, S. M.; Jensen, L., Understanding the Molecule-Surface Chemical Coupling in SERS. *Journal of the American Chemical Society* **2009**, *131* (11), 4090-4098.
85. Otto, A., The 'chemical' (electronic) contribution to surface-enhanced Raman scattering. *Journal of Raman Spectroscopy* **2005**, *36* (6-7), 497-509.
86. Le Ru, E. C.; Blackie, E.; Meyer, M.; Etchegoin, P. G., Surface enhanced Raman scattering enhancement factors: a comprehensive study. *Journal of Physical Chemistry C* **2007**, *111* (37), 13794-13803.

87. Barhoumi, A.; Halas, N. J., Label-Free Detection of DNA Hybridization Using Surface Enhanced Raman Spectroscopy. *Journal of the American Chemical Society* **2010**, *132* (37), 12792-12793.
88. Dondapati, S. K.; Sau, T. K.; Hrelescu, C.; Klar, T. A.; Stefani, F. D.; Feldmann, J., Label-free Biosensing Based on Single Gold Nanostars as Plasmonic Transducers. *Acs Nano* **2010**, *4* (11), 6318-6322.
89. Papadopoulou, E.; Bell, S. E. J., Label-Free Detection of Single-Base Mismatches in DNA by Surface-Enhanced Raman Spectroscopy. *Angewandte Chemie-International Edition* **2011**, *50* (39), 9058-9061.
90. Xu, L. J.; Lei, Z. C.; Li, J. X.; Zong, C.; Yang, C. J.; Ren, B., Label-Free Surface-Enhanced Raman Spectroscopy Detection of DNA with Single-Base Sensitivity. *Journal of the American Chemical Society* **2015**, *137* (15), 5149-5154.
91. Braun, G. B.; Lee, S. J.; Laurence, T.; Fera, N.; Fabris, L.; Bazan, G. C.; Moskovits, M.; Reich, N. O., Generalized Approach to SERS-Active Nanomaterials via Controlled Nanoparticle Linking, Polymer Encapsulation, and Small-Molecule Infusion. *Journal of Physical Chemistry C* **2009**, *113* (31), 13622-13629.
92. Fabris, L.; Dante, M.; Nguyen, T. Q.; Tok, J. B. H.; Bazan, G. C., SERS aptatags: New responsive metallic nanostructures for heterogeneous protein detection by surface enhanced Raman spectroscopy. *Advanced Functional Materials* **2008**, *18* (17), 2518-2525.
93. Indrasekara, A.; Paladini, B. J.; Naczynski, D. J.; Starovoytov, V.; Moghe, P. V.; Fabris, L., Dimeric Gold Nanoparticle Assemblies as Tags for SERS-Based Cancer Detection. *Advanced Healthcare Materials* **2013**, *2* (10), 1370-1376.
94. Perets, E. A.; Indrasekara, A.; Kurmis, A.; Atlasevich, N.; Fabris, L.; Arslanoglu, J., Carboxy-terminated immuno-SERS tags overcome non-specific aggregation for the robust detection and localization of organic media in artworks. *Analyst* **2015**, *140* (17), 5971-5980.
95. West, P. R.; Ishii, S.; Naik, G. V.; Emani, N. K.; Shalaev, V. M.; Boltasseva, A., Searching for better plasmonic materials. *Laser Photon. Rev.* **2010**, *4* (6), 795-808.
96. Shukla, R.; Bansal, V.; Chaudhary, M.; Basu, A.; Bhonde, R. R.; Sastry, M., Biocompatibility of gold nanoparticles and their endocytotic fate inside the cellular compartment: A microscopic overview. *Langmuir* **2005**, *21* (23), 10644-10654.
97. Carville, N. C.; Neumayer, S. M.; Manzo, M.; Gallo, K.; Rodriguez, B. J., Biocompatible Gold Nanoparticle Arrays Photodeposited on Periodically Proton

Exchanged Lithium Niobate. *Acs Biomaterials Science & Engineering* **2016**, 2 (8), 1351-1356.

98. Lee, K. S.; El-Sayed, M. A., Gold and silver nanoparticles in sensing and imaging: Sensitivity of plasmon response to size, shape, and metal composition. *Journal of Physical Chemistry B* **2006**, 110 (39), 19220-19225.

99. Lee, H. K.; Lee, Y. H.; Koh, C. S. L.; Gia, C. P. Q.; Han, X. M.; Lay, C. L.; Sim, H. Y. F.; Kao, Y. C.; An, Q.; Ling, X. Y., Designing surface-enhanced Raman scattering (SERS) platforms beyond hotspot engineering: emerging opportunities in analyte manipulations and hybrid materials. *Chemical Society Reviews* **2019**, 48 (3), 731-756.

100. Gabudean, A. M.; Focsan, M.; Astilean, S., Gold Nanorods Performing as Dual-Modal Nanoprobes via Metal-Enhanced Fluorescence (MEF) and Surface-Enhanced Raman Scattering (SERS). *Journal of Physical Chemistry C* **2012**, 116 (22), 12240-12249.

101. Qian, J.; Jiang, L.; Cai, F.; Wang, D.; He, S., Fluorescence-surface enhanced Raman scattering co-functionalized gold nanorods as near-infrared probes for purely optical in vivo imaging. *Biomaterials* **2011**, 32 (6), 1601-1610.

102. Wu, X.; Chen, J.; Li, X.; Zhao, Y.; Zughailer, S. M., Culture-free diagnostics of *Pseudomonas aeruginosa* infection by silver nanorod array based SERS from clinical sputum samples. *Nanomedicine-Nanotechnology Biology and Medicine* **2014**, 10 (8), 1863-1870.

103. Esenturk, E. N.; Walker, A. R. H., Surface-enhanced Raman scattering spectroscopy via gold nanostars. *Journal of Raman Spectroscopy* **2009**, 40 (1), 86-91.

104. Reyes, M.; Piotrowski, M.; Ang, S. K.; Chan, J. Q.; He, S. A.; Chu, J. J. H.; Kah, J. C. Y., Exploiting the Anti-Aggregation of Gold Nanostars for Rapid Detection of Hand, Foot, and Mouth Disease Causing Enterovirus 71 Using Surface-Enhanced Raman Spectroscopy. *Analytical Chemistry* **2017**, 89 (10), 5373-5381.

105. Trigari, S.; Rindi, A.; Margheri, G.; Sottini, S.; Dellepiane, G.; Giorgetti, E., Synthesis and modelling of gold nanostars with tunable morphology and extinction spectrum. *Journal of Materials Chemistry* **2011**, 21 (18), 6531-6540.

106. Wu, H. L.; Chen, C. H.; Huang, M. H., Seed-Mediated Synthesis of Branched Gold Nanocrystals Derived from the Side Growth of Pentagonal Bipyramids and the Formation of Gold Nanostars. *Chemistry of Materials* **2009**, 21 (1), 110-114.

107. Sanchez-Purra, M.; Roig-Solvas, B.; Rodriguez-Quijada, C.; Leonardo, B. M.; Hamad-Schifferli, K., Reporter Selection for Nanotags in Multiplexed Surface Enhanced Raman Spectroscopy Assays. *Acs Omega* **2018**, 3 (9), 10733-10742.

108. Reguera, J.; Langer, J.; de Aberasturi, D. J.; Liz-Marzan, L. M., Anisotropic metal nanoparticles for surface enhanced Raman scattering. *Chemical Society Reviews* **2017**, *46* (13), 3866-3885.
109. Sanchez-Purra, M.; Roig-Solvas, B.; Versiani, A.; Rodriguez-Quijada, C.; de Puig, H.; Bosch, I.; Gehrke, L.; Hamad-Schifferli, K., Design of SERS nanotags for multiplexed lateral flow immunoassays. *Molecular Systems Design & Engineering* **2017**, *2* (4), 401-409.
110. Yuan, H. K.; Khoury, C. G.; Hwang, H.; Wilson, C. M.; Grant, G. A.; Vo-Dinh, T., Gold nanostars: surfactant-free synthesis, 3D modelling, and two-photon photoluminescence imaging. *Nanotechnology* **2012**, *23* (7).
111. Rodriguez-Lorenzo, L.; Alvarez-Puebla, R. A.; Pastoriza-Santos, I.; Mazzucco, S.; Stephan, O.; Kociak, M.; Liz-Marzan, L. M.; de Abajo, F. J. G., Zeptomol Detection Through Controlled Ultrasensitive Surface-Enhanced Raman Scattering. *Journal of the American Chemical Society* **2009**, *131* (13), 4616-+.
112. Yuan, H.; Ma, W. H.; Chen, C. C.; Zhao, J. C.; Liu, J. W.; Zhu, H. Y.; Gao, X. P., Shape and SPR evolution of thorny gold nanoparticles promoted by silver ions. *Chemistry of Materials* **2007**, *19* (7), 1592-1600.
113. Zapata-Urzuza, C.; Perez-Ortiz, M.; Acosta, G. A.; Mendoza, J.; Yedra, L.; Estrade, S.; Alvarez-Lueje, A.; Nunez-Vergara, L. J.; Albericio, F.; Lavilla, R.; Kogan, M. J., Hantzsch dihydropyridines: Privileged structures for the formation of well-defined gold nanostars. *Journal of Colloid and Interface Science* **2015**, *453*, 260-269.
114. Sau, T. K.; Rogach, A. L.; Doblinger, M.; Feldmann, J., One-Step High-Yield Aqueous Synthesis of Size-Tunable Multispiked Gold Nanoparticles. *Small* **2011**, *7* (15), 2188-2194.
115. Piella, J.; Bastus, N. G.; Puntès, V., Size-Controlled Synthesis of Sub-10-nanometer Citrate-Stabilized Gold Nanoparticles and Related Optical Properties. *Chemistry of Materials* **2016**, *28* (4), 1066-1075.
116. Turkevich, J.; Stevenson, P. C.; Hillier, J., A STUDY OF THE NUCLEATION AND GROWTH PROCESSES IN THE SYNTHESIS OF COLLOIDAL GOLD. *Discussions of the Faraday Society* **1951**, (11), 55-&.
117. Li, J. F.; Zhang, Y. J.; Ding, S. Y.; Panneerselvam, R.; Tian, Z. Q., Core-Shell Nanoparticle-Enhanced Raman Spectroscopy. *Chemical Reviews* **2017**, *117* (7), 5002-5069.
118. Fan, M. K.; Lai, F. J.; Chou, H. L.; Lu, W. T.; Hwang, B. J.; Brolo, A. G., Surface-enhanced Raman scattering (SERS) from Au:Ag bimetallic nanoparticles: the effect of the molecular probe. *Chemical Science* **2013**, *4* (1), 509-515.

119. Zhang, W. Q.; Liu, J.; Niu, W. X.; Yan, H.; Lu, X. M.; Liu, B., Tip-Selective Growth of Silver on Gold Nanostars for Surface-Enhanced Raman Scattering. *Acs Applied Materials & Interfaces* **2018**, *10* (17), 14850-14856.
120. Kustner, B.; Gellner, M.; Schutz, M.; Schoppler, F.; Marx, A.; Strobel, P.; Adam, P.; Schmuck, C.; Schlucker, S., SERS Labels for Red Laser Excitation: Silica-Encapsulated SAMs on Tunable Gold/Silver Nanoshells. *Angewandte Chemie-International Edition* **2009**, *48* (11), 1950-1953.
121. Rodriguez-Lorenzo, L.; Krpetic, Z.; Barbosa, S.; Alvarez-Puebla, R. A.; Liz-Marzan, L. M.; Prior, I. A.; Brust, M., Intracellular mapping with SERS-encoded gold nanostars. *Integrative Biology* **2011**, *3* (9), 922-926.
122. Lee, S.; Chon, H.; Yoon, S. Y.; Lee, E. K.; Chang, S. I.; Lim, D. W.; Choo, J., Fabrication of SERS-fluorescence dual modal nanoprobe and application to multiplex cancer cell imaging. *Nanoscale* **2012**, *4* (1), 124-129.
123. Zhang, H.; Harpster, M. H.; Wilson, W. C.; Johnson, P. A., Surface-Enhanced Raman Scattering Detection of DNAs Derived from Virus Genomes Using Au-Coated Paramagnetic Nanoparticles. *Langmuir* **2012**, *28* (8), 4030-4037.
124. Enoki, S.; Iino, R.; Morone, N.; Kaihatsu, K.; Sakakihara, S.; Kato, N.; Noji, H., Label-Free Single-Particle Imaging of the Influenza Virus by Objective-Type Total Internal Reflection Dark-Field Microscopy. *Plos One* **2012**, *7* (11).
125. Verebes, G. S.; Melchiorre, M.; Garcia-Leis, A.; Ferreri, C.; Marzetti, C.; Torreggiani, A., Hyperspectral enhanced dark field microscopy for imaging blood cells. *Journal of Biophotonics* **2013**, *6* (11-12), 960-967.
126. Zamora-Perez, P.; Tsoutsis, D.; Xu, R. X.; Rivera-Gil, P., Hyperspectral-Enhanced Dark Field Microscopy for Single and Collective Nanoparticle Characterization in Biological Environments. *Materials* **2018**, *11* (2), 13.
127. Yim, S. Y.; Park, J. H.; Kim, M. G., Dark-field spectral imaging microscope for localized surface plasmon resonance-based biosensing. In *International Conference on Nano-Bio Sensing, Imaging, and Spectroscopy 2015*, Kim, D.; Kim, M. G.; Park, S. H., Eds. 2015; Vol. 9523.
128. Jenkins, S. V.; Qu, H. O.; Mudalige, T.; Ingle, T. M.; Wang, R. R.; Wang, F.; Howard, P. C.; Chen, J. Y.; Zhang, Y. B., Rapid determination of plasmonic nanoparticle agglomeration status in blood. *Biomaterials* **2015**, *51*, 226-237.
129. Indrasekara, A. S. D.; Johnson, S. F.; Odion, R. A.; Vo-Dinh, T., Manipulation of the Geometry and Modulation of the Optical Response of Surfactant-Free Gold Nanostars: A Systematic Bottom-Up Synthesis. *Acs Omega* **2018**, *3* (2), 2202-2210.

130. Fales, A. M.; Yuan, H. K.; Vo-Dinh, T., Development of Hybrid Silver-Coated Gold Nanostars for Nonaggregated Surface-Enhanced Raman Scattering. *Journal of Physical Chemistry C* **2014**, *118* (7), 3708-3715.



Recent Advancement in the Surface-Enhanced Raman Spectroscopy-Based Biosensors for Infectious Disease Diagnosis

Logan Hamm, Amira Gee and A. Swarnapali De Silva Indrasekara * 

Department of Chemistry, University of North Carolina at Charlotte, 9201 University City Blvd, Charlotte, NC 28203, USA; lhamm2@uncc.edu (L.H.); agee2@uncc.edu (A.G.)

* Correspondence: adesilva@uncc.edu; Tel.: +1-704-687-7848



Received: 4 March 2019; Accepted: 3 April 2019; Published: 6 April 2019

Abstract: Diagnosis is the key component in disease elimination to improve global health. However, there is a tremendous need for diagnostic innovation for neglected tropical diseases that largely consist of mosquito-borne infections and bacterial infections. Early diagnosis of these infectious diseases is critical but challenging because the biomarkers are present at low concentrations, demanding bioanalytical techniques that can deliver high sensitivity with ensured specificity. Owing to the plasmonic nanomaterials-enabled high detection sensitivities, even up to single molecules, surface-enhanced Raman spectroscopy (SERS) has gained attention as an optical analytical tool for early disease biomarker detection. In this mini-review, we highlight the SERS-based assay development tailored to detect key types of biomarkers for mosquito-borne and bacterial infections. We discuss in detail the variations of SERS-based techniques that have developed to afford qualitative and quantitative disease biomarker detection in a more accurate, affordable, and field-transferable manner. Current and emerging challenges in the advancement of SERS-based technologies from the proof-of-concept phase to the point-of-care phase are also briefly discussed.

Keywords: optical biosensors; plasmonics; surface-enhanced Raman scattering; SERS; malaria; bacterial infections; diagnostics

1. Introduction

Accurate and timely diagnosis of infectious diseases is crucial for effective disease management and epidemic preparedness. Infectious diseases caused by parasites, viruses, bacteria, and fungi are responsible for 15 million deaths each year, while more than 95% of these deaths take place in low-income countries [1]. Among them, most of the mosquito-borne and bacterial infectious diseases are included in the list of neglected tropical diseases declared by World Health organization (WHO) that need to be controlled by 2030 [2,3], which emphasizes the current urge to develop rapid diagnostic tests for the early detection of infectious diseases. Current diagnostic modalities rely on highly sensitive polymerase chain reaction (PCR), which is technically challenging and expensive for widespread implementation in resource-

Appl. Sci. **2019**, *9*, 1448

limited settings, or light microscopy-based cytological examination, which has high specificity but poor sensitivity. Therefore, it is a timely need to develop new detection modalities that bring affordable, accurate, and highly sensitive characteristics to diagnostic tests.

Among new detection modalities, surface-enhanced Raman spectroscopy (SERS) has emerged as a powerful analytical technique for molecular analysis, which can be particularly advantageous for diagnostic purposes when the Raman spectroscopy is combined with inherent optical and chemical properties of plasmonic nanoparticles [4–13]. SERS is the main method of enhancing the inherently weak Raman intensity, such that Raman scattering can be widely utilized in analytical applications.

In general, the Raman signal enhancement (commonly known as the SERS enhancement) is proposed to be a result of a combination of two main contributing phenomena, (i) electromagnetic enhancement (then main contributor) and (ii) chemical enhancement [14]. The electromagnetic enhancement is known to originate from the unique optical properties of plasmonic nanoparticles such as gold (Au) and silver (Ag). Plasmonic nanoparticles are known to generate localized electromagnetic field when their size is smaller than the wavelength of the interacting light, which is known as localized surface plasmon resonance (LSPR) [15,16]. In SERS, this intense localized electromagnetic field of the plasmonic substrate is exploited to amplify the intrinsically weak Raman scattering cross-section of analytes when they are either on or in close proximity to a plasmonic substrate [14]. The LSPR and the magnitude of SERS enhancement can be modulated by changing the size, composition, shape, and the local environment of the NP [17–25]. In the context of SERS, plasmonic nanomaterial are referred to as SERS substrates and their effectiveness as a SERS substrate is evaluated by the SERS enhancement factor [26–29].

In SERS-based sensing applications, the optical transducer (SERS substrate) and the molecular functional interface are the two main elements that dictate the performance of sensors. The optical properties of a SERS substrate affect the analytical sensitivity while the functional interface of a SERS substrate determines the detection specificity. A great deal of work has been done in designing different types of plasmonic nanoscale substrates to improve the SERS enhancement factor, hence the analytical sensitivities. The first generation of SERS substrates were mainly composed of spherical gold or silver nanoparticles or substrates [30–33]. Anisotropic nanoparticles such as rod-, cubic-, triangle-, and star-shaped plasmonic nanoparticles and two-dimensional plasmonic substrates were then introduced [25,34–39]. Due to the higher electromagnetic field concentration imparted by the antenna effect of the sharp features of the second-generation SERS substrates, higher SERS enhancement factors could be achieved [38]. As the next generation of SERS substrates, nanoparticle assemblies and three-dimensional nanoscale plasmonic substrates were then emerged, and they contain plasmonic “hot spots”, where the SERS enhancement factor is much greater [21,40–42]. In these nanoparticle assemblies, Raman active molecules are chemically or physically placed at the narrow gap between nanoparticles (“SERS hot spot”) where they can experience the maximum SERS signal enhancement [14,29,43,44]. The evolution of SERS substrates has resulted in 10–12 orders of maximum Raman signal enhancement, which, under optimum condition, could facilitate even single-molecule detection.

The molecular functional interface of a biosensor, which is the interface between the optical transducer (plasmonic nanomaterials in SERS) and the biological environment, is the key element that needs to be carefully designed in order to attain high specificity, and hence, optimize the performance of a biosensor. There are two main factors that need to be considered when designing a functional interface of a nanobiosensor on SERS-based detection; (i) the stability of the SERS substrate in a biological sample matrix and (ii) the molecular recognition moieties (proteins, peptides, nucleic acids, aptamers) that specifically capture biomarkers such as cell membrane proteins, polysaccharides, lipids, or nucleic acids

Appl. Sci. **2019**, *9*, 1448

or a matrix that capture and retain the biomarkers or pathogens or infected cells. In addition, the physical distance between the transducer and the analyte should be kept at an optimum, which is <5 nm, to obtain the higher SERS signal enhancement [14,45,46]. Therefore, the distance dependence of the SERS signal intensity should also be taken into consideration when designing the molecular recognition moieties and/or spacers. Polymer-derivatives, polyethylene glycol, and surfactants are usually used as capping ligands or surface passivation ligands to ensure the colloidal stability of plasmonic SERS substrates and also to control the non-specific surface adsorption of biomolecules in biological samples [47,48]. Molecular recognition elements such as antibodies, enzymes, complementary nucleic acid, aptamers, and peptides are either use directly as it is or attached to a passivation ligand or a molecular spacer and then incorporated in the functional interface. Surface functionalization of SERS substrate with molecular recognition elements and surface passivation ligands takes the advantage of inherent high affinity of gold and silver nanomaterials towards molecules bearing highly electronegative or charged atoms such as nitrogen, sulfur, oxygen, etc., [49]. Therefore, molecular recognition elements are usually modified to contain a functional group such as thiol (SH), primary amine (NH₂), and carboxylic acid (COOH) that can be attached to SERS substrates through dative covalent bonds to ensure strong and lasting surface attachment [50–53]. In some cases, molecular recognition elements such as proteins naturally possess primary amines or sulfur, which allows their direct attachment to nanoparticle surfaces. Ligands and molecular recognition elements modified with zwitterionic groups or the charged domains of the molecular recognition elements are also used to electrostatically attach them to plasmonic nanomaterial surfaces. Electrostatic interaction between the charged domains of the biomarkers, such as cell membrane proteins, are often used to directly capture, isolate, and retain the biomarker on plasmonic surfaces. In this case, the overall surface charge of the SERS substrate is modified using charged surface passivation ligands to tailor the functional interface depending on the biomarker of interest.

SERS as an analytical tool has been integrated into various disease diagnostic assays, including infectious diseases in two main formats; (1) label-free direct detection and (2) Raman label-enabled indirect detection. The direct detection format involves the adsorption of an analyte or the presence of an analyte in close proximity to a SERS substrate, which allows the analyte identification or quantification based on its unique SERS spectral fingerprints (intrinsic SERS signal) [54–59]. On the other hand, the indirect detection format uses a molecular recognition moiety on a SERS substrate, which capture analytes/biomarkers and bring them closer to the SERS substrate. The successful capture of analytes is then confirmed indirectly by monitoring the intense SERS signal of “reporter molecule” associated with the SERS substrate (extrinsic SERS signal) [20,21,33,40]. Reporter molecules are usually a dye or a molecule with high Raman scattering cross section that yield an intense SERS signal. Direct detection has the advantage of high specificity and capability to detect analytes without a known specific recognition element, but the spectral interference from the other components in the biological/sample matrix is a common issue. On the other hand, in indirect detection, spectral interference from the sample matrix is minimal as the analytes are isolated using molecular recognition elements, but it has the disadvantage of not being able to acquire the molecular information of the analyte/biomarker itself. Depending on the diagnostic need (binary identification, quantification, or multiplexing), and the sample matrix, the most appropriate SERS detection format could be selected.

In general, SERS-based sensing approaches have become more attractive and advantageous over conventional methods such as fluorescence due to ultra-sensitivity, even up to single-molecule detection, rich spectroscopic information provided on the molecular structure of interest that enable direct biomarker detection, and higher multiplexing capability [8,34,60–70]. Among these advantages, the multiplexed SERS detection, in particular, is very attractive in clinical settings as it allows for the detection of a panel of biomarkers ensuring higher confidence in the diagnosis and poses as a better alternative to

Appl. Sci. **2019**, *9*, 1448

the commonly used fluorescence-based multiplexed biosensing. This is because, (i) in comparison to fluorophores, Raman tags or Raman-active molecules are highly photostable, hence leading to stable SERS signal over a much longer analysis time. (ii) Raman/SERS peak widths are much narrower than fluorescence peaks, which leads to better spectral resolution, thereby facilitating higher-order multiplexing (in theory, >10) with spectrally unique Raman reporters, and (iii) different SERS tags used in a multiplexed assay can be detected under single-laser excitation source, but for each fluorophore used in a multiplexed biosensing assay, a separate laser excitation source is required. That means the less sophistication in instrumentation and experimental setup needed for SERS multiplexing is much more appealing when developing biosensors for point-of-care (POC) applications.

In this mini-review, we highlight the progress in the development in SERS-based diagnostic assays mainly for bacterial infections and mosquito-borne infections. In each section, the current SERS-based assays for common disease biomarkers (nucleic acid, proteins, and metabolites) followed by pre-sample preparation for SERS analysis and diagnostic device designs are discussed. Throughout the review, analytical figure of merits is provided as a guide to the reader to decide the quantitative and qualitative detection capabilities and limitations of each SERS-based diagnostic assays. Challenges and areas of improvements in designing SERS substrates and devices to transform these SERS-based technologies from the lab bench to the field are also briefly discussed. A summary of the highlighted work outlining the disease, biomarker, type of SERS detection (direct/indirect), transducer, and limit of detection (LOD) is also provided for the readers' benefit in the Table 1.

2. Bacterial Infections

SERS-based methods have enabled the detection of various types of bacterial biomarkers ranging from nucleic acids to proteins. The evolution of SERS-based detection methods improves the possibility of POC diagnostics by fabricating functional nanoparticles to achieve specific biomarker identification and higher SERS sensitivities. The functionality of nanoparticles can affect the efficiency and accuracy of target biomarker(s) detection. Device fabrication also plays a major role in the SERS-based detection of bacterial infections, particularly for field transferable applications. Recent advancements that have led to improved sensitivity and specificity in SERS-based bacterial infection detection are discussed in the following sections.

2.1. Nucleic Acid Biomarkers

Nucleic acids are a well-established group of biomarkers for detecting bacterial infections [5,59,66,71–74]. Knowing the pathogenic DNA and RNA sequences facilitates the design of complementary strand(s) to specifically capture pathogenic RNA or single-stranded DNA, and hence, to identify them either directly or indirectly using SERS [72,75,76]. The nature of DNA and RNA, however, poses challenges in preparing sample to develop SERS-based diagnostic assays. The presence of smaller copy numbers of pathogenic nucleic acid biomarkers at the early stages of disease onset and their extraction and isolation from sample matrices make nucleic acid biomarker detection with no amplification very challenging. Therefore, as a common practice, synthetic nucleic acid sequences and also polymerase chain reaction (PCR)-amplified nucleic acid biomarkers from clinical samples are usually used in the proof-of-concept assays to optimize the assay parameters, and hence, the assay performance. Once the assay is optimized for analytical sensitivities and specificities, analysis in real biological/clinical samples with no nucleic acid amplification is carried out for field-transferable adaptation and optimization of the SERS-based diagnostic assays.

Most of the studies have used cultured bacterial suspensions to test SERS-based assays as a preliminary step for proof-of-concept testing [7,59,66,72,73,77–86]. The extraction of the DNA/RNA from

Appl. Sci. **2019**, *9*, 1448

the cultured bacterial cells of interest is crucial in order to remove background noise from other biomarkers, like cell membrane and metabolite biomarkers. The extracted nucleic acid is often amplified using PCR in order to reach the analytical sensitivities of the instrumentation as the concentrations of nucleic acid biomarkers are very low at early disease stages. For instance, Popp's group developed a combinatorial approach using PCR and SERS to detect epizootic pathogen DNA from cultured cells [72]. However, the sample preparation can be extensive when using PCR as it requires culturing of bacterial cells to extract DNA, followed by extensive purification and isolation steps. Clinical/biological samples have high background noise in SERS assays, which originates from the biological matrix in which the target DNA resides, therefore it requires more sample preparation. While sample preparation for nucleic acid detection has its inherent challenges, SERS-based high sensitivities at the picomolar to attomolar levels can still be achieved. For instance, in 2010, Bongsoo et al. used bacterial genomic DNA as the biomarker for four different pathogenic strains of bacteria and reported a limit of detection (LOD) of each pathogen ranging from 10 pM–10 nM using indirect SERS [66]. In their method, the target genomic DNA from four bacterial pathogens that causes various infections were first extracted and then amplified by PCR. The target DNA biomarkers for this study originated from reference bacteria and as well as clinically isolated samples such as cerebrospinal fluid, stool, pus, and sputum.

Among SERS-based nucleic acid detection methods, direct and indirect sandwich assays are the most common approach. It involves hybridization of a target nucleic acid sequence (target probe) with a capture sequence (capture probe) and reporter sequence linked to a Raman tag (reporter probe) and a plasmonic nanoparticle. For instance, Kim et al. presented an indirect SERS detection of PCR-amplified pathogenic DNA using a sandwich assay (Figure 1) [66]. They used two modified complementary DNA sequences, a 3'-thiol modified sequence attached to a gold nanowire (capture probe) and a 5'-Raman tag-modified sequence attached to gold nanoparticles through the 3'-thiol functional group (reporter probe), that hybridize specifically to two different sequence positions of the target DNA sequence. The complete hybridization of these three sequences is exhibited by the unique SERS signal of the Raman tag, indicating the presence of target DNA and resulting in a low LOD. Recently, Faulds's group also developed a new assay format for multiplexed SERS-based indirect detection and quantification of three meningitis pathogens using a sandwich assay [5]. They used two modified complementary DNA sequences to the target DNA sequence, a 3'-biotinylated modified sequence (capture probe) and a 5'-Raman tag-modified sequence (reporter probe). The newly formed duplex is retained on a streptavidin functionalized bead. Then, they used I-exonuclease to digest the double-stranded DNA. The DNA sequences are designed in such a way that the digestion product contains the Raman tag. The digestion products were then added to a solution containing silver nanoparticles for the SERS detection of the digestion product. The complete hybridization of these three sequences provides the unique SERS signal of the Raman tag, indicating the presence of the target DNA and resulting the LOD in the picomolar range. This approach provides higher specificity due to the hybridization between the target and two complementary sequences.

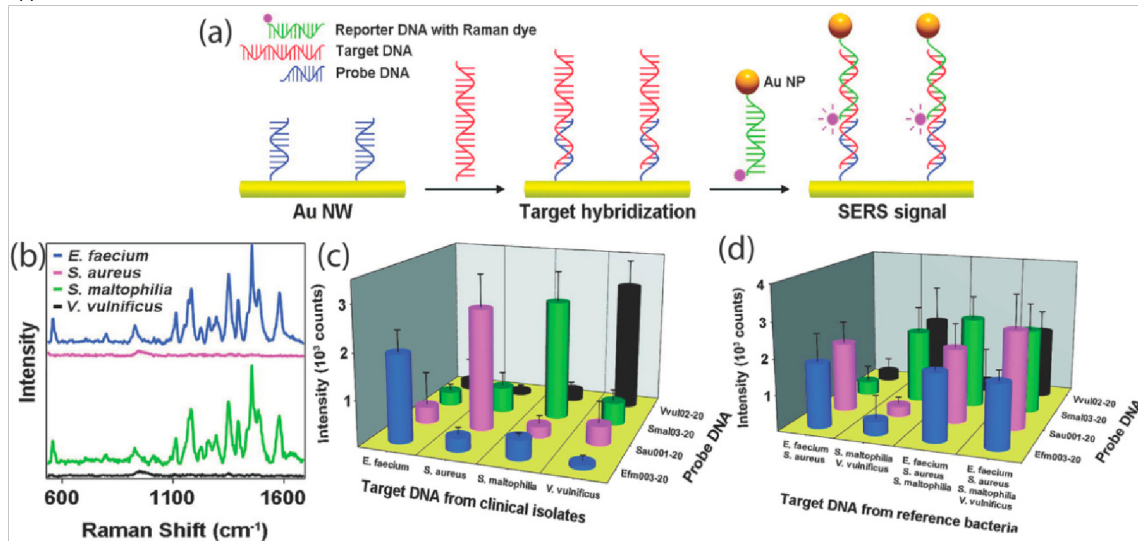


Figure 1. (a) An indirect surface-enhanced Raman spectroscopy (SERS)-based method for PCR-amplified pathogenic DNA detection. This method utilizes a sandwich hybridization event between a capture DNA sequence on gold nanowires and Raman reporter-labeled DNA sequence on with a target pathogenic DNA. (b) SERS spectra from each of the four nanowire systems in the presence of only the target DNAs of *Enterococcus faecium* and *Stenotrophomonas maltophilia*. SERS spectra of the Raman reporter (Cy5) detected only for *E. faecium* and *S. maltophilia* sensors. (c) SERS-based identification of amplified pathogenic DNA in clinical samples. (d) SERS-based multiplexed detection when all four target DNAs are present at 10^{-8} M each. Reproduced with permission from Reference [66] American Chemical Society (2010).

Direct, label-free SERS detection of nucleic acids has also been used despite common indirect detection methods [73,74]. Kaminska et al. introduced a new class of label-free (direct SERS) SERS-based assay to detect *Neisseria meningitidis*, *Streptococcus pneumoniae*, and *Haemophilus influenzae* in cerebrospinal fluid (CSF) using their unique cell membrane biomarkers such as lipids and polysaccharides [74]. Their assay is based on the Au–Ag coated polycarbonate membranes that allow simultaneous filtration of CSF and immobilization of CSF components to enhance their intrinsic SERS signature. This approach facilitates the direct detection of nitrogenous bases of target DNA and neopterin at the single-bacteria cell level. Direct detection of nucleic acids can be challenging because of the background noise from the biological matrix.

SERS-based diagnostic methods using clinical samples have also been conducted to determine the applicability towards POC applications [78–80,87–90]. Porter’s group reported a novel sandwich SERS immunoassay for an antigenic biomarker for tuberculosis found in bodily fluids using a handheld Raman spectrometer [90]. They used serum samples to detect phospho-myo-inositol-capped lipoarabinomannan (PILAM), a stimulant of an antigenic biomarker found in tuberculosis infected patients. Their method requires sample pretreatment in order to eliminate any possible non-specific interaction between the PILAM and the other constituents found naturally in the serum sample. It is important to eliminate unnecessary biological interactions to ensure high detection specificity and, more importantly, to remove the biological matrix interferences to achieve high signal-to-noise ratio in SERS signal for high analytical sensitivity. The sample was acidified in order to denature proteins that could bind to PILAM. These denatured proteins and insoluble components were separated from the PILAM by centrifugation. The PILAM-enriched supernatant was extracted and neutralized to be used for a SERS assay. While the added

Appl. Sci. **2019**, *9*, 1448

sample pretreatment is not an extensive protocol, it shows the necessity of developing methods that require minimum or no sample preparation to transform these assays towards POC diagnosis of infectious bacterial diseases.

With impressive technological and technical growth in the microbiology and gene sequencing, a wide range of nucleic acids (DNA, RNA, non-coding RNA) biomarkers for disease diagnosis are being reported more frequently than before. Having access to such rich genetic information is highly beneficial to the scientists working in the POC SERS diagnostics as it will allow us to design SERS probes and assays that ensure high detection specificities and high-throughput detection protocols. This will immensely assist the performance of analysis in biological samples with no nucleic acid amplification carried out in the field-transferable adaptation and optimization of the SERS-based diagnostic assays.

2.2. Cell Membrane Biomarkers

Cellular membrane macromolecules, especially proteins, have proven to be a major pathogenic biomarker for SERS-based diagnostics [7,72,73,79–81,84–88,91]. Cell membrane proteins have been used as biomarkers to detect various bacterial infections such as Methicillin-resistant *Staphylococcus aureus* (MRSA) [73,86], urinary tract infection (UTI) [85], and strep throat [88]. For instance, Konkel's group used silver nanoparticles in solution for the direct, label-free SERS detection of proteins and nucleic acids in MRSA [73]. Cell membrane proteins in *Escherichia coli* and *Proteus mirabilis* cells that cause urinary tract infections have also been detected using intrinsic Raman signature (e.g., ring breathing/stretching, carbohydrate, and protein vibrations). In this study, the required sensitivity for intrinsic SERS-based detection was achieved using a SERS platform that was composed of silver nanoparticles decorated on a glass substrate [85]. Assay development for cell membrane biomarker detection has been integrated into microfluidic devices [7,73,79] and in solution assays [80,81]. For instance, in 2013, Ray et al. reported the use of intrinsic SERS signature a cell membrane biomarker to detect MRSA with a 10 CFU/mL limit [86]. The SERS spectra produced from the MRSA cell wall consisted of peaks corresponding to ring breathing of tyrosine protein, saturated lipids, and other vibrational modes of cell membrane biomarkers. In order to achieve such high sensitivity in label-free detection, they used graphene oxide modified with an aptamer that selectively binds to Enterotoxin B, which is a prominent MRSA protein, and gold nanopopcorn that provides good resolving power for SERS-based detection. It is reported that a higher analytical sensitivity was able to be achieved because they used the hybrid graphene oxide-based SERS substrates, which exhibited around 2 orders of magnitude higher SERS enhancement than only gold nanoparticle-based SERS substrates. They attributed the higher SERS enhancement effect originated from the hybrid graphene oxide-based SERS substrates to the contribution from both the electromagnetic and chemical enhancement effects simultaneously. This is an example that displays the improvements of the analytical sensitivities achieved by tailored designing of the SERS substrates.

In SERS-based diagnostic methods, protein biomarkers offer more advantages; (i) the ability to capture bacterial antigens using antibodies and (ii) the availability and accessibility of a larger quantity of proteins in comparison to nucleic acid biomarkers. Krause et al. used P30 and P65 proteins to detect and differentiate *Mycoplasma pneumoniae* strains FH, M129, and II-3 from clinical throat swabs and cultured bacteria [80]. They observed a variation in the concentration of proteins of interests between different strains of *M. pneumoniae*. Their results showed >97% accuracy in identifying the strains from the throat swabs; thus, further displaying the clinical possibilities of SERS-based detection of protein biomarkers. This work shows the high sensitivity of SERS that enables protein biomarker detection that can even discriminate different bacterial pathogenic strains with increased specificity. Antibodies can act as good capture moieties due to specific binding affinity of proteins to antibodies, which ensures high analytical specificity for proteins biomarkers. Peripheral proteins, or surface proteins, are typically targeted as they

Appl. Sci. **2019**, *9*, 1448

can be easily accessible by nanoparticles to come in close proximity for SERS signal enhancement [79,80]. If a specific integral protein or a protein naturally found inside the cell is targeted, then the sample preparation for that method would require protein extraction from the bacterial cells. Added sample preparation can result in POC diagnosis being out of reach, however, protein has still proven to be a good biomarker for possible diagnosis in clinical settings [77,80,82,84–86,88,91]. Han et al. detected muramidase-released protein antibody against *Streptococcus suis II* in pig serum to demonstrate the potential clinical applicability of their indirect immuno-SERS assay [88]. While not all methods are clinically viable, some can be adapted for field-transferable applications. For example, Boyacı, Ismail et al. developed a method for indirect detection of *E. coli* in a water sample using a biotin-conjugated polyclonal antibody, which could be used by environmental scientists in the field [84].

Both direct and indirect SERS assays are commonly utilized for protein and cellular membrane biomarker detection. In comparison to nucleic acids, protein detection involves less sample preparation and nanoparticle fabrication. The close proximity of nanoparticles to the target bacteria provides an amplified Raman signal of the proteins, lipids, and carbohydrates directly, hence no extensive surface functionalization of nanoparticles is required [79,82,86,91]. Choi et al. used a gold nanoparticle-deposited paper for direct detection of cell membrane biomarkers in infectious keratoconjunctivitis (Figure 2) [91]. This method exhibited a SERS enhancement factor of 7.8×10^8 , which shows that the current approach can result in good sensitivities without the functionalization of nanoparticles. Depending on what proteins are being detected, extraction may be necessary. Extracted protein samples can still be used in direct SERS detection assays. Indirect detection of proteins involves antibodies adhered to the nanoparticles through bioconjugation method. For instance, Boyacı, Ismail et al. used gold nanorods labeled with a Raman reporter and gold-coated magnetic nanoparticles both of which are functionalized with anti-*E. coli* antibodies for the detection of *E. coli* [84]. In this approach, immunoaffinity between the *E. coli* and anti-*E. coli* antibodies immobilized on gold-coated magnetic nanoparticles is first used to selectively separate and concentrate *E. coli* from the rest of the sample. Then, the resultant complex is allowed to form a sandwich with the anti-*E. coli* antibodies immobilized on gold nanorods for identification and quantification of *E. coli* using the SERS signal originated from the Raman reporter encoded in gold nanorods. Using this approach, they were able to achieve 8 CFU mL⁻¹ LOD and 24 CFU mL⁻¹ limit of quantification.

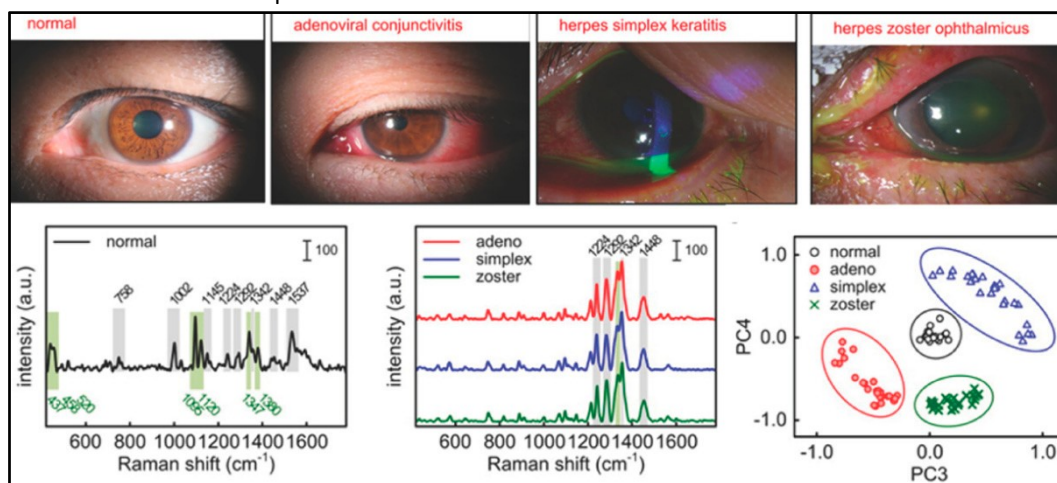


Figure 2. Direct, label-free cell membrane biomarker detection in bodily fluid using SERS. (Top) Photographs of a healthy and three types of keratoconjunctivitis, an infectious eye disease. Raman spectrum of (bottom left) a normal eye fluid and (bottom middle) fluid from the three types of eye

Appl. Sci. **2019**, *9*, 1448

infections. (Bottom right) PCA score plot classifying the normal and the three infected eyes based on the SERS spectra. Reproduced with permission from Reference [91] American Chemical Society (2016).

In general, immunoassays (traditional and SERS-based) that use protein biomarkers are still the most commonly used, widely studied, and even integrated into the commercialized diagnostics. However, in moving forward, we have two main important challenges to overcome; (i) the need for a known antibody for each protein biomarker and the cost associated with the production of antibodies for indirect SERS detection, and (ii) the complexity of the intrinsic SERS signature of proteins in direct SERS-based detection schemes. On a positive note, we believe that the current progress in finding alternatives to monoclonal antibodies, such as aptamers, and the machine learning for complex spectral analysis could contribute to overcome the abovementioned issues.

2.3. Metabolites as Biomarkers

In comparison to proteins and nucleic acids, cellular metabolites are not yet a common biomarker for SERS-based pathogen detection [74,77,78,83,87,90]. Metabolic processes can differ between bacteria that cause infections, therefore certain metabolites are targeted for increased specificity. Intrinsic SERS of metabolites is mostly used in direct SERS detection methods [74,78,87]. With the lack of work done on metabolites compared to proteins and nucleic acids, detection schemes are limited. Zughaier et al. targeted pyocyanin (PCN), a major secondary metabolic biomarker of *Pseudomonas aeruginosa*, which can cause pneumonia and urinary tract infections [78]. They and other groups reported above 90% sensitivity that can be achieved using similar bacterial metabolites [74,78,87]. Extensive background knowledge of the bacterium is necessary to understand the proper sample preparation and where the largest concentration of the metabolite resides. Sample fluids for metabolite detection of a bacterial pathogen can vary, ranging from clinical sputum, cerebrospinal fluid (CSF), to blood samples [74,78,90]. Sample preparation for metabolites can be challenging. Device substrates such as a “lab-on-a-chip” SERS platforms are common for metabolite detection. Ziegler et al. used an aggregated gold nanoparticle-covered silica substrate as a SERS substrate to detect urinary tract infection pathogens [87]. They used an in situ, two-step reduction method to synthesize the aggregated gold nanoparticles on the silica substrate (Figure 3). With this device, they directly detected the vibrational modes of nucleic acid metabolic degradation metabolites such as adenine, hypoxanthine, xanthine, guanine, uric acid, and adenosine monophosphate. Direct detection suits for this method because of the varying concentrations of abovementioned metabolites in the extracellular region of different bacterial strains creating unique, intrinsic SERS spectra. Their work displayed >95% sensitivity and >99% specificity for direct SERS detection of target metabolites. With current methods achieving high sensitivities, metabolite detection does have a promising future in POC applications [74,78,87,90]. While it is still in its infancy to exploit the metabolites of the pathogen in the SERS biosensing assay, in our opinion, the metabolites could be one of the best biomarker options as they facilitate simple label-free SERS detection. Simplicity in the assay development and the detection scheme could be highly favorable for POC applications. We hope that more metabolite-based SERS diagnostic assays will be seen in the future as biologists better understand the molecular level processes of the pathogens.

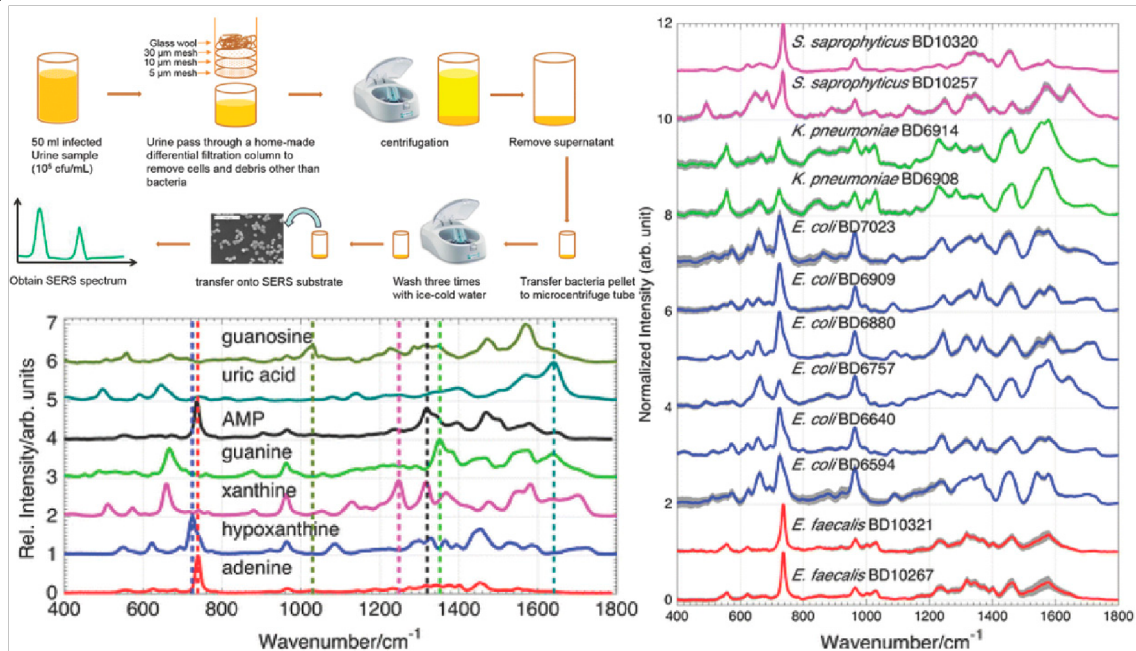


Figure 3. (Top Left) Sample preparation steps for urine samples spiked with bacterial strains of urinary tract infection (UTI) clinical isolates for SERS-based direct detection of nucleic acid metabolites. (Right) SERS spectra of 12 different UTI bacterial strains exhibiting unique biomarker signatures that were produced from sample on an aggregated gold nanoparticle-covered silica substrate. (Bottom Left) Intrinsic SERS spectra of seven key metabolite biomarkers used in the differentiation of the 12 UTI bacterial strains. Reproduced with permission from Reference [87] Springer (2017).

3. Mosquito-Borne Infections

Mosquito-borne diseases such as Malaria, dengue, West Nile Virus, River Valley Fever, and Zika are caused by either a virus or parasite, and they have gained the most attention in the global health-focused communities for the last few decades. These diseases are usually diagnosed by a blood test to identify the presence of parasites or virus. In order to improve the timely diagnosis of mosquito-borne infectious disease, specific biomarkers must be analyzed through more robust diagnostics. Herein, we discuss advances in the SERS-based approaches for the sensitive detection of mosquito-borne infectious disease biomarkers.

3.1. Nucleic Acid Biomarker Detection

Nucleic acids, both DNAs and RNAs (coding and non-coding), are valuable biomarkers for infectious disease detection. In 2011, Zhang et al. designed a proof-of-concept SERS assay to detect DNA oligonucleotides obtained from the West Nile virus (WNV) genome. They used the classical sandwich assay where hybridization between the complementary oligonucleotide probes covalently linked to paramagnetic nanoparticle (capture probe) and Raman-reporter conjugated-gold nanoparticles (reporter probe) and the target DNA sequence to design an indirect SERS assay for WNV detection [92]. They later simplified this method to do multiplexed detection of viral DNA of WNV and Rift Valley virus (RVFV) and also intensify the SERS response by magnetic enrichment [93]. They used a capture probe attached to a gold-coated paramagnetic nanoparticle that have both magnetic and SERS properties, and a reporter probe with a Raman tag as the key components. Each of these probes has specific complementary oligonucleotide sequences to the opposing ends of the target WNV DNA sequence. In the presence of the

Appl. Sci. **2019**, *9*, 1448

target DNA, a hybridized complex between capture–target–reporter probe is formed. It is then magnetically enriched using Au-coated paramagnetic nanoparticle and the SERS signal is recorded. Herein, the capture of target DNA is indirectly detected by monitoring the SERS spectrum of the Raman tag associated with the reporter probe. The LOD was determined to be in the low nanomolar range (20–100 nM) requiring only 1 h for the assay.

Lab-on-a-chip SERS substrates are another common approach for DNA biomarker detection. The Vo-Dinh group at Duke University developed a bioassay-on-chip using plasmonic bimetallic nanowave to detect dengue viral DNA [94]. They used gold and silver nanowaves to develop a highly sensitive SERS substrate, which was subsequently functionalized with reporter probes carrying a Raman tag for dengue viral DNA. They designed a new type of reporter probe with a placeholder, which is covalently linked to the plasmonic nanowaves. In the absence of the target sequence, the reporter probe and the placeholder maintain a partially duplex complex. It keeps the Raman tag at the end of the reporter probe away from the SERS substrate at a distance where the SERS effect is negligible and therefore no significant SERS signal is detected—SERS “off” state. In the presence of target viral DNA, placeholder hybridizes with the target DNA, leaving the reporter probe to form a hair loop.

This hair loop structure brings the Raman tag back into very close proximity to the SERS substrate (SERS “ON”) hence producing a measurable SERS signal. The LOD of this approach was determined to be 6 attomoles. The same group later developed another simpler detection strategy based on sandwich DNA hybridization to detect malaria DNA biomarkers [95]. The target DNA was identified using single nucleotide polymorphism discrimination via ultrabright SERS nanoparticles known as nanorattles and then enriched using magnetic beads. The ultrabright nanorattles are functionalized with SERS reporter DNA probes and the magnetic beads are coated with the capture DNA probes. Once the target DNA is introduced, complexation of magnetic beads and nanorattles takes place due to the sandwich DNA hybridization between target-capture and reporter DNA probes. This allowed them to concentrate hybridized complex in a localized position using a magnet for SERS measurements and achieve LOD at 3 picomolar.

The most recent work by the Vo-Dinh group reported a highly sensitive SERS-based diagnostic assay to detect Malaria ribosomal RNA (rRNA) in blood lysates without target amplification [96]. They introduced a lab-in-a-stick portable device concept that process blood samples for SERS-based detection of 18s rRNA (unamplified) from the Malaria parasite (Figure 4). Their detection strategy involves ultrabright SERS-encoded nanorattles. The nanorattle-based sandwich assay used magnetic beads functionalized with capture probes and nanorattles with reporter probes. In the presence of target, hybridized nanoparticle complex forms a pellet, which is localized inside the capillary tube using a magnet while leaving any unreacted analytes or other biological components behind. Passing the pellet through different washing compartments inside the capillary tube with the assistance of a magnet, non-specific binding can be largely eliminated/removed, thereby ensuring high specificity in the recorded SERS measurements. The most appealing feature of this approach is that it involves no RNA extraction nor PCR amplification yet achieves an LOD at 200 fM in Malaria-infected blood samples, which exhibits more field-transferable characteristics for a SERS diagnostic assay.

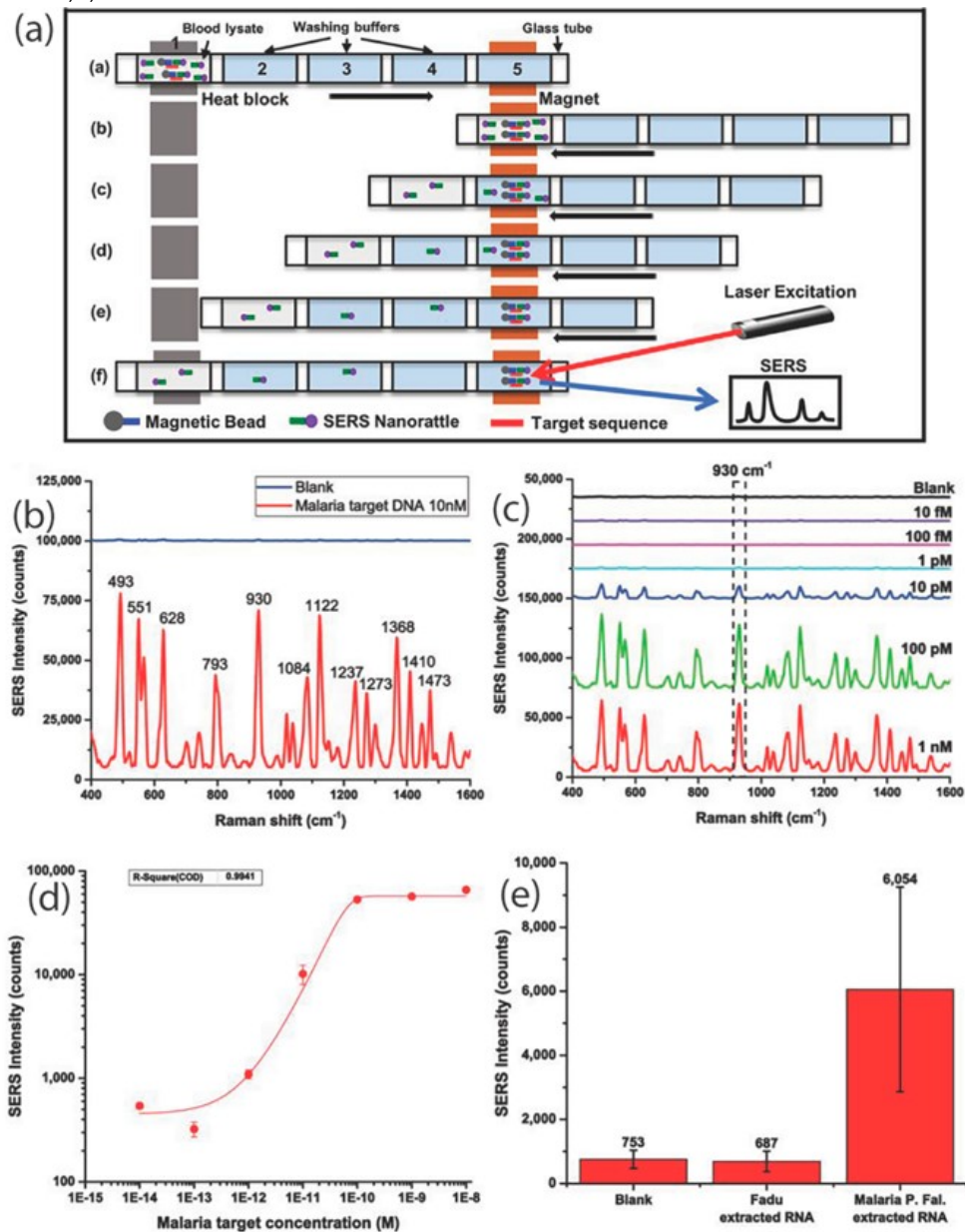


Figure 4. (a) Direct detection of *plasmodium falciparum*, malaria parasite, using an unamplified DNA and RNA biomarker. RNA biomarker sequence hybridized to the capture probe sequence on a magnetic bead and the reporter probe sequence on an ultra-bright SERS nanorattle with in a lab-in-a-stick device detection scheme. (b) SERS spectra displaying malaria synthetic DNA versus blank and (c) Malaria synthetic DNA with a concentration range of 10 fM to 1 nM. (d) Quantification of target DNA using the SERS intensity at the reporter signature peak at 930 cm^{-1} , (e). Malaria *P. falciparum* 18S rRNA detection in blood lysate. Reproduced with permission from Reference [96] Scientific Reports (2018).

3.2. Proteins

Antibodies are used in immunoassays to detect protein biomarkers associated with infectious diseases. Brolo et al. used SERS nanoprobe in an immunoassay to detect Zika virus [97]. They used gold shell-isolated nanoparticles as the SERS substrate, where a Raman reporter (Nile Blue) is embedded in a

Appl. Sci. **2019**, *9*, 1448

silica shell to prevent leaching and the silica surface is functionalized with monoclonal anti-Zika NS1 antigens. This method was able to ensure high specificity that they observed no cross-reactivity with DENV NS1 antigens and to provide 10 ng/mL LOD for ZIKV NS1. In 2010, Johnson et al. focused on designing a SERS immunoassay to detect the WNV. They used WNV antigen-coated gold nanostars and matchite green Raman reporter-conjugated proteins. When the antigen functionalized gold nanostars captures the target WNV proteins, it can be detected using the Raman spectral signature of matchite green. The LOD of this SERS immunoassay was determined to be 2 ng/mL while resulting sensitivity of 50 pg/mL [98]. Later, they designed another type of SERS immunoassay to detect the surface envelope and capsid antigens of WNV and RVF. Raman reporter coated-gold nanoparticles and paramagnetic nanoparticles were conjugated with disease specific polyclonal antibodies, which resulted LOD near 5 fg/mL [99]. Then, in 2018, they reported multiplexed immunoSERS for the detection of viral pathogenic antigens associated with WNV, RVF, and *Yersinia pestis* [100]. Both magnetic nanoparticles and SERS reporter-embedded silica-coated gold nanoparticles were functionalized with the polyclonal antibodies in order to capture the disease specific antigens. An external magnetic field was used to aggregate the antigen-, magnetic nanoparticle-, and silica-coated gold nanoparticle complex. The unique SERS spectrum of the Raman tags embedded in the silica-coated gold nanoparticles was then used to indirectly detect each captured antigen, which has enabled the multiplexed SERS-based protein biomarker detection with the LOD at 10 pg/mL.

Protein-induced plasmonic nanoparticle aggregation has also been used to detect protein biomarkers using their intrinsic SERS signatures (direct SERS). Kah et al. used gold nanostars (GNS) to design an approach for label-free direct SERS detection of Enterovirus 71 (EV71) [101]. This approach is very attractive for POC diagnosis given the fact that it is based on the intrinsic SERS of proteins (Figure 5). In this study, GNS were conjugated to a recombinant scavenger receptor class B, member 2 (SCARB2) protein, which has an established affinity for EV71. When the GNS-SCARB2 is introduced to the infected sample, they conjugate to EV71 hence facilitating the direct detection of EV71 while preventing GNS aggregation. This method has yield LOD comparable to other approaches at 10^6 to 10^8 pfu/mL. In addition, the high sensitivity (10^7 pfu/ mL), low amount of sample preparation, and only 15-minute analysis time are favorable characteristics, which make this assay more appealing for POC applications. Recently, Hamad-Schifferli's group developed a multiplexed SERS-based dipstick immunoassay to distinguish between Zika and dengue [102]. In this study, they used SERS tags-encoded GNS conjugated to Zika and dengue specific antibodies to detect nonstructural protein 1 (NS 1) specific to Zika and dengue as the biomarkers (Figure 6). This diagnostic assay combined the simplicity of lateral flow assay (LFA) with the high sensitivity of SERS where 15-fold and 7-fold LOD for Zika and dengue biomarkers, respectively. Serum and saliva have also been used as sources of diagnostic protein biomarkers for mosquito-borne diseases. Ray et al. used anti-flavivirus 4G2 antibody conjugated gold nanoparticle with Raman probes to detect dengue and WNV in serum samples. The LOD was determined to be 10 PFU/mL for both dengue and WNV due to the plasmon coupling in nanoassembly [103].

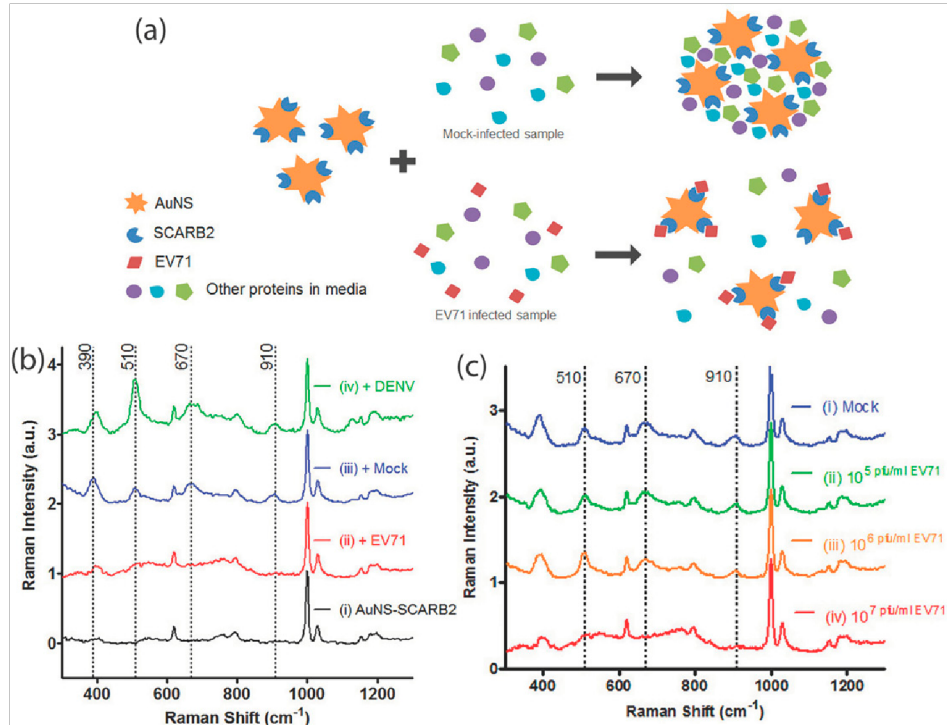


Figure 5. Direct, label-free SERS-based detection of enterovirus 71 using gold nanostars conjugated to recombinant scavenger receptor class B, member 2 (SCARB2) protein. (a) Schematic representation of the enterovirus 71 detection by SCARB2 protein-functionalized gold nanoparticles. (b) SERS spectral differences of AuNS-SCARB2 in the presence of EV71 in comparison to other control proteins, which indicates analytical specificity of this approach and (c) concentration dependence of the SERS intensity of the AuNS-SCARB2- EV71 conjugate. Reproduced with permission from Reference [101] American Chemical Society (2011).

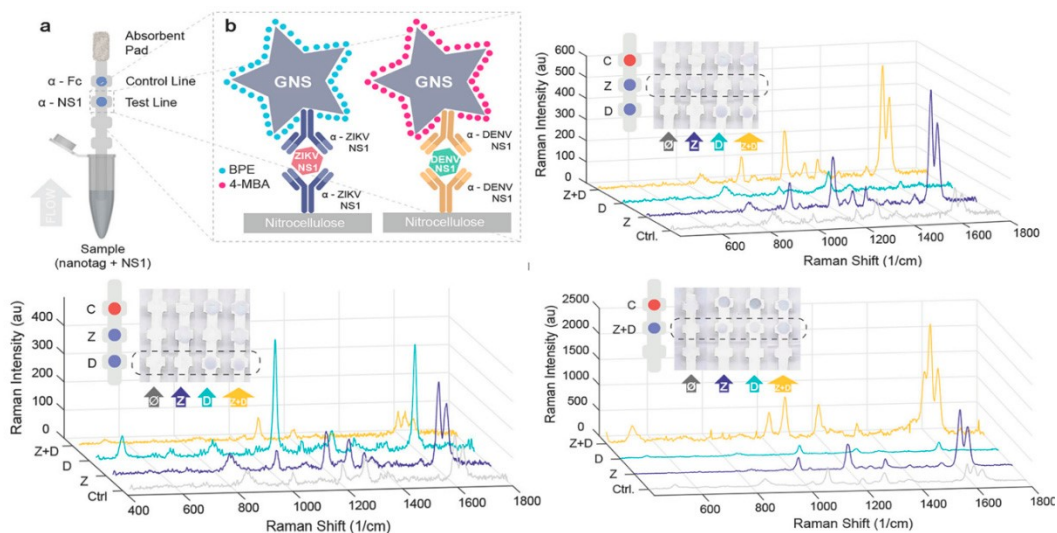


Figure 6. Multiplexed SERS-based indirect detection of Zika and dengue using dipstick sandwich immunoassay. (top left) Schematic diagram of dipstick immunoassay where sandwiches are formed by each antibody pair, NS1, and gold nanostars–Ab conjugate for both ZIKV and DENV NS1. SERS spectra of the conjugates

Appl. Sci. **2019**, *9*, 1448

(top left) Zika and (bottom left) dengue test line separately and (bottom right) both Zika and dengue in the same test line. Samples: The control (C) (gray), ZIKV NS1 (blue), DENV NS1 (cyan), and a mixture of ZIKV and DENV NS1 (yellow). Reproduced with permission from Reference [102] American Chemical Society (2011).

3.3. Metabolites as Biomarkers

Changes in the red blood cells (RBC) have been traditionally used to detect mosquito-borne infection, and it has also been found that some of the molecular changes in RBC can also be detected using SERS to potentially achieve high diagnostic sensitivities. Zhao's group at the University of Georgia used the SERS spectral features apparent in RBC infected with *Plasmodium falciparum* (iRBC) to differentiate varying stages of the parasite in the blood as iRBC at different post-invasion times exhibit different cell membrane modifications [104]. In this study, they analyzed and compared the intrinsic spectral signatures of healthy RBC and iRBC on silver nanorod array substrates. For instance, a unique SERS peak at $\Delta\nu = 1599 \text{ cm}^{-1}$ for ring stage iRBCs, and a SERS speak characteristic to trophozoite, and schizoid stages were at $\Delta\nu = 723 \text{ cm}^{-1}$ identified while none of them were present in healthy RBC (Figure 7). This intrinsic SERS-based assay reported $1.5 \times 10^7/\text{mL}$ LOD for both RBCs and iRBCs. In addition, there are several other reports that uses either Raman or resonance Raman to identify the erythrocyte membrane alterations at iRBC at different post-invasion times [105–108].

Hemozoin, a metabolite found in malaria-infected blood has also been used as a biomarker for early malaria diagnosis [109–112]. In 2012, Yuen et al. used SERS-active magnetic nanoparticles composed of iron oxide core and silver shell to detect hemozoin in iRBC based on its intrinsic SERS signature [113]. Hemozoin, which is paramagnetic in nature, was enriched using an external magnetic field on the iron oxide core and then the amplified SERS signal on silver shell was measured. They observed that the SERS signal without the use of the magnetic field is about two orders of magnitude lower than signals reported without the magnetic enrichment (Figure 7). The LOD for β -hematin was determined to be 5 nM, which is approximately equivalent to 30 parasites/ μL present at the early stages of malaria infection [113]. The same group later developed a method for SERS-based hemozoin detection in iRBC using only plasmonic nanoparticle, but with no need for an external magnetic field [109]. This improvement was done in order to eliminate any additional variation in SERS readings that could have originated from the magnetic enrichment and hence improve the SERS-based quantification capability. They used two approaches; (i) synthesized silver nanoparticles in the blood or (ii) pre-synthesized silver nanoparticles added to a blood sample. The first approach has exhibited lower variation in the SERS measurement, which could be more suitable for quantification of the parasitemia level. On the other hand, the second method has resulted in a higher sensitivity, with the LOD as low as 0.00005% parasitemia level in the ring stage, which is approximately 2.5 parasites/ μL of blood. The reported LOD is comparable to the most sensitive detection techniques currently available, thus this approach could be more effective in early malaria diagnosis. Wood et al. also developed a novel SERS platform, which is composed of gold-coated butterfly wings for SERS-based direct detection of malarial hemozoin in lysed blood samples [114]. Using this new SERS platform, they identified key characteristic spectral features of the hemozoin in the iRBC lysate (e.g., strong pyrrole in-phase breathing vibration peak at 1375 cm^{-1}) that indicate the presence of early-ring stage parasitemia levels and provided the LOD between 0.0005% and 0.005%.

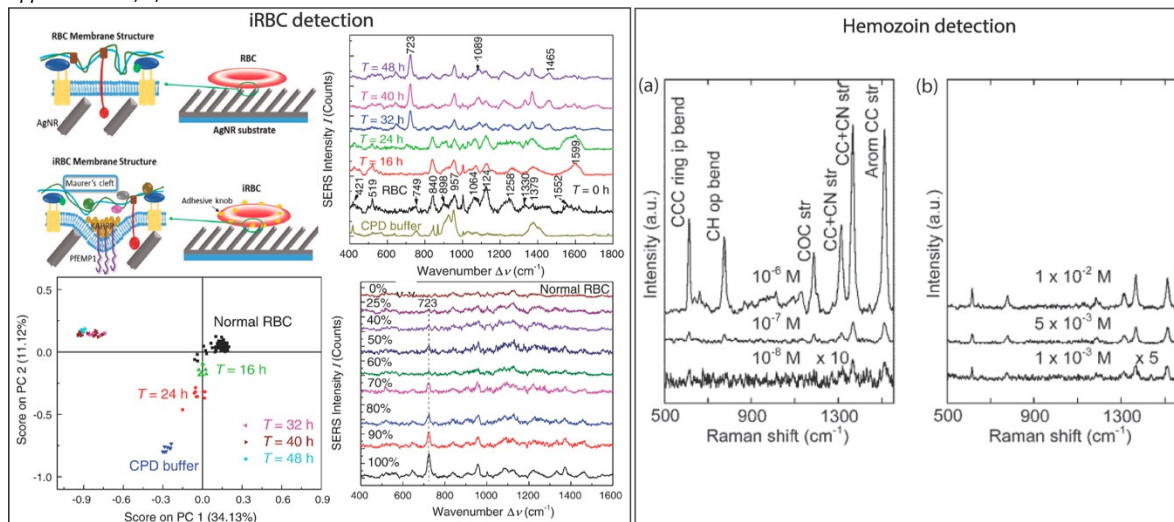


Figure 7. SERS-based malaria metabolite detection. Intrinsic SERS signature of infected red blood cells (iRBC) using silver nanoparticle substrates. (top right) iRBCs with different infection time (up to 24 h: ring stage, after 32 h: late-stage trophozoite and schizont stage iRBCs). (bottom left) Principle component analysis (PCA) score plot for RBCs and different stages of iRBCs based on their SERS spectra. (bottom right) The SERS spectra of the mixtures of RBCs and schizont stage iRBCs at varying percentages. Reproduced with permission from Reference [104] Science Direct (2016). Detection of β -hematin crystals in blood as a malaria metabolite biomarker using magnetic nanoparticles with iron oxide and a silver shell. (a) Intrinsic SERS spectra showing the unique peak profile of β -hematin at varying concentrations and (b) changes in concentration of the target biomarker. Reproduced with permission from Reference [113] SPIE (2012).

4. SERS-Based Diagnostic Devices and Assay Platforms

Integration of biosensors into technological platforms/prototypes for field testing is critical in its transformation from the bench to the clinics or field. In particular, The World Health Organization (WHO) has identified the characteristics of a POC diagnostic that are appropriate for even the lowest-resource limited settings. They coined the acronym “ASSURED” to highlight affordable, sensitive, specific, user-friendly, rapid and robust, equipment free, and deliverable to users as the main characteristics of a diagnostic biosensor. While accuracy, accessibility, and affordability are the three main important factors, some characteristics have to be traded off to prioritize others based on the application.

Table 1. Summary of SERS-based biomarker detection methods for bacteria and mosquito-borne infectious diseases.

Disease	Target	Detection Scheme	Transducer	LOD	Ref.
Bacterial Infections					
Various bacterial infections: <i>E. faecium</i> , <i>S. aureus</i> , <i>S. Maltophilia</i> and <i>V. vulnificus</i>	DNA extracted from clinical samples of cerebrospinal fluid, stool, and sputum	Indirect SERS	Gold nanowires & nanoparticles	10 pM	[66]
Bacterial meningitis pathogens: <i>N. meningitidis</i> , <i>S. pneumoniae</i> and <i>H. influenzae</i>	Synthetic DNA	Indirect SERS	Silver nanoparticles	pM range	[5]
contagious bovine pleuropneumonia (CBPP)	<i>MmmSC_1046</i> (lipoprotein lppQ), <i>MmmSC_0136</i> (hypothetical transmembrane protein), and <i>Botau_125</i> (mitochondrial 12S rRNA)	Indirect SERS	streptavidin-modified magnetic nanoparticles & silver nanoparticles	Not reported	[72]
Bacterial meningitis pathogens: <i>N. meningitidis</i> , <i>S. pneumoniae</i> and <i>H. influenzae</i>	Unique Nitrogen base composition of target DNA & Neopterin (metabolites)	Direct SERS	polycarbonate membranes coated with gold & silver	Neopterin: nM range	[74]
Tuberculosis	mannose-capped lipoarabinomannan (ManLAM), a stimulant of antigenic biomarker in serum	Indirect SERS	Gold film-coated substrate & gold nanoparticles	handheld Raman system (0.18 ng/mL) & Ramaninstrument (0.032 ng/mL)	[90]
methicillin-resistant <i>S. aureus</i> (MRSA) and methicillin-sensitive <i>S. aureus</i> (MSSA)	<i>mecA</i> gene and cellular proteins	Direct SERS	Silver nanocolloids	5% to 100%	[73]
Urinary tract infection caused by <i>E. coli</i> and <i>P. mirabilis</i>	cell membrane proteins	Direct SERS	Silver nanoparticles	Not reported	[85]
Pneumonia caused by <i>M. pneumoniae</i>	Surface proteins of bacteria in clinical throat swabs	Direct SERS	Silver nanorod arrays	82 CFU/sample	[80]
Infections caused by <i>Streptococcus suis</i> II	Muramidase released protein (MRP) antibody in pig serum	Indirect SERS	Thorny gold nanoparticles	0.1 pg/mL	[88]
<i>E. coli</i>	Cellular surface antigens in real water samples	Indirect SERS	Gold nanorods with gold-coated magnetic nanoparticles	8 CFU/mL	[84]
Keratoconjunctivitis	Protein biomarkers in eye fluid	Direct SERS	Gold nanoparticles	1 pM	[91]
<i>Pseudomonas aeruginosa</i>	Pyocyanin metabolite in clinical sputum samples	Indirect SERS	Silver nanorod array	5 ppb	[78]

Table 1. Cont.

Disease	Target	Detection Scheme	Transducer	LOD	Ref.
Mosquito-borne Infectious Diseases					
West Nile Virus	Viral DNA	Indirect SERS	Paramagnetic nanoparticles and gold nanoparticles	20–100 nM	[92]
Dengue	Viral DNA	Indirect SERS	Gold and silver Nanowaves	6 attomoles	[94]
Malaria	Parasitic DNA	Indirect SERS	nanorattles and magnetic beads	3 picomolar	[95]
Malaria	Ribosomal RNA in infected blood lysates	Indirect SERS	Nanorattles and magnetic beads	200 fM	[96]
Zika	ZIKV Nonstructural protein 1 (NS1) protein	Indirect SERS	Silica-coated gold nanoparticles	10 ng/mL	[97]
West Nile Virus	WNV protein	Indirect SERS	Gold Nanostars	2 ng/mL	[98]
West Nile Virus and Rift Valley Virus	Antigens of WNV and RVF	Indirect SERS	Gold nanoparticles and Paramagnetic nanoparticles	5 fg/mL	[99]
West Nile Virus, Valley Fever Virus and Yersinia pestis	Viral pathogenic antigens	Indirect SERS	Silica-coated gold nanoparticles and Paramagnetic nanoparticles	10 pg/mL	[100]
Hand, Foot and Mouth Disease causing virus	Enterovirus 71 (EV71)	Direct SERS	Gold Nanostars	10 ⁶ to 10 ⁸ pfu/mL	[101]
Zika and Dengue	Nonstructural protein 1 (NS1)	Indirect SERS	Gold Nanostars	0.72 ng/mL of ZIKV NS1 and 7.67 ng/mL of DENV NS1	[102]
West Nile Virus and Dengue	DENV-2 and WNV proteins in serum	Direct SERS	Gold nanoparticles	10 pfu/mL	[103]
Malaria	<i>Plasmodium falciparum</i> infected red blood cells (iRBC)	Direct SERS	Silver nanorod	1.5 × 10 ⁷ /mL	[104]
Malaria	Hemozoin in iRBC	direct SERS	Iron oxide core and silver shell nanoparticles	5 nM	[113]
Malaria	Hemozoin in iRBC	direct SERS	Silver nanoparticles	2.5 parasites/ μ L	[109]
Malaria	Hemozoin in iRBC lysate	direct SERS	Gold-coated butterfly wings	0.0005% and 0.005%	[114]

Among many different approaches, microfluidic devices, lateral-flow assays, and lab-on-a-chip assays are the most common diagnostic assay platforms that have been developed and tested for infectious diseases [94,115–120]. SERS-based assays have been integrated into these devices to be used for both qualitative and quantitative biomarker detection [7,8,70,73,91,94,121–124]. Integration of SERS detection schemes into lateral flow assays are commonly seen in the recent work related to infectious disease diagnosis [91,122]. Paper-based immunoassays such as LFA are desirable at the POC as they are cost-efficient and can be user friendly for a non- technically specialized end user. For instance, Choo, et al. developed a simplified LFA using hollow gold nanoparticles encoded with Raman tags and functionalized with antibodies as the SERS detection probe to specifically capture and detect staphylococcal enterotoxin B (SEB), which is a common food-poisoning pathogen (Figure 8) [122]. This approach was able to yield highly sensitive quantitative detection of SEB based on the SERS signals measured at the test zone, where the SEB-antibody conjugated SERS probe complex exist. The reported LOD for SEB using this SERS-based LFA strip was estimated to be 0.001 ng mL^{-1} , which is in the range required for SEB to cause intoxication (less than 1 ng mL^{-1}). In comparison to the enzyme-linked immunosorbent assay (ELISA)-based method, the SERS-based LFA provides approximately three orders of magnitude higher detection sensitivity. Hamad-Schifferli's group also developed LFAs using SERS nanotags for dengue and Zika detection [70,125]. The importance of their study is that they systematically examined the importance of gold nanostar morphological features and Raman reporter selection in order to optimize the SERS enhancement and multiplexed detection in LFAs, respectively. They investigated the effect of the morphological features of gold nanoparticles (spherical vs. star-shaped and the varying tip curvature of gold nanostars) as SERS substrates on the sensitivity of SERS-based LFA [70]. The SERS enhancement of the Raman reporter molecules 1,2-bis(4-pyridyl)ethylene and 4-mercaptobenzoic acid were optimized and compared using different types of gold nanoparticles for multiplexed detection of Zika and dengue non-structural protein 1 (NS1). They concluded that the nanoparticles with sharp tips such as nanostars provide higher enhancement factors, hence enabling higher sensitivities in SERS immunoassays. In addition, they also observed that the SERS intensity distribution within the test zone is greater in the area where the fluid first encounters the immobilized antibody, and such factors can be used to strategically design LFA to decrease the overall assay cost. In 2018, the same group focused on selecting Raman reporters for quantitative multiplexed SERS detection of protein (IgG) biomarkers in a dipstick immunoassay [125]. In this study, gold nanostars conjugated to polyclonal anti-human IgG antibodies were tagged with 15 different Raman reporters. They used machine learning to evaluate the spectral overlap and quantitative contribution of Raman reporters. Using the information gathered from the comprehensive correlation matrix analysis, they were able to select multiple reporters that provide sufficient spectral resolution and higher quantitative accuracy in multiplexed SERS-based IgG biomarker detection in LFAs.

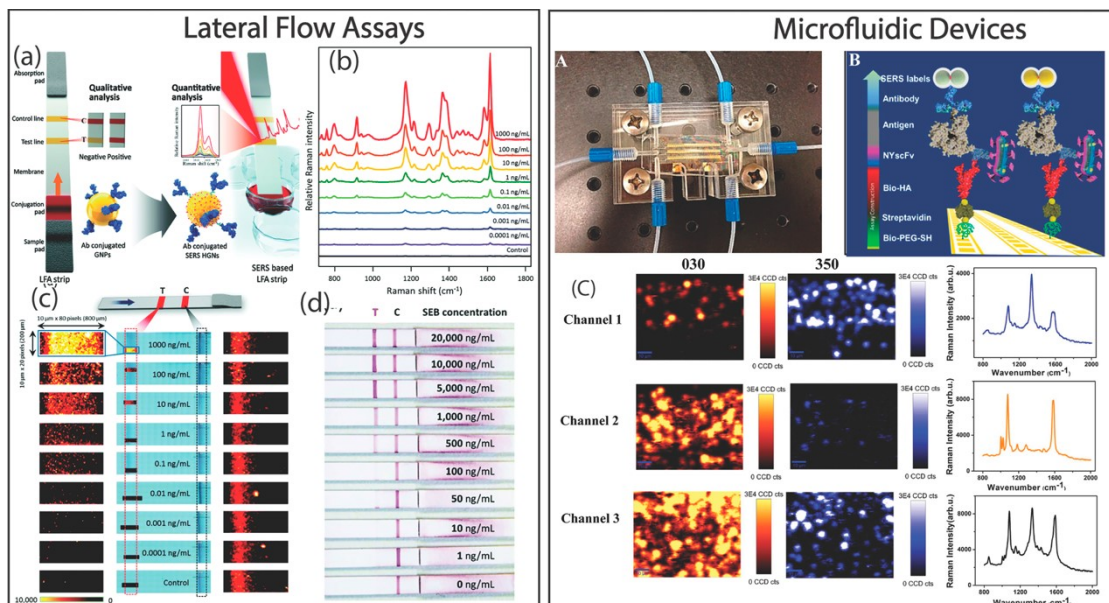


Figure 8. SERS-based diagnostic devices and assay platforms. Lateral flow assay (LFA) designs: (a) Representation of a traditional LFA and a SERS-based LFA that utilized Raman reporter-labeled hollow gold nanospheres to detect the presence of *staphylococcal enterotoxin B* (SEB). (b) Average SERS spectra at the mapping area of the test zone for varying concentrations of SEB. (c) SERS maps acquired using a peak intensity at 1650 cm^{-1} for varying concentrations of SEB concentrations. (d) Photograph of the LFA strip at varying concentrations of SEB concentrations. Reproduced with permission from Reference [122] Royal Society of Chemistry (2016). Microfluidic devices. (a) Microfluidic device used for the detection of *Entamoeba histolytica* using antigen as the biomarker. (b) Schematic representation of an indirect detection scheme designed to detect *Entamoeba histolytica* antigen biomarkers. It uses gold nanoparticle clusters functionalized with aromatic thiols as Raman reporters. (c) The duplex detection of pathogen in the three-channel microfluidic device using false-color SERS images and the corresponding average SERS spectra. Reproduced with permission from Reference [7] American Chemical Society (2014).

Microfluidic SERS immunoassays using antigen–antibody interactions are also a popular device architecture for POC infectious disease detection in clinical samples [7,73,124]. Trau et al. developed a conceptually new SERS diagnostic assay integrated into a microfluidic devices for duplex detection of two antigen biomarkers of the *Entamoeba histolytica* pathogen [7]. The bioassay platform was designed using a glass chip-coated with Raman tags-encoded gold nanoparticles (SERS substrate) which was then then fixed into a microfluidic device (Figure 8). The glass chip (SERS substrate) is comprised of multiple channels that carry different Raman tags-encoded gold nanoparticles for multiplexed detection of antigens. In order to reduce the cost associated with the device fabrication, this platform used inexpensive nanoyeast single-chain variable fragments (NYScFv) reagents instead of antibodies as the recognition moieties of antigen biomarkers. Using this new SERS-based microfluid bioassays, they achieved highly specific and highly sensitive detection of individual *E. histolytica* antigen EHI_115350 and EHI_182030 at the LOD of 1 pg/mL and 10 pg/mL, respectively. Overall this microfluid device exhibits greater potential as a SERS-based analytical platform for high throughput multiplexed detection of pathogen antigens. Konkel et al. introduced a microfluidic system coupled to a “lab-on-a-chip” system that enables label-free SERS-based rapid detection and differentiation of *Staphylococcus aureus* (MRSA) and methicillin-sensitive *S. aureus* (MSSA) in clinical isolates [73]. This integrated device is based on the working principle of an optofluidic system where the SERS detection is carried under controlled flow conditions as opposed to traditional

stationary conditions. A microfluidic SERS-based assay with an optofluidic design provides many advantages such as highly reliable handling of small sample volumes and high sample throughput. By coupling the novel optofluidic-based “lab-on-a-chip” detection system to a confocal micro-Raman spectroscopic system, they were able to use the intrinsic SERS signature of MRSA and MSSA to investigate their epidemiology in clinical samples isolated from infected humans.

5. Conclusions and Outlook

The work highlighted in this review demonstrates the greater potential and the POC applicability of SERS spectroscopy as a bioanalytical technique for both qualitative and quantitative infectious disease diagnostics using biomarkers ranging from nucleic acids to proteins to metabolites. Intrinsic SERS enables the monitoring of the molecular structural changes of biomarkers during disease progression, and Raman labels- and molecular recognition elements-assisted indirect SERS detection of biomarkers offer versatile POC diagnostic potentials. Enabled by the excellent optical properties of plasmonic nanomaterials, the high sensitivity, selectivity, and multiplexing capability of SERS-based bioassays, collectively, offer characteristics of a powerful diagnostic tool that can be integrated into field-transferable devices for early and rapid infectious disease detection.

While many of the SERS-based techniques demonstrate excellent and versatile biomarker detection capabilities, it is crucial to reconsider the sensory characteristics and practical needs for their clinical and/or POC applications. In order for SERS-based sensing platforms to reach the front line of the POC detection, technique standardization and validation is highly important. The performance of the SERS-based diagnostic assays mainly depends on the quality of plasmonic nanomaterials and the nano-bio functional interface. Therefore, we have to address two main aspects of the nanoparticles-based SERS diagnostic systems to further advance them for POC diagnosis; (i) both the SERS signal stability and the SERS enhancement factor depend on the quality of the plasmonic NPs. Therefore, it is vital to ensure the batch-to-batch consistency and reproducibility of plasmonic nanoparticles-based SERS substrates for reliable and quantitative SERS-based biomarker detection. (ii) In addition, the careful fabrication of the functional nano-bio interface is critical to obtain high diagnostic specificity and accuracy. Thus, synthetic approaches for stable and reproducible surface functionalization of SERS substrates with molecular recognition elements and surface passivation ligands are needed. It will help eliminating non-specific biological interactions hence reducing SERS spectral interference and ensuring colloidal stability for stable SERS signal acquisition. An appreciable amount of effort is currently being invested by the research community to investigate these fundamental aspects of the nanoparticle-based SERS diagnostic assays [7,17,70,73,125,126]. Combining the current exponential improvement in both fundamental chemistry and device engineering, the widespread use of SERS-based diagnostics for infectious diseases at the POC and clinical setting is only a very few years away from us.

Author Contributions: Writing—original draft preparation, L.H. and A.G.; Conceptualization, writing—review and editing, A.S.D.S.I.

Funding: This work was funded by University of North Carolina at Charlotte.

Conflicts of Interest: The authors declare no conflict of interest.

References

1. Qasim, M.; Lim, D.-J.; Park, H.; Na, D. Nanotechnology for Diagnosis and Treatment of Infectious Diseases. *J. Nanosci. Nanotechnol.* **2014**, *14*, 7374–7387. [[CrossRef](#)]
2. Peeling, R.W.; Holmes, K.K.; Mabey, D.; Ronald, A. Rapid tests for sexually transmitted infections (STIs): the way forward. *Sex. Transm. Infect.* **2006**, *82*, v1–v6. [[CrossRef](#)] [[PubMed](#)]

Appl. Sci. **2019**, *9*, 1448

3. Mabey, D.; Peeling, R.W.; Ustianowski, A.; Perkins, M.D. Diagnostics for the developing world. *Nat. Rev. Microbiol.* **2004**, *2*, 231–240. [[CrossRef](#)]
4. Manohar, C.; Andrea, T.; Anisha, G.; Gobind, D.; Zaccaria, R.P.; Roman, K.; Eliana, R.; Marco, L.; Carlo, L.; De, A.F.; et al. 3D Nanostar Dimers with a Sub-10-nm Gap for Single-/Few-Molecule Surface-Enhanced Raman Scattering. *Adv. Mater.* **2014**, *26*, 2353–2358.
5. Gracie, K.; Correa, E.; Mabbott, S.; Dougan, J.A.; Graham, D.; Goodacre, R.; Faulds, K. Simultaneous detection and quantification of three bacterial meningitis pathogens by SERS. *Chem. Sci.* **2014**, *5*, 1030–1040. [[CrossRef](#)]
6. Domke, K.F. Surface Enhanced Raman Spectroscopy. Analytical, Biophysical and Life Science Applications. Edited by Sebastian Schlücker. *Angew. Chem. Int. Ed.* **2011**, *50*, 8226. [[CrossRef](#)]
7. Wang, Y.; Rauf, S.; Grewal, Y.S.; Spadafora, L.J.; Shiddiky, M.J.; Cangelosi, G.A.; Schlucker, S.; Trau, M. Duplex microfluidic SERS detection of pathogen antigens with nanoyeast single-chain variable fragments. *Anal. Chem.* **2014**, *86*, 9930–9938. [[CrossRef](#)] [[PubMed](#)]
8. Tran, V.; Walkenfort, B.; König, M.; Salehi, M.; Schlucker, S. Rapid, Quantitative, and Ultrasensitive Point-of-Care Testing: A Portable SERS Reader for Lateral Flow Assays in Clinical Chemistry. *Angew. Chem. Int. Ed. Engl.* **2019**, *58*, 442–446. [[CrossRef](#)]
9. Graham, D.; Mallinder, B.J.; Smith, W.E. Detection and identification of labeled DNA by surface enhanced resonance Raman scattering. *Biopolymers* **2000**, *57*, 85–91. [[CrossRef](#)]
10. Harper, M.M.; Dougan, J.A.; Shand, N.C.; Graham, D.; Faulds, K. Detection of SERS active labelled DNA based on surface affinity to silver nanoparticles. *Analyst* **2012**, *137*, 2063–2068. [[CrossRef](#)]
11. McQueenie, R.; Stevenson, R.; Benson, R.; MacRitchie, N.; McInnes, I.; Maffia, P.; Faulds, K.; Graham, D.; Brewer, J.; Garside, P. Detection of inflammation in vivo by surface-enhanced Raman scattering provides higher sensitivity than conventional fluorescence imaging. *Anal. Chem.* **2012**, *84*, 5968–5975. [[CrossRef](#)]
12. Alvarez-Puebla, R.A.; Liz-Marzan, L.M. SERS-Based Diagnosis and Biodetection. *Small* **2010**, *6*, 604–610. [[CrossRef](#)]
13. Bodelon, G.; Montes-Garcia, V.; Lopez-Puente, V.; Hill, E.H.; Hamon, C.; Sanz-Ortiz, M.; Rodal-Cedeira, S.; Costas, C.; Celiksoy, S.; Perez-Juste, I.; et al. Detection and imaging of quorum sensing in *Pseudomonas aeruginosa* biofilm communities by surface-enhanced resonance Raman scattering. *Nat. Mater.* **2016**, *15*, 1203–1211. [[CrossRef](#)]
14. Moskovits, M. Surface-enhanced Raman spectroscopy: A brief retrospective. *J. Raman Spectrosc.* **2005**, *36*, 485–496. [[CrossRef](#)]
15. Hao, E.; Schatz, G.; Hupp, J. Synthesis and Optical Properties of Anisotropic Metal Nanoparticles. *J. Fluoresc.* **2004**, *14*, 331–341. [[CrossRef](#)]
16. Kelly, K.L.; Coronado, E.; Zhao, L.L.; Schatz, G.C. The optical properties of metal nanoparticles: The influence of size, shape, and dielectric environment. *J. Phys. Chem. B* **2003**, *107*, 668. [[CrossRef](#)]
17. De Silva Indrasekara, A.S.; Johnson, S.F.; Odion, R.A.; Vo-Dinh, T. Manipulation of the Geometry and Modulation of the Optical Response of Surfactant-Free Gold Nanostars: A Systematic Bottom-Up Synthesis. *ACS Omega* **2018**, *3*, 2202–2210. [[CrossRef](#)]
18. Indrasekara, A.S.D.; Thomas, R.; Fabris, L. Plasmonic properties of regiospecific core–satellite assemblies of gold nanostars and nanospheres. *Phys. Chem. Chem. Phys.* **2015**, *17*, 21133–21142. [[CrossRef](#)]
19. Fabris, L.; Indrasekara, A.S. Gold Nanostar Substrates for SERS Sensing in the Femtomolar Regime. US Patent No US10024800B2, 2015.
20. Perets, E.A.; Indrasekara, A.S.D.S.; Kurmis, A.; Atlasevich, N.; Fabris, L.; Arslanoglu, J. Carboxy-terminated immuno-SERS tags overcome non-specific aggregation for the robust detection and localization of organic media in artworks. *Analyst* **2015**, *140*, 5971–5980. [[CrossRef](#)]
21. Indrasekara, A.S.D.S.; Paladini, B.J.; Naczynski, D.J.; Starovoytov, V.; Moghe, P.V.; Fabris, L. Dimeric Gold Nanoparticle Assemblies as Tags for SERS-Based Cancer Detection. *Adv. Healthc. Mater.* **2013**, *2*, 1370–1376. [[CrossRef](#)]
22. Personick, M.L.; Langille, M.R.; Zhang, J.; Mirkin, C.A. Shape Control of Gold Nanoparticles by Silver Underpotential Deposition. *Nano Lett.* **2011**, *11*, 3394–3398. [[CrossRef](#)]

Appl. Sci. **2019**, *9*, 1448

23. Xue, C.; Millstone, J.E.; Li, S.; Mirkin, C.A. Plasmon-Driven Synthesis of Triangular Core/Shell Nanoprisms from Gold Seeds. *Angew. Chem. Int. Ed.* **2007**, *46*, 8436–8439. [[CrossRef](#)]
24. Rosi, N.L.; Mirkin, C.A. Nanostructures in biodiagnostics. *Chem. Rev.* **2005**, *105*, 1547–1562. [[CrossRef](#)]
25. Murphy, C.J.; Sau, T.K.; Gole, A.M.; Orendorff, C.J.; Gao, J.; Gou, L.; Hunyadi, S.E.; Li, T. Anisotropic Metal Nanoparticles: Synthesis, Assembly, and Optical Applications. *J. Phys. Chem. B* **2005**, *109*, 13857–13870. [[CrossRef](#)]
26. Kleinman, S.L.; Sharma, B.; Blaber, M.G.; Henry, A.-I.; Valley, N.; Freeman, R.G.; Natan, M.J.; Schatz, G.C.; Van Duyne, R.P. Structure Enhancement Factor Relationships in Single Gold Nanoantennas by Surface-Enhanced Raman Excitation Spectroscopy. *J. Am. Chem. Soc.* **2013**, *135*, 301–308. [[CrossRef](#)]
27. Sharma, B.; Fernanda Cardinal, M.; Kleinman, S.L.; Greeneltch, N.G.; Frontiera, R.R.; Blaber, M.G.; Schatz, G.C.; Van Duyne, R.P. High-performance SERS substrates: Advances and challenges. *MRS Bull.* **2013**, *38*, 615–624. [[CrossRef](#)]
28. Greeneltch, N.G.; Blaber, M.G.; Henry, A.-I.; Schatz, G.C.; Van Duyne, R.P. Immobilized Nanorod Assemblies: Fabrication and Understanding of Large Area Surface-Enhanced Raman Spectroscopy Substrates. *Anal. Chem.* **2013**, *85*, 2297–2303. [[CrossRef](#)]
29. Stiles, P.L.; Dieringer, J.A.; Shah, N.C.; Van Duyne, R.P. Surface-Enhanced Raman Spectroscopy. *Annu. Rev. Anal. Chem.* **2008**, *1*, 601–626. [[CrossRef](#)]
30. Kneipp, K.; Dasari, R.R.; Wang, Y. Near-Infrared Surface-Enhanced Raman-Scattering (Nir Sers) on Colloidal Silver and Gold. *Appl. Spectrosc.* **1994**, *48*, 951–955. [[CrossRef](#)]
31. Michota, A.; Bukowska, J. Surface-enhanced Raman scattering (SERS) of 4-mercaptobenzoic acid on silver and gold substrates. *J. Raman Spectrosc.* **2003**, *34*, 21–25. [[CrossRef](#)]
32. Alvarez-Puebla, R.; Dos, S., Jr.; Aroca, R.F. Surface-enhanced Raman scattering for ultrasensitive chemical analysis of 1 and 2-naphthalenethiols. *Analyst* **2004**, *129*, 1251–1256. [[CrossRef](#)]
33. Fabris, L.; Dante, M.; Nguyen, T.-Q.; Tok, J.B.H.; Bazan, G.C. SERS Aptatags: New Responsive Metallic Nanostructures for Heterogeneous Protein Detection by Surface Enhanced Raman Spectroscopy. *Adv. Funct. Mater.* **2008**, *18*, 2518–2525. [[CrossRef](#)]
34. Indrasekara, A.S.D.S.; Meyers, S.; Shubeita, S.; Feldman, L.C.; Gustafsson, T.; Fabris, L. Gold nanostar substrates for SERS-based chemical sensing in the femtomolar regime. *Nanoscale* **2014**, *6*, 8891–8899. [[CrossRef](#)]
35. Millstone, J.E.; Park, S.; Shuford, K.L.; Qin, L.; Schatz, G.C.; Mirkin, C.A. Observation of a Quadrupole Plasmon Mode for a Colloidal Solution of Gold Nanoprisms. *J. Am. Chem. Soc.* **2005**, *127*, 5312–5313. [[CrossRef](#)]
36. Fales, A.M.; Yuan, H.; Vo-Dinh, T. Silica-Coated Gold Nanostars for Combined Surface-Enhanced Raman Scattering (SERS) Detection and Singlet-Oxygen Generation: A Potential Nanoplatfor for Theranostics. *Langmuir* **2011**, *27*, 12186–12190. [[CrossRef](#)]
37. Hsiangkuo, Y.; Christopher, G.K.; Hanjun, H.; Christy, M.W.; Gerald A Grant and, T.V. Gold nanostars: surfactant-free synthesis, 3D modelling, and two-photon photoluminescence imaging. *Nanotechnology* **2012**, *23*, 075102.
38. Hao, F.; Nehl, C.L.; Hafner, J.H.; Nordlander, P. Plasmon Resonances of a Gold Nanostar. *Nano Lett.* **2007**, *7*, 729–732. [[CrossRef](#)] [[PubMed](#)]
39. Alvarez-Puebla, R.; Liz-Marzán, L.M.; de Abajo, F.J.G. Light Concentration at the Nanometer Scale. *J. Phys. Chem. Lett.* **2010**, *1*, 2428–2434. [[CrossRef](#)]
40. Braun, G.B.; Lee, S.J.; Laurence, T.; Fera, N.; Fabris, L.; Bazan, G.C.; Moskovits, M.; Reich, N.O. Generalized Approach to SERS-Active Nanomaterials via Controlled Nanoparticle Linking, Polymer Encapsulation, and Small-Molecule Infusion. *J. Phys. Chem. C* **2009**, *113*, 13622–13629. [[CrossRef](#)]
41. Talley, C.E.; Jackson, J.B.; Oubre, C.; Grady, N.K.; Hollars, C.W.; Lane, S.M.; Huser, T.R.; Nordlander, P.; Halas, N.J. Surface-Enhanced Raman Scattering from Individual Au Nanoparticles and Nanoparticle Dimer Substrates. *Nano Lett.* **2005**, *5*, 1569–1574. [[CrossRef](#)]

Appl. Sci. **2019**, *9*, 1448

42. Schutz, M.; Schlucker, S. Molecularly linked 3D plasmonic nanoparticle core/satellite assemblies: SERS nanotags with single-particle Raman sensitivity. *Phys. Chem. Chem. Phys.* **2015**, *17*, 24356. [[CrossRef](#)]
43. Romo-Herrera, J.; Alvarez-Puebla, R.; Liz-Marzan, L. Controlled assembly of plasmonic colloidal nanoparticle clusters. *Nanoscale* **2011**, *3*, 1304–1315. [[CrossRef](#)]
44. Chen, G.; Wang, Y.; Yang, M.; Xu, J.; Goh, S.J.; Pan, M.; Chen, H. Measuring Ensemble-Averaged Surface-Enhanced Raman Scattering in the Hotspots of Colloidal Nanoparticle Dimers and Trimers. *J. Am. Chem. Soc.* **2010**, *132*, 3644–3645. [[CrossRef](#)]
45. Malinsky, M.D.; Kelly, K.L.; Schatz, G.C.; Van Duyne, R.P. Chain Length Dependence and Sensing Capabilities of the Localized Surface Plasmon Resonance of Silver Nanoparticles Chemically Modified with Alkanethiol Self-Assembled Monolayers. *J. Am. Chem. Soc.* **2001**, *123*, 1471–1482. [[CrossRef](#)]
46. Wustholz, K.L.; Henry, A.-I.; McMahon, J.M.; Freeman, R.G.; Valley, N.; Piotti, M.E.; Natan, M.J.; Schatz, G.C.; Duyne, R.P.V. Structure-Activity Relationships in Gold Nanoparticle Dimers and Trimers for Surface-Enhanced Raman Spectroscopy. *J. Am. Chem. Soc.* **2010**, *132*, 10903–10910. [[CrossRef](#)]
47. Rahme, K.; Chen, L.; Hobbs, R.G.; Morris, M.A.; O'Driscoll, C.; Holmes, J.D. PEGylated gold nanoparticles: Polymer quantification as a function of PEG lengths and nanoparticle dimensions. *RSC Adv.* **2013**, *3*, 6085–6094. [[CrossRef](#)]
48. Chen, S.; Yang, M.; Hong, S.; Lu, C. Nonionic fluorosurfactant as an ideal candidate for one-step modification of gold nanorods. *Nanoscale* **2014**. [[CrossRef](#)]
49. Austin, L.A.; Mackey, M.A.; Dreaden, E.C.; El-Sayed, M.A. The optical, photothermal, and facile surface chemical properties of gold and silver nanoparticles in biodiagnostics, therapy, and drug delivery. *Arch. Toxicol.* **2014**, *88*, 1391–1417. [[CrossRef](#)]
50. Park, S.Y.; Lee, J.-S.; Georganopoulou, D.; Mirkin, C.A.; Schatz, G.C. Structures of DNA-Linked Nanoparticle Aggregates. *J. Phys. Chem. B* **2006**, *110*, 12673–12681. [[CrossRef](#)]
51. Brennan, J.L.; Hatzakis, N.S.; Tshikhudo, T.R.; Razumas, V.; Patkar, S.; Vind, J.; Svendsen, A.; Nolte, R.J.M.; Rowan, A.E.; Brust, M. Bionanoconjugation via Click Chemistry: The Creation of Functional Hybrids of Lipases and Gold Nanoparticles. *Bioconj. Chem.* **2006**, *17*, 1373–1375. [[CrossRef](#)]
52. Krpetic, Ž.; Nativo, P.; Porta, F.; Brust, M. A Multidentate Peptide for Stabilization and Facile Bioconjugation of Gold Nanoparticles. *Bioconj. Chem.* **2009**, *20*, 619–624. [[CrossRef](#)]
53. Kanaras, A.G.; Kamounah, F.S.; Schaumburg, K.; Kiely, C.J.; Brust, M. Thioalkylated tetraethylene glycol: A new ligand for water soluble monolayer protected gold clusters. *Chem. Commun.* **2002**, 2294–2295. [[CrossRef](#)]
54. Barhoumi, A.; Halas, N.J. Label-Free Detection of DNA Hybridization Using Surface Enhanced Raman Spectroscopy. *J. Am. Chem. Soc.* **2010**, *132*, 12792–12793. [[CrossRef](#)]
55. Dondapati, S.K.; Sau, T.K.; Hrelescu, C.; Klar, T.A.; Stefani, F.D.; Feldmann, J. Label-free Biosensing Based on Single Gold Nanostars as Plasmonic Transducers. *ACS Nano* **2010**, *4*, 6318–6322. [[CrossRef](#)]
56. Papadopoulou, E.; Bell, S.E.J. Label-Free Detection of Single-Base Mismatches in DNA by Surface-Enhanced Raman Spectroscopy. *Angew. Chem. Int. Ed.* **2011**, *50*, 9058–9061. [[CrossRef](#)]
57. Ngo, H.T.; Wang, H.-N.; Fales, A.M.; Vo-Dinh, T. Label-Free DNA Biosensor Based on SERS Molecular Sentinel on Nanowave Chip. *Anal. Chem.* **2013**, *85*, 6378–6383. [[CrossRef](#)]
58. Xu, L.-J.; Lei, Z.-C.; Li, J.; Zong, C.; Yang, C.J.; Ren, B. Label-Free Surface-Enhanced Raman Spectroscopy Detection of DNA with Single-Base Sensitivity. *J. Am. Chem. Soc.* **2015**, *137*, 5149–5154. [[CrossRef](#)]
59. Dina, N.E.; Zhou, H.; Colnita, A.; Leopold, N.; Szoke-Nagy, T.; Coman, C.; Haisch, C. Rapid single-cell detection and identification of pathogens by using surface-enhanced Raman spectroscopy. *Analyst* **2017**, *142*, 1782–1789. [[CrossRef](#)]
60. Graham, D.; Mallinder, B.J.; Whitcombe, D.; Watson, N.D.; Smith, W.E. Simple Multiplex Genotyping by Surface-Enhanced Resonance Raman Scattering. *Anal. Chem.* **2002**, *74*, 1069–1074. [[CrossRef](#)]
61. Yu, C.; Irudayaraj, J. Quantitative Evaluation of Sensitivity and Selectivity of Multiplex NanoSPR Biosensor Assays. *Biophys. J.* **2007**, *93*, 3684–3692. [[CrossRef](#)]

Appl. Sci. **2019**, *9*, 1448

62. Sun, L.; Yu, C.; Irudayaraj, J. Raman multiplexers for alternative gene splicing. *Anal. Chem.* **2008**, *80*, 3342–3349. [[CrossRef](#)]
63. von Maltzahn, G.; Centrone, A.; Park, J.-H.; Ramanathan, R.; Sailor, M.J.; Hatton, T.A.; Bhatia, S.N. SERS-Coded Gold Nanorods as a Multifunctional Platform for Densely Multiplexed Near-Infrared Imaging and Photothermal Heating. *Adv. Mater.* **2009**, *21*, 3175–3180. [[CrossRef](#)]
64. Zavaleta, C.L.; Smith, B.R.; Walton, I.; Doering, W.; Davis, G.; Shojaei, B.; Natan, M.J.; Gambhir, S.S. Multiplexed imaging of surface enhanced Raman scattering nanotags in living mice using noninvasive Raman spectroscopy. *Proc. Natl. Acad. Sci. USA* **2009**, *106*, 13511–13516. [[CrossRef](#)]
65. Fabris, L.; Schierhorn, M.; Moskovits, M.; Bazan, G.C. Aptatag-Based Multiplexed Assay for Protein Detection by Surface-Enhanced Raman Spectroscopy. *Small* **2010**, *6*, 1550–1557. [[CrossRef](#)]
66. Kang, T.; Yoo, S.M.; Yoon, I.; Lee, S.Y.; Kim, B. Patterned Multiplex Pathogen DNA Detection by Au Particle-on-Wire SERS Sensor. *Nano Lett.* **2010**, *10*, 1189–1193. [[CrossRef](#)]
67. Pallaoro, A.; Braun, G.B.; Moskovits, M. Quantitative ratiometric discrimination between noncancerous and cancerous prostate cells based on neuropilin-1 overexpression. *Proc. Natl. Acad. Sci. USA* **2011**. [[CrossRef](#)]
68. Kim, J.-Y.; Lee, J.-S. Multiplexed DNA Detection with DNA-Functionalized Silver and Silver/Gold Nanoparticle Superstructure Probes. *Bull. Korean Chem. Soc.* **2012**, *33*, 221–226. [[CrossRef](#)]
69. Wang, H.-N.; Crawford, B.M.; Fales, A.M.; Bowie, M.L.; Seewaldt, V.L.; Vo-Dinh, T. Multiplexed Detection of MicroRNA Biomarkers Using SERS-Based Inverse Molecular Sentinel (iMS) Nanoprobes. *J. Phys. Chem. C* **2016**, *120*, 21047–21055. [[CrossRef](#)]
70. Sánchez-Purrà, M.; Roig-Solvas, B.; Versiani, A.; Rodriguez-Quijada, C.; de Puig, H.; Bosch, I.; Gehrke, L.; Hamad-Schifferli, K. Design of SERS nanotags for multiplexed lateral flow immunoassays. *Mol. Syst. Des. Eng.* **2017**, *2*, 401–409. [[CrossRef](#)]
71. Wang, H.-N.; Fales, A.M.; Zaas, A.K.; Woods, C.W.; Burke, T.; Ginsburg, G.S.; Vo-Dinh, T. Surface-enhanced Raman scattering molecular sentinel nanoprobe for viral infection diagnostics. *Anal. Chim. Acta* **2013**, *786*, 153–158. [[CrossRef](#)]
72. Strelau, K.K.; Brinker, A.; Schnee, C.; Weber, K.; Moeller, R.; Popp, J. Detection of PCR products amplified from DNA of epizootic pathogens using magnetic nanoparticles and SERS. *J. Raman Spectrosc.* **2011**, *42*, 243–250. [[CrossRef](#)]
73. Lu, X.; Samuelson, D.R.; Xu, Y.; Zhang, H.; Wang, S.; Rasco, B.A.; Xu, J.; Konkell, M.E. Detecting and tracking nosocomial methicillin-resistant *Staphylococcus aureus* using a microfluidic SERS biosensor. *Anal. Chem.* **2013**, *85*, 2320–2327. [[CrossRef](#)]
74. Kamin'ska, A.; Witkowska, E.; Kowalska, A.; Skoczyn'ska, A.; Ronkiewicz, P.; Szymborski, T.; Waluk, J. Rapid detection and identification of bacterial meningitis pathogens in ex vivo clinical samples by SERS method and principal component analysis. *Anal. Methods* **2016**, *8*, 4521–4529. [[CrossRef](#)]
75. De, S.I.; Fabris, L. SERS-based approaches toward genetic profiling. *Bioanalysis* **2015**, *7*, 263–278.
76. Negri, P.; Dluhy, R.A. Detection of genetic markers related to high pathogenicity in influenza by SERS. *Analyst* **2013**, *138*, 4877–4884. [[CrossRef](#)]
77. Lee, C.; Carney, R.P.; Hazari, S.; Smith, Z.J.; Knudson, A.; Robertson, C.S.; Lam, K.S.; Wachsmann-Hogiu, S. 3D plasmonic nanobowl platform for the study of exosomes in solution. *Nanoscale* **2015**, *7*, 9290–9297. [[CrossRef](#)]
78. Wu, X.; Chen, J.; Li, X.; Zhao, Y.; Zughaier, S.M. Culture-free diagnostics of *Pseudomonas aeruginosa* infection by silver nanorod array based SERS from clinical sputum samples. *Nanomedicine* **2014**, *10*, 1863–1870. [[CrossRef](#)]
79. Hennigan, S.L.; Driskell, J.D.; Ferguson-Noel, N.; Dluhy, R.A.; Zhao, Y.; Tripp, R.A.; Krause, D.C. Detection and differentiation of avian mycoplasmas by surface-enhanced Raman spectroscopy based on a silver nanorod array. *Appl. Environ. Microbiol.* **2012**, *78*, 1930–1935. [[CrossRef](#)]
80. Hennigan, S.L.; Driskell, J.D.; Dluhy, R.A.; Zhao, Y.; Tripp, R.A.; Waites, K.B.; Krause, D.C. Detection of *Mycoplasma pneumoniae* in simulated and true clinical throat swab specimens by nanorod array-surface-enhanced Raman spectroscopy. *PLoS ONE* **2010**, *5*, e13633. [[CrossRef](#)]

Appl. Sci. **2019**, *9*, 1448

81. Fan, Z.; Senapati, D.; Khan, S.A.; Singh, A.K.; Hamme, A.; Yust, B.; Sardar, D.; Ray, P.C. Popcorn-shaped magnetic core-plasmonic shell multifunctional nanoparticles for the targeted magnetic separation and enrichment, label-free SERS imaging, and photothermal destruction of multidrug-resistant bacteria. *Chemistry* **2013**, *19*, 2839–2847. [[CrossRef](#)]
82. Muhamadali, H.; Subaihi, A.; Mohammadtaheri, M.; Xu, Y.; Ellis, D.I.; Ramanathan, R.; Bansal, V.; Goodacre, R. Rapid, accurate, and comparative differentiation of clinically and industrially relevant microorganisms via multiple vibrational spectroscopic fingerprinting. *Analyst* **2016**, *141*, 5127–5136. [[CrossRef](#)]
83. Prucek, R.; Ranc, V.; Kvitek, L.; Panacek, A.; Zboril, R.; Kolar, M. Reproducible discrimination between gram-positive and gram-negative bacteria using surface enhanced Raman spectroscopy with infrared excitation. *Analyst* **2012**, *137*, 2866–2870. [[CrossRef](#)]
84. Guven, B.; Basaran-Akgul, N.; Temur, E.; Tamer, U.; Boyaci, I.H. SERS-based sandwich immunoassay using antibody coated magnetic nanoparticles for Escherichia coli enumeration. *Analyst* **2011**, *136*, 740–748. [[CrossRef](#)]
85. Mircescu, N.E.; Zhou, H.; Leopold, N.; Chis, V.; Ivleva, N.P.; Niessner, R.; Wieser, A.; Haisch, C. Towards a receptor-free immobilization and SERS detection of urinary tract infections causative pathogens. *Anal. Bioanal. Chem.* **2014**, *406*, 3051–3058. [[CrossRef](#)]
86. Fan, Z.; Kanchanapally, R.; Ray, P.C. Hybrid Graphene Oxide Based Ultrasensitive SERS Probe for Label-Free Biosensing. *J. Phys. Chem. Lett.* **2013**, *4*, 3813–3818. [[CrossRef](#)]
87. Premasiri, W.R.; Chen, Y.; Williamson, P.M.; Bandarage, D.C.; Pyles, C.; Ziegler, L.D. Rapid urinary tract infection diagnostics by surface-enhanced Raman spectroscopy (SERS): identification and antibiotic susceptibilities. *Anal. Bioanal. Chem.* **2017**, *409*, 3043–3054. [[CrossRef](#)]
88. Chen, K.; Han, H.; Luo, Z. Streptococcus suis II immunoassay based on thorny gold nanoparticles and surface enhanced Raman scattering. *Analyst* **2012**, *137*, 1259–1264. [[CrossRef](#)]
89. MacLaughlin, C.M.; Mullailthilaga, N.; Yang, G.; Ip, S.Y.; Wang, C.; Walker, G.C. Surface-enhanced Raman scattering dye-labeled Au nanoparticles for triplexed detection of leukemia and lymphoma cells and SERS flow cytometry. *Langmuir* **2013**, *29*, 1908–1919. [[CrossRef](#)]
90. Owens, N.A.; Laurentius, L.B.; Porter, M.D.; Li, Q.; Wang, S.; Chatterjee, D. Handheld Raman Spectrometer Instrumentation for Quantitative Tuberculosis Biomarker Detection: A Performance Assessment for Point-of-Need Infectious Disease Diagnostics. *Appl. Spectrosc.* **2018**, *72*, 1104–1115. [[CrossRef](#)]
91. Kim, W.; Lee, J.C.; Shin, J.H.; Jin, K.H.; Park, H.K.; Choi, S. Instrument-Free Synthesizable Fabrication of Label-Free Optical Biosensing Paper Strips for the Early Detection of Infectious Keratoconjunctivitis. *Anal. Chem.* **2016**, *88*, 5531–5537. [[CrossRef](#)]
92. Zhang, H.; Harpster, M.H.; Park, H.J.; Johnson, P.A. Surface-Enhanced Raman Scattering Detection of DNA Derived from the West Nile Virus Genome Using Magnetic Capture of Raman-Active Gold Nanoparticles. *Anal. Chem.* **2011**, *83*, 254–260. [[CrossRef](#)]
93. Zhang, H.; Harpster, M.H.; Wilson, W.C.; Johnson, P.A. Surface-Enhanced Raman Scattering Detection of DNAs Derived from Virus Genomes Using Au-Coated Paramagnetic Nanoparticles. *Langmuir* **2012**, *28*, 4030–4037. [[CrossRef](#)]
94. Ngo, H.T.; Wang, H.N.; Fales, A.M.; Nicholson, B.P.; Woods, C.W.; Vo-Dinh, T. DNA bioassay-on-chip using SERS detection for dengue diagnosis. *Analyst* **2014**, *139*, 5655–5659. [[CrossRef](#)]
95. Ngo, H.T.; Gandra, N.; Fales, A.M.; Taylor, S.M.; Vo-Dinh, T. Sensitive DNA detection and SNP discrimination using ultrabright SERS nanorattles and magnetic beads for malaria diagnostics. *Biosens. Bioelectron.* **2016**, *81*, 8–14. [[CrossRef](#)]
96. Ngo, H.T.; Freedman, E.; Odion, R.A.; Strobbia, P.; De Silva Indrasekara, A.S.; Vohra, P.; Taylor, S.M.; Vo-Dinh, T. Direct Detection of Unamplified Pathogen RNA in Blood Lysate using an Integrated Lab-in-a-Stick Device and Ultrabright SERS Nanorattles. *Sci. Rep.* **2018**, *8*, 4075. [[CrossRef](#)]
97. Camacho, S.A.; Sobral-Filho, R.G.; Aoki, P.H.B.; Constantino, C.J.L.; Brolo, A.G. Zika Immunoassay Based on Surface-Enhanced Raman Scattering Nanoproboscopes. *ACS Sens.* **2018**, *3*, 587–594. [[CrossRef](#)]

Appl. Sci. **2019**, *9*, 1448

98. Neng, J.; Harpster, M.H.; Zhang, H.; Mecham, J.O.; Wilson, W.C.; Johnson, P.A. A versatile SERS-based immunoassay for immunoglobulin detection using antigen-coated gold nanoparticles and malachite green-conjugated protein A/G. *Biosens. Bioelectron.* **2010**, *26*, 1009–1015. [[CrossRef](#)]
99. Neng, J.; Harpster, M.H.; Wilson, W.C.; Johnson, P.A. Surface-enhanced Raman scattering (SERS) detection of multiple viral antigens using magnetic capture of SERS-active nanoparticles. *Biosens. Bioelectron.* **2013**, *41*, 316–321. [[CrossRef](#)]
100. Neng, J.; Li, Y.; Driscoll, A.J.; Wilson, W.C.; Johnson, P.A. Detection of Multiple Pathogens in Serum Using Silica-Encapsulated Nanotags in a Surface-Enhanced Raman Scattering-Based Immunoassay. *J. Agric. Food Chem.* **2018**, *66*, 5707–5712. [[CrossRef](#)]
101. Reyes, M.; Piotrowski, M.; Ang, S.K.; Chan, J.; He, S.; Chu, J.J.H.; Kah, J.C.Y. Exploiting the Anti-Aggregation of Gold Nanostars for Rapid Detection of Hand, Foot, and Mouth Disease Causing Enterovirus 71 Using Surface-Enhanced Raman Spectroscopy. *Anal. Chem.* **2017**, *89*, 5373–5381. [[CrossRef](#)]
102. Sanchez-Purra, M.; Carre-Camps, M.; de Puig, H.; Bosch, I.; Gehrke, L.; Hamad-Schifferli, K. Surface-Enhanced Raman Spectroscopy-Based Sandwich Immunoassays for Multiplexed Detection of Zika and Dengue Viral Biomarkers. *ACS Infect. Dis.* **2017**, *3*, 767–776. [[CrossRef](#)]
103. Paul, A.M.; Fan, Z.; Sinha, S.S.; Shi, Y.; Le, L.; Bai, F.; Ray, P.C. Bio-Conjugated Gold Nanoparticle Based SERS Probe for Ultrasensitive Identification of Mosquito-Borne Viruses Using Raman Fingerprinting. *J. Phys. Chem. C Nanomater. Interfaces* **2015**, *119*, 23669–23775. [[CrossRef](#)]
104. Chen, F.; Flaherty, B.R.; Cohen, C.E.; Peterson, D.S.; Zhao, Y. Direct detection of malaria infected red blood cells by surface enhanced Raman spectroscopy. *Nanomedicine* **2016**, *12*, 1445–1451. [[CrossRef](#)]
105. Bilal, M.; Saleem, M.; Amanat, S.T.; Shakoor, H.A.; Rashid, R.; Mahmood, A.; Ahmed, M. Optical diagnosis of malaria infection in human plasma using Raman spectroscopy. *J. Biomed. Opt.* **2015**, *20*, 017002. [[CrossRef](#)]
106. Bruckner, M.; Becker, K.; Popp, J.; Frosch, T. Fiber array based hyperspectral Raman imaging for chemical selective analysis of malaria-infected red blood cells. *Anal. Chim. Acta* **2015**, *894*, 76–84. [[CrossRef](#)]
107. Hobro, A.J.; Konishi, A.; Coban, C.; Smith, N.I. Raman spectroscopic analysis of malaria disease progression via blood and plasma samples. *Analyst* **2013**, *138*, 3927–3933. [[CrossRef](#)]
108. Kozicki, M.; Czepiel, J.; Biesiada, G.; Nowak, P.; Garlicki, A.; Weselucha-Birczynska, A. The ring-stage of *Plasmodium falciparum* observed in RBCs of hospitalized malaria patients. *Analyst* **2015**, *140*, 8007–8016. [[CrossRef](#)]
109. Chen, K.; Yuen, C.; Aniwah, Y.; Preiser, P.; Liu, Q. Towards ultrasensitive malaria diagnosis using surface enhanced Raman spectroscopy. *Sci. Rep.* **2016**, *6*, 20177. [[CrossRef](#)]
110. Wood, B.R.; Langford, S.J.; Cooke, B.M.; Glenister, F.K.; Lim, J.; McNaughton, D. Raman imaging of hemozoin within the food vacuole of *Plasmodium falciparum* trophozoites. *FEBS Lett.* **2003**, *554*, 247–252. [[CrossRef](#)]
111. Wood, B.R.; Langford, S.J.; Cooke, B.M.; Lim, J.; Glenister, F.K.; Duriska, M.; Unthank, J.K.; McNaughton, D. Resonance Raman Spectroscopy Reveals New Insight into the Electronic Structure of β -Hematin and Malaria Pigment. *J. Am. Chem. Soc.* **2004**, *126*, 9233–9239. [[CrossRef](#)]
112. Frosch, T.; Koncarevic, S.; Becker, K.; Popp, J. Morphology-sensitive Raman modes of the malaria pigment hemozoin. *Analyst* **2009**, *134*, 1126–1132. [[CrossRef](#)]
113. Yuen, C.; Liu, Q. Magnetic field enriched surface enhanced resonance Raman spectroscopy for early malaria diagnosis. *Biomed. Opt.* **2012**, *17*, 017005. [[CrossRef](#)]
114. Garrett, N.L.; Sekine, R.; Dixon, M.W.; Tilley, L.; Bambery, K.R.; Wood, B.R. Bio-sensing with butterfly wings: Naturally occurring nano-structures for SERS-based malaria parasite detection. *Phys. Chem. Chem. Phys.* **2015**, *17*, 21164–21168. [[CrossRef](#)]
115. DeChiara, N.S.; Wilson, D.J.; Mace, C.R. An Open Software Platform for the Automated Design of Paper-Based Microfluidic Devices. *Sci. Rep.* **2017**, *7*, 16224. [[CrossRef](#)]

Appl. Sci. **2019**, *9*, 1448

116. Fu, E.; Liang, T.; Spicar-Mihalic, P.; Houghtaling, J.; Ramachandran, S.; Yager, P. Two-dimensional paper network format that enables simple multistep assays for use in low-resource settings in the context of malaria antigen detection. *Anal. Chem.* **2012**, *84*, 4574–4579. [[CrossRef](#)]
117. Anderson, C.E.; Holstein, C.A.; Strauch, E.M.; Bennett, S.; Chevalier, A.; Nelson, J.; Fu, E.; Baker, D.; Yager, P. Rapid Diagnostic Assay for Intact Influenza Virus Using a High Affinity Hemagglutinin Binding Protein. *Anal. Chem.* **2017**, *89*, 6608–6615. [[CrossRef](#)]
118. Zagorovsky, K.; Chan, W.C. A plasmonic DNAzyme strategy for point-of-care genetic detection of infectious pathogens. *Angew. Chem. Int. Ed. Engl.* **2013**, *52*, 3168–3171. [[CrossRef](#)]
119. Grant, B.D.; Smith, C.A.; Karvonen, K.; Richards-Kortum, R. Highly Sensitive Two-Dimensional Paper Network Incorporating Biotin-Streptavidin for the Detection of Malaria. *Anal. Chem.* **2016**, *88*, 2553–2557. [[CrossRef](#)]
120. Shanmukh, S.; Jones, L.; Zhao, Y.P.; Driskell, J.D.; Tripp, R.A.; Dluhy, R.A. Identification and classification of respiratory syncytial virus (RSV) strains by surface-enhanced Raman spectroscopy and multivariate statistical techniques. *Anal. Bioanal. Chem.* **2008**, *390*, 1551–1555. [[CrossRef](#)]
121. Fu, X.; Cheng, Z.; Yu, J.; Choo, P.; Chen, L.; Choo, J. A SERS-based lateral flow assay biosensor for highly sensitive detection of HIV-1 DNA. *Biosens. Bioelectron.* **2016**, *78*, 530–537. [[CrossRef](#)]
122. Hwang, J.; Lee, S.; Choo, J. Application of a SERS-based lateral flow immunoassay strip for the rapid and sensitive detection of staphylococcal enterotoxin B. *Nanoscale* **2016**, *8*, 11418–11425. [[CrossRef](#)]
123. Park, H.J.; Yang, S.C.; Choo, J. Early Diagnosis of Influenza Virus A Using Surface-enhanced Raman Scattering-based Lateral Flow Assay. *Bull. Korean Chem. Soc.* **2016**, *37*, 2019–2024. [[CrossRef](#)]
124. Kaminska, A.; Witkowska, E.; Winkler, K.; Dziecielewski, I.; Weyher, J.L.; Waluk, J. Detection of Hepatitis B virus antigen from human blood: SERS immunoassay in a microfluidic system. *Biosens. Bioelectron.* **2015**, *66*, 461–467. [[CrossRef](#)]
125. Sanchez-Purra, M.; Roig-Solvas, B.; Rodriguez-Quijada, C.; Leonardo, B.M.; Hamad-Schifferli, K. Reporter Selection for Nanotags in Multiplexed Surface Enhanced Raman Spectroscopy Assays. *ACS Omega* **2018**, *3*, 10733–10742. [[CrossRef](#)]
126. De Silva Indrasekara, A.S.; Norton, S.J.; Geitner, N.K.; Crawford, B.M.; Wiesner, M.R.; Vo-Dinh, T. Tailoring the Core–Satellite Nanoassembly Architectures by Tuning Internanoparticle Electrostatic Interactions. *Langmuir* **2018**, *34*, 14617–14623. [[CrossRef](#)]



© 2019 by the authors. Licensee MDPI, Basel, Switzerland. This article is an open access article distributed under the terms and conditions of the Creative Commons Attribution (CC BY) license (<http://creativecommons.org/licenses/by/4.0/>).

APPENDIX B

The information provided in this section is for the Ag@AuNS SERS substrate development. The synthesis of the AuNS for the Ag@AuNS substrate followed a two-step procedure. The first step was the synthesis of 12 nm spherical gold nanoparticles (AuNP) to function as the core of the second step branch formation. Below in Figure B1 is the UV-VIS and TEM data for the AuNP stock solution. The synthesis was performed using the Turkevich method and provided AuNP with an average size of $12.9 \text{ nm} \pm 0.8 \text{ nm}$. The max wavelength of the AuNP from the UV-VIS data is 521 nm. Successful synthesis of AuNP allowed for use of solution in the second reduction of gold to form the AuNS.

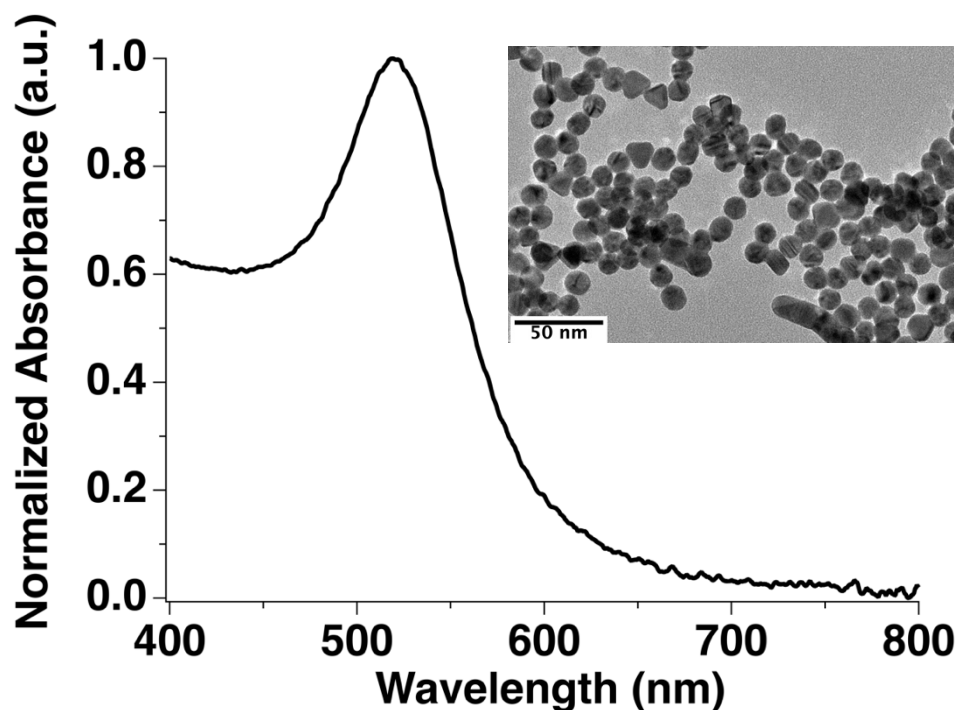


Figure B1. UV-VIS and TEM data for synthesized 12 nm AuNP solution. The max wavelength of absorbance resides at 521 nm. The average size of the AuNP was calculated using ImageJ and determined to be $12.9 \text{ nm} \pm 0.8 \text{ nm}$.

Multiple silver coating trials were performed in order to determine the optimal amount of silver nitrate to use for developing the Ag@AuNS. Three different concentrations of silver nitrate were used: 50 mM, 25 mM and 10 mM. 10 mM addition of silver nitrate was performed at two different volumes to see if any improvements could be made to the UV-VIS results (Figure B2). The results for the 25 mM and 10 mM reactions show very broad absorbance which indicates either the formation of silver nanoparticles or a varying distribution of the silver over the AuNS. The 50 mM silver nitrate addition, based on a narrower wavelength range of absorbance, was determined the best of the silver coating trials. The TEM of the 50 mM silver nitrate addition substrate can also be found in Figure B2.

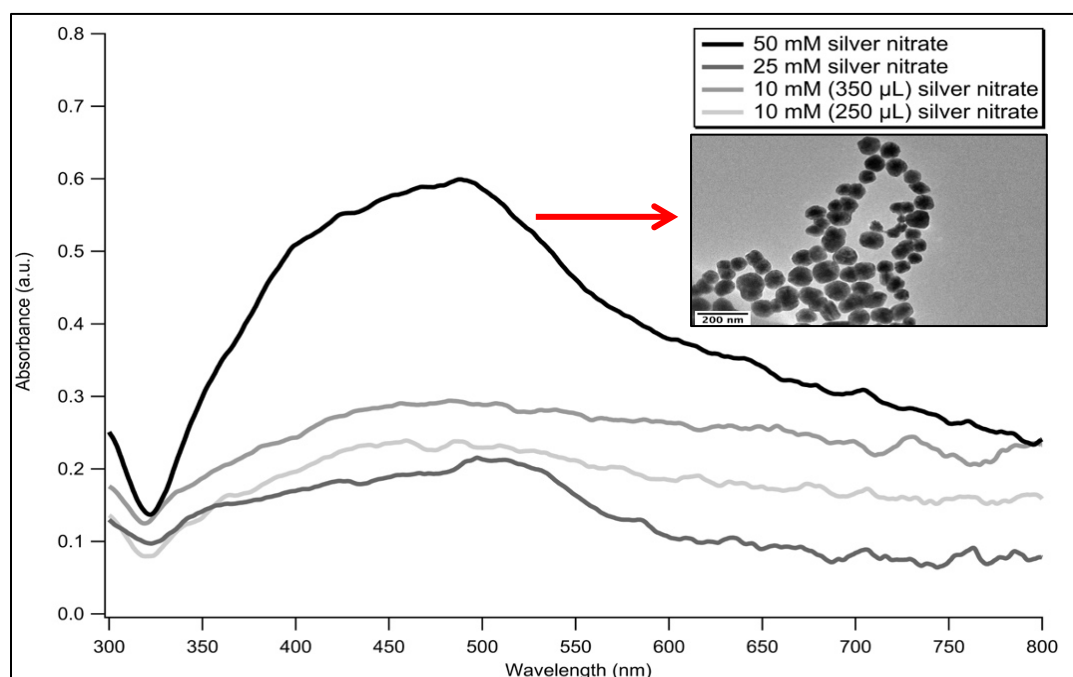


Figure B2. UV-VIS comparison of the 50 mM, 25 mM and 10 mM silver nitrate coating additions for the formation of Ag@AuNS. TEM image (inset) is the 50 mM silver nitrate sample that displayed the best UV-VIS profile.

During the Ag@AuNS substrate synthesis, 4-MBA was used as a placeholder Raman tag to understand how the silver would coat the samples with a tag embedded. For actual SERS measurements and use in the hybridization reactions, CVL was embedded as the Raman tag of choice. However, after running blank SERS measurements (capture probe spectral profile) and low concentration hybridization reactions in buffer, a spectral overlap was observed (Figure B3). This spectral overlap was prominent only at low concentrations making it difficult to distinguish the complexes versus the blank measurements. The CVL Raman profile shows Raman bands with good resolution at 1607.81 cm^{-1} , 1440.92 cm^{-1} , 1353.84 cm^{-1} , and 1157.57 cm^{-1} . When analyzing the blank and 200 nM hybridized complex SERS measurements there is an overlap at all of these peaks which makes developing a biosensor with a low limit of detection difficult. Thus, choosing another Raman tag was necessary to find a Raman band that does not have spectral overlap with the blank measurements.

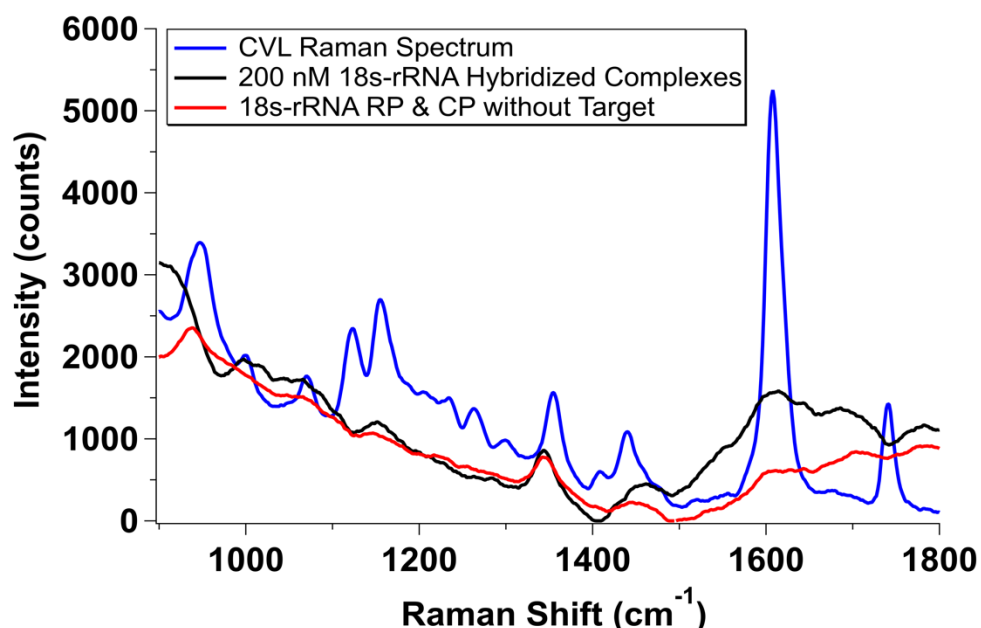


Figure B3. Comparison of SERS spectral profiles for CVL, 200 nM hybridized complexes, and blank hybridization measurements. All measurements were obtained with five replicates using the 638 nm laser excitation, one second acquisition, and 10 accumulations. Spectral overlap between the 200 nM complexes and the blanks can be observed at the CVL main peaks 1607.81 cm^{-1} , 1440.92 cm^{-1} , 1353.84 cm^{-1} , and 1157.57 cm^{-1} .

After consulting literature on different Raman tags used and their spectral profiles, Rose Bengal dye was determined to be a good fit for the work in this thesis. SERS measurements were taken to compare Rose Bengal, CVL, and hybridization blank measurements (Figure B4). Rose Bengal does show some overlap of the CVL Raman bands at 1607.81 cm^{-1} and 1157.57 cm^{-1} . In spite of these two peaks overlapping, Rose Bengal shows other notable peaks at 1489.11 cm^{-1} , 1292.10 cm^{-1} and 1267.21 cm^{-1} . The intensity of the 1489.11 cm^{-1} peak relative to the other peaks makes it the ideal Raman band to use for detecting the nucleic acid biomarker in hybridization reactions. Not only is this the dominant peak in the Rose Bengal profile but the 1489.11 cm^{-1} position shows

the lowest intensity in the blank measurement spectral profile. These factors were the main reason that Rose Bengal dye was used as the Raman tag throughout this thesis.

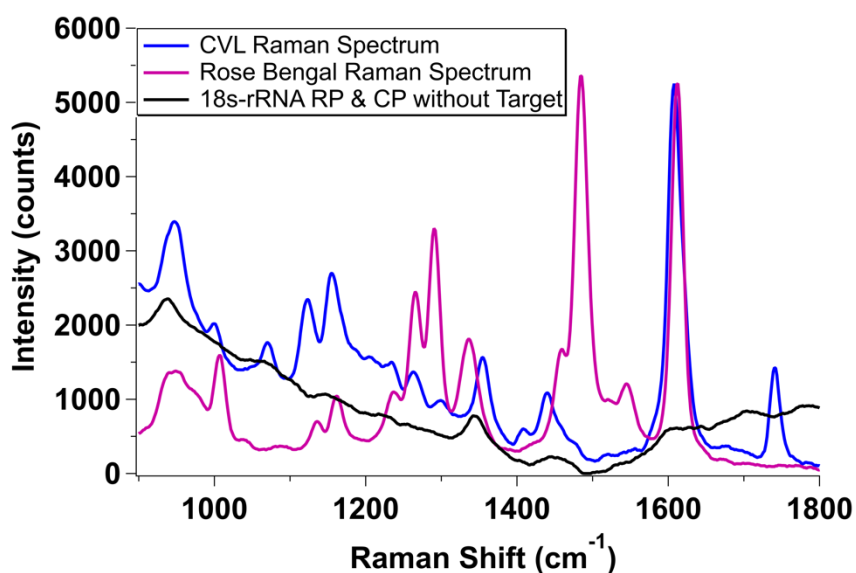


Figure B4. Comparison of Rose Bengal dye, CVL, and blank hybridization SERS measurements. Measurements were obtained using the 638 nm excitation, one second acquisition, and 10 accumulations. The dominant Rose Bengal peak at 1489.11 cm^{-1} showed no overlap with the blank signal measurements, thus making it the peak of interest for the hybridization reactions.

APPENDIX C

Synthesis of the novel Au@AgNS substrate required multiple attempts at applying the gold coating onto the AgNS surface. As mentioned in the main text, two methods were attempted for reducing gold onto the AgNS: CTAB surfactant stabilization and chitosan biopolymer. For the CTAB gold coating method, four different volumes of 0.1 M gold (III) chloride solution (20 μL , 50 μL , 100 μL , and 200 μL) were added in different trials as an attempt to optimize Au@AgNS synthesis. Abbreviations for these samples correspond to the CTAB coating and the volume of 0.1 M gold solution used in microliters (CTAB20, CTAB50, CTAB100 and CTAB200). The UV-VIS data for these samples (Figure C1) indicate the lower two volumes of gold addition produce substrates that interact with light in the visible region with some homogeneity of the formed particles. However, the absorbance of particles CTAB20 (20 μL addition) and CTAB50 (50 μL addition), is still broad across a few hundred nanometers. Analyzing the TEM images were the next step in identifying which substrate would work best for the CTAB coating method.

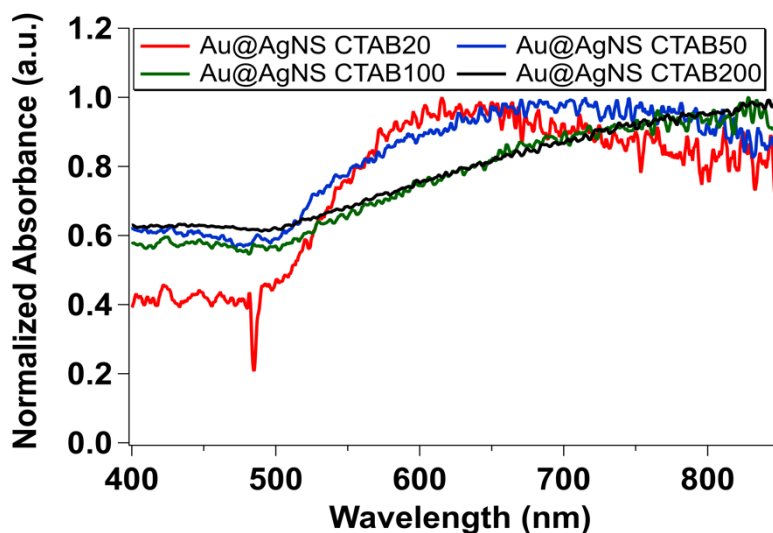


Figure C1. UV-VIS data for the four different CTAB coating methods to synthesize Au@AgNS. Each trial is denoted by the word CTAB with the number corresponding to the volume (μL) of 0.1 M gold used in each reaction.

The TEM images for all four CTAB samples can be found below in Figure C2. CTAB100 and CTAB200 show a spherical morphology with short branches which do not match the original shape of the AgNS used for the synthesis of these substrates. Of the two substrates of interest CTAB20 and CTAB50, the CTAB20 sample produced substrates that retained some of the original morphology from AgNS. This combined with the UV-VIS data indicated that CTAB20 was the best of the four CTAB methods for synthesizing Au@AgNS. Once a substrate using the CTAB coating method was produced, it was compared to the best chitosan substrate for determining which would be the best Au@AgNS substrate.

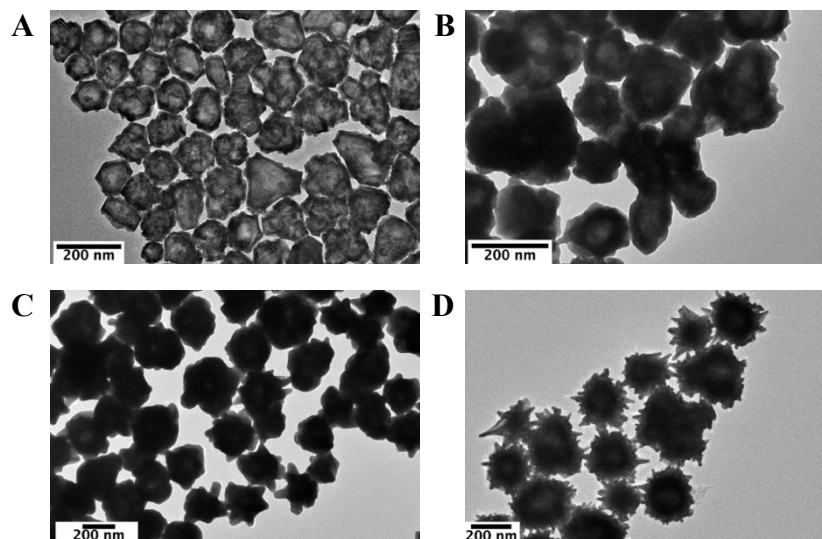


Figure C2. TEM images for all four CTAB synthesized Au@AgNS. Images correspond to: (A) CTAB20, (B) CTAB50, (C) CTAB 100 and (D) CTAB200. Morphology indicates that CTAB20 is the closest to maintaining the original shape of the AgNS core.

For chitosan only two different trials were attempted using a similar approach as the CTAB trials. Only the volume of gold was adjusted while keeping the other parameters the same. The two chitosan trials consisted of using 10 μL (chitosan10) and 25 μL (chitosan25) of a 0.1 M gold solution. With these trials a control sample was performed with the absence of AgNS in the reaction to see how the chitosan behaves with only 10 μL of 0.1 M gold solution (control10). The UV-VIS and TEM can be found below (Figure C3) for the comparison of chitosan10 and chitosan25 plus the control10 sample. The UV-VIS profile for all of three of these samples were similar in shape; however, the higher absorbance of chitosan10 and chitosan25 indicates the substrate was made due to a higher interaction with the light in the spectrophotometer. The TEM also supports since the overall morphology of chitosan10 and chitosan25 shows larger clusters or coated AgNS compared to the control10 sample. Overall, the chitosan10 sample exhibits the

original morphology of the AgNS much better than the chitosan25 sample. The characterization of chitosan10 displays the more optimized synthetic method than the chitosan25 sample and should be compared to the CTAB20 sample.

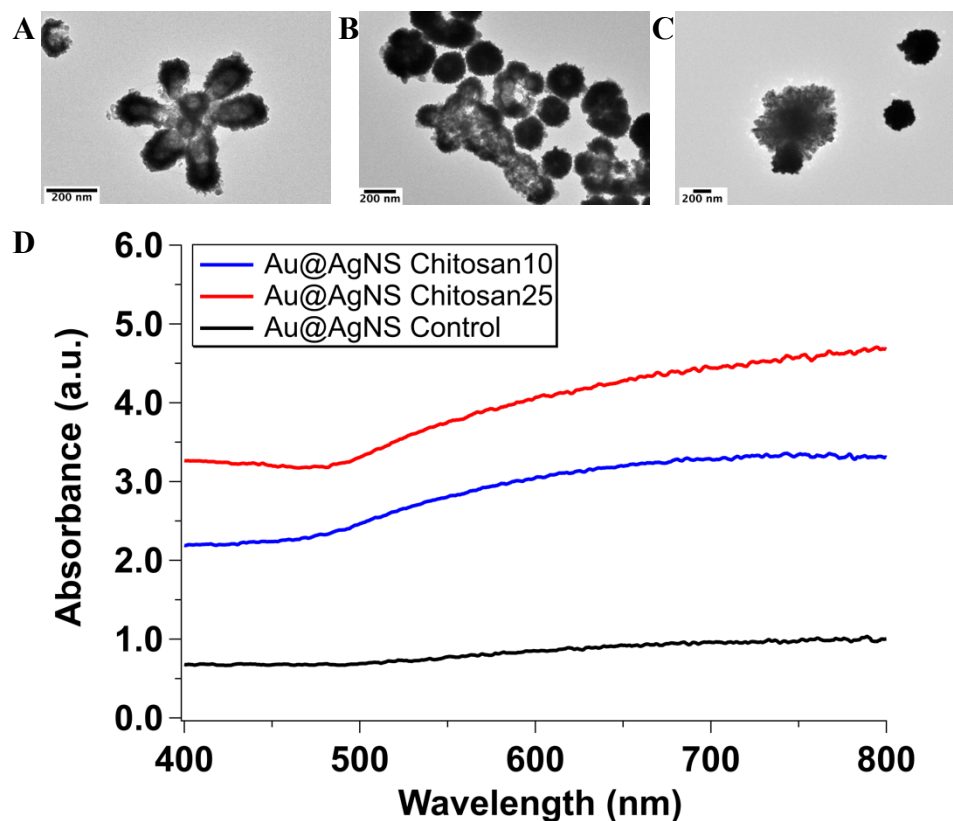


Figure C3. TEM and UV-VIS characterization data for chitosan10, chitosan25 and control10. TEM images are in the order of: (A) chitosan10, (B) chitosan25 and (C) control10. D) UV-VIS data for all three samples. Chitosan10 and chitosan25 display similar profiles based on shape and absorbance compared to control10.

APPENDIX D

For the blood lysate reactions, the focus of the work and quantification of the assay was performed while using the 638 nm laser excitation. In this appendix is the SERS spectra and calibration curve in blood lysate for the 785 nm laser excitation (Figure D1). The measurements were done using the same parameters as the 638 nm laser with the only switch being the laser excitation. The 785 nm laser was used to gain a better understanding of how changing the excitation could impact the SERS intensity after hybridization reactions in blood. The change of matrix from buffer to blood can cause complications in some systems which is why it was necessary to not only collect data with the 638 nm laser but the 785 nm laser as well. The overall counts for each concentration in the calibration range of 125 nM to 10 μ M were much lower for the 785 nm excitation. However, the blank signal measurements were also lower when using the 785 nm excitation. The trend remained the same between the two laser types as seen in between the two calibration curves. The linear range of this assay was approximately from 125 nM to 1 μ M. This data supports that either laser source can be used for the hybridization assay in blood lysate even with lower overall intensity.

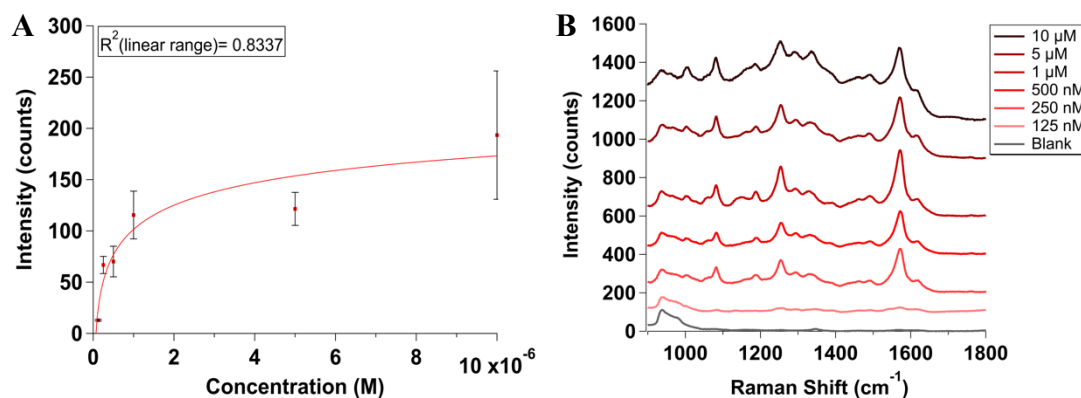


Figure D1. Calibration curve and SERS spectra for hybridization reactions in blood lysate when using 785 nm excitation. Measurements were acquired using the 10x objective, one second acquisition and 10 accumulations. A) Calibration curve ranging from 125 nM to 10 μ M concentrations. Error bars are from the standard deviation of the intensity across five replicate samples for each concentration. Linear range was approximately from 125 nM to 1 μ M. B) Averaged SERS spectra for every concentration in the calibration curve plus the blank average signal.